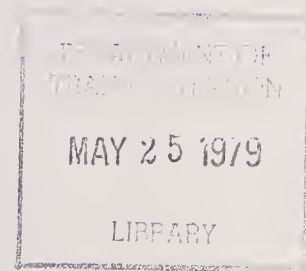


TE
662
.A35
no.
FHWA-
RD-
76-
181

Report No. FHWA-RD-76-181

NDOMDEC: MATHEMATICAL BACKGROUND AND APPLICATION TO DETECTION OF STRUCTURAL DETERIORATION IN BRIDGES



September 1976

Final Report

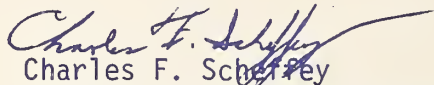
Document is available to the public through
the National Technical Information Service,
Springfield, Virginia 22161

Prepared for
FEDERAL HIGHWAY ADMINISTRATION
Offices of Research & Development
Washington, D. C. 20590

FOREWORD

This report presents the results of analytical, laboratory, and field studies of the "Randomdec" technique for analyzing random bridge vibrations to detect bridge structural member deterioration. The report is being distributed by memorandum to researchers in this field.

Research on bridge inspection and analysis is included in the Federal Highway Administration Federally Coordinated Program of Highway Research and Development Project 5F "Structural Integrity and Life Expectancy of Bridges." Mr. Craig A. Ballinger is the Project Manager.



Charles F. Scherfey
Director, Office of Research
Federal Highway Administration

NOTICE

This document is disseminated under the sponsorship of the Department of Transportation and the National Aeronautics and Space Administration in the interest of information exchange. The United States Government assumes no liability for its contents or use thereof.

The contents of this report reflect the views of the authors who are responsible for the facts and the accuracy of the data presented herein. The contents do not necessarily reflect the official views or policy of the Department of Transportation or the National Aeronautics and Space Administration. This report does not constitute a standard, specification, or regulation.

The United States Government does not endorse products or manufacturers. Trade or manufacturers' names appear herein only because they are considered essential to the object of this document.

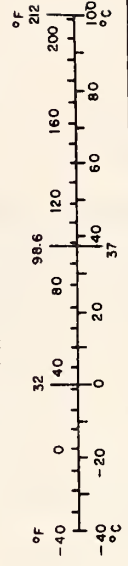
1. Report No. FHWA-RD-76-181	2. Government Accession No.	3. Recipient's Catalog No.	
4. Title and Subtitle RANDOMDEC: MATHEMATICAL BACKGROUND AND APPLICATION TO DETECTION OF STRUCTURAL DETERIORATION IN BRIDGES		5. Report Date September 1976	
		6. Performing Organization Code	
7. Author(s) R. E. Reed, Jr. and H. A. Cole, Jr.		8. Performing Organization Report No. NEAR TR 124	
9. Performing Organization Name and Address Nielsen Engineering & Research, Inc. 510 Clyde Avenue Mountain View, California 94043		10. Work Unit No. (TRAIS)	
12. Sponsoring Agency Name and Address National Aeronautics and Space Administration Washington, D.C. 20546 Federal Highway Administration Washington, D.C. 20590		11. Contract or Grant No. NAS2-8702	
		13. Type of Report and Period Covered Final Report 12/20/74 to 12/15/76	
14. Sponsoring Agency Code			
15. Supplementary Notes FHWA Contract Manager: C. A. Ballinger (HRS-11) NASA Contract Manager: R. J. Miller			
16. Abstract The application of Randomdec analysis to the detection of flaws in highway bridges is investigated analytically and experimentally. The analytical study shows basic properties of the method including the relationship between the Randomdec signature, the amplitude spectrum and the modal response of the system. The experimental program included a field study on five bridges and a laboratory study on samples with induced fatigue cracks. The bridge work produced results on signature characteristics of different types of structural members and on the detection of structural changes in a bridge under dynamic testing. The laboratory study showed that within the frequency range of 1-10 KHz, crack growth in the range of 0.25 to 0.7 cm can be detected at distances up to about one meter.			
17. Key Words Failure Detection Bridges Nondestructive testing (NDT) Structures		18. Distribution Statement No restrictions. This document is available to the public through the National Technical Information Service, Springfield, Virginia 22161	
19. Security Classif. (of this report) Unclassified	20. Security Classif. (of this page) Unclassified	21. No. of Pages 180	22. Price

PREFACE

This work was done under NASA Contract NAS2-8702, which was jointly funded by NASA/Headquarters and the Federal Highway Administration (FHWA). The program was monitored by Robert Miller of NASA/Ames Research Center and Craig Ballinger of FHWA. The authors are grateful to Charles Seim and others of the Toll Bridge Administration of the State of California for their cooperation in providing access to the bridges in California. Also, thanks are extended to the group of faculty members at the University of Missouri headed by James Baldwin for their cooperation and help in obtaining field measurements on the bridge in Missouri.

METRIC CONVERSION FACTORS

Approximate Conversions to Metric Measures				Approximate Conversions from Metric Measures			
Symbol	When You Know	Multiply by	To Find	Symbol	When You Know	Multiply by	To Find
LENGTH				LENGTH			
in	inches	2.5	centimeters	mm	millimeters	0.04	inches
ft	feet	30	centimeters	cm	centimeters	0.4	inches
yd	yards	0.9	meters	m	meters	3.3	feet
mi	miles	1.6	kilometers	km	kilometers	1.1	yards
						0.6	miles
AREA				AREA			
in ²	square inches	6.5	square centimeters	cm ²	square centimeters	0.16	square inches
ft ²	square feet	0.09	square meters	m ²	square meters	1.2	square yards
yd ²	square yards	0.8	square meters	km ²	square kilometers	0.4	square miles
mi ²	square miles	2.6	square kilometers	ha	hectares (10,000 m ²)	2.5	acres
	acres	0.4	hectares				
MASS (weight)				MASS (weight)			
oz	ounces	28	grams	g	grams	0.035	ounces
lb	pounds	0.45	kilograms	kg	kilograms	2.2	pounds
	short tons (2000 lb)	0.9	tonnes	t	tonnes (1000 kg)	1.1	short tons
VOLUME				VOLUME			
tsp	teaspoons	5	milliliters	ml	milliliters	0.03	fluid ounces
Tbsp	tablespoons	15	milliliters	l	liters	2.1	pints
fl oz	fluid ounces	30	milliliters	l	liters	1.06	quarts
c	cups	0.24	liters	l	liters	0.26	gallons
pt	pints	0.47	liters	m ³	cubic meters	35	cubic feet
qt	quarts	0.95	liters	m ³	cubic meters	1.3	cubic yards
gal	gallons	3.8	liters				
ft ³	cubic feet	0.03	cubic meters				
yd ³	cubic yards	0.76	cubic meters				
TEMPERATURE (exact)				TEMPERATURE (exact)			
°F	Fahrenheit temperature	5/9 (after subtracting 32)	Celsius temperature	°C	Celsius temperature	9/5 (then add 32)	Fahrenheit temperature



*1 in = 2.54 (exactly). For other exact conversions and more detailed tables, see NBS Misc. Publ. 286, Units of Weights and Measures, Price \$2.25, SD Catalog No. C13.10.286.

TABLE OF CONTENTS

<u>Section</u>	<u>Page</u>
INTRODUCTION.	1
SCOPE OF WORK	2
Analytical Study	2
Field Study.	3
Laboratory Study	4
BACKGROUND OF RANDOMDEC ANALYSIS.	5
ANALYTICAL STUDY.	7
Randomdec and Fourier Series Representations of Time History . .	7
Signatures of Linear Oscillatory Systems	11
Numerical Examples for a Two-Mode System	16
Signature Accuracy	18
Effect of Filtering on Signatures.	19
FIELD STUDY	22
Operational Procedures	22
Installation of accelerometers.	23
Excitation.	23
Record lengths.	24
Filter settings	24
Hardware configurations	24
Calibration	25
Interpretation of signatures.	25
85-101 Separation Bridge	26
Signal Bridge.	27
West Carquinez Bridge.	28
Missouri Bridge.	31
Signatures from dolly excitation.	33
Signatures from actuator excitation	34
Simulation of Flaws.	37

TABLE OF CONTENTS (CONCLUDED)

<u>Section</u>	<u>Page</u>
East Carquinez Bridge	37
Sawcuts in a laboratory beam.	38
Location of Flaws.	39
East Carquinez Bridge signatures.	40
West Carquinez Bridge - traveling waves	42
LABORATORY STUDY.	44
Excitation of Specimens.	44
Crack Histories.	45
Specimen no. 1.	45
Specimen no. 2.	45
Specimen no. 3.	46
Specimen no. 4.	46
Specimen no. 5.	46
Specimen no. 6.	47
Specimen no. 7.	47
DISCUSSION OF RESULTS	48
Analytical Basis for Signature Interpretation.	48
Signature Characteristics for Different Structures	48
Similarity of Signatures for Similar Members	49
Sensitivity of Signatures to Cracks.	49
CONCLUSIONS	50
RECOMMENDATIONS	51
Field Work	51
Laboratory Work.	51
Analytical Work.	51
REFERENCES.	53
APPENDIX A - TWO-DEGREE-OF-FREEDOM SYSTEM	55
APPENDIX B - LABORATORY TEST PROGRAM.	59

LIST OF ILLUSTRATIONS

<u>Figure</u>		<u>Page</u>
1	Definition of Randomdec signature.	66
2	Comparison of forward and backward analysis of time history.	67
3	Numerical cases for two-degree-of-freedom analytical model.	68
4	Comparison of system step response y_1 and Randomdec signature, case 1.	69
5	Comparison of system step response y_2 and Randomdec signature, case 1.	70
6	Comparison of system step response y_1 and acceleration signature, case 1.	71
7	Standard deviation of segments versus signature amplitude.	72
8	Randomdec signature of white noise subjected to ideal low-pass filter.	73
9	Randomdec signature of white noise subjected to ideal band-pass filter.	74
10	Instrumentation for field measurements.	75
11	Highway 85-101 Bridge, looking north on Highway 101.	76
12	85-101 Bridge accelerometer locations.	77
13	Signatures of 85-101 Bridge, girder A.	78
14	Signatures of 85-101 Bridge, girder B.	79
15	Cross-Randomdec signatures, 85-101 Bridge.	80
16	Repeatability of signatures on 85-101 Separation Bridge.	81
17	Signal Bridge, looking north across east approach to San Francisco Bay Bridge.	82
18	Signatures of lower West chord.	83
19	Signatures of lower east chord and upper diagonal member.	84
20	Carquinez Bridges, West Carquinez Bridge in foreground.	85
21	Locations of eyebar removal on West Carquinez Bridge.	86
22	Eyebars configuration at removal location.	87
23	Eyebars replacement, Bar No. 10.	88
24	Eyebars replacement; south end; Bar No. 9.	89

LIST OF ILLUSTRATIONS (CONTINUED)

<u>Figure</u>		<u>Page</u>
25	Eyebar replacement; south end; Bar No. 8.	90
26	Eyebar replacement; north end; Bar No. 9.	91
27	Eyebar replacement; north end; Bar No. 8.	92
28	Hanger eyebar locations.	93
29	Signatures of hanger eyebars; 2/22/75.	94
30	Signatures of hanger eyebars; 3/4/75.	95
31	Signatures of hanger eyebars; 3/20/75.	96
32	Signatures of hanger eyebars; 5/20/75.	97
33	Signatures of hanger bars; east side; 5/20/75.	98
34	Test bridge in Missouri for dynamic fatigue study.	99
35	Ballast loading and actuator on Missouri Bridge.	100
36	Cracks in bottom flange of Missouri Bridge.	101
37	Transducer locations on Missouri Bridge.	102
38	Station 3; top flange.	103
39	Station 6; top flange.	104
40	Station 9; top flange.	105
41	Station 12; top flange.	106
42	Station 12; top flange.	107
43	Station 15; top flange.	108
44	Station 18; top flange.	109
45	Station 21; top flange.	110
46	Station 24; top flange.	111
47	Comparison of bottom flange signatures, Stations 1 and 2.	112
48	Comparison of bottom flange signatures, Stations 4 and 5.	113
49	Comparison of bottom flange signatures, Stations 7 and 8.	114
50	Comparison of bottom flange signatures, Stations 10 and 11.	115
51	Comparison of bottom flange signatures, Stations 16 and 17.	116

LIST OF ILLUSTRATIONS (CONTINUED)

<u>Figure</u>		<u>Page</u>
52	Comparison of bottom flange signatures, Stations 16 and 17.	117
53	Comparison of bottom flange signatures, Stations 19 and 20.	118
54	Comparison of bottom flange signatures, Stations 22 and 23.	119
55	Check of structural linearity.	120
56	Check of repeatability.	121
57	Station 10, bottom flange.	122
58	Station 11, bottom flange.	123
59	Station 1, bottom flange.	124
60	Station 2, bottom flange.	125
61	Station 3, top flange.	126
62	Station 6, top flange.	127
63	Station 9, top flange.	128
64	Station 12, top flange.	129
65	Station 19, bottom flange.	130
66	Station 20, bottom flange.	131
67	Station 21, top flange.	132
68	Failure of interior girder at midspan on Missouri Bridge.	133
69	Bolt simulator and accelerometer stations, East Carquinez Bridge.	134
70	Station 1, flaw simulation.	135
71	Station 2, flaw simulation.	136
72	Station 3, flaw simulation.	137
73	Station 4, flaw simulation.	138
74	Station 5, flaw simulation.	139
75	Simulation of crack with a sawcut in beam.	140
76	Sawcut in beam, Station 1.	141
77	Sawcut in beam, Station 2.	142

LIST OF ILLUSTRATIONS (CONCLUDED)

<u>Figure</u>		<u>Page</u>
78	Signatures superposed on standard, Station 1.	143
79	Signatures superposed on standard, Station 2.	144
80	Effect of flaw simulation and possible location of flaw.	145
81	Traveling wave in West Carquinez eyebar.	146
82	Traveling waves in West Carquinez eyebar.	147
83	Laboratory specimen with fillet welded cover plate.	148
84	Laboratory specimen with butt weld.	149
85	Development of machine failure.	150
86	Specimen #1 - top accelerometer.	151
87	Specimen #1 - bottom accelerometer.	152
88	Specimen #2 - top accelerometer.	153
89	Specimen #3 - top accelerometer.	154
90	Specimen #3 - top accelerometer.	155
91	Specimen #4 - top accelerometer.	156
92	Specimen #4 - top accelerometer.	157
93	Specimen #5 - top accelerometer.	158
94	Specimen #6 - top accelerometer.	159
95	Specimen #6 - top accelerometer.	160
96	Specimen #7.	161
97	Specimen #7 - comparison of signatures.	162

LIST OF TABLES

<u>Table</u>		<u>Page</u>
1	Transducer locations, 85-101 Bridge.	163
2	Visual crack sizes on lower flanges of Missouri Bridge.	164
3	Numerical differences between signatures of Missouri Bridge bottom flange.	165
4	Laboratory test log.	166

LIST OF SYMBOLS

a	k_1/k_2
A	Fourier amplitude coefficient
b	m_1/m_2
C	confidence factor
C_i	damping coefficient
d	$C_2/(2\sqrt{k_2 m_2})$
e	C_1/C_2
E	modulus of elasticity
F	excitation force
F_s	fractional error of signature
h	thickness
i, j, m, n, p	indices
I	area moment of inertia
k_i	spring constant of i^{th} spring
K	number of peaks encountered
$L()$	differential operator
m_i	mass of i^{th} element
M	number of frequency components
N	number of segments in ensemble
Q	complex frequency
r	correlation factor
t	time
T	half record length
V_s	initial slope of signature
W	$\sqrt{k_2/m_2}$
y	displacement
Y_s	initial amplitude of signature

LIST OF SYMBOLS (CONCLUDED)

δ	Randomdec signature
λ	frequency parameter, $\lambda^2 = A\rho/EI$
ϕ	phase angle
ρ	mass density
τ	time coordinate of signature
ω	circular frequency
σ_{ϵ}	standard deviation of ensemble average
σ_y	rms value of time history
$(\bar{})$	mean value of variables in parenthesis

RANDOMDEC: MATHEMATICAL BACKGROUND AND APPLICATION
TO DETECTION OF STRUCTURAL DETERIORATION
IN BRIDGES

R. E. Reed, Jr. and H. A. Cole, Jr.
Nielsen Engineering & Research, Inc.

INTRODUCTION

The ability to detect flaws in bridges before the flaws affect the integrity of the structure is becoming more necessary as the ages of the vast number of bridges built in the last few decades increase and approach their expected service lives. At present, visual inspection is the only method that is used as a general inspection technique. Its obvious shortcomings have instituted the development of additional techniques, with several methods appearing feasible although no simple method can be applied reliably and economically to all types of applications that exist.

Randomdec analysis is a method that appears feasible for many applications. It is a technique for analyzing the dynamic response of a structure to random excitation. Usually, the dynamic response of the structure to in-service loads is recorded onto magnetic tape for later analysis. Using the Randomdec technique, the analysis produces a signature that is characteristic of the structure and relatively independent of the random excitation.

The method was originally developed (ref. 1) to measure the damping of aircraft models in wind tunnel flutter tests. The method is presently being used by the aerospace industry for this application and also for flight flutter testing of actual aircraft (ref. 2). The flaw detection capability became apparent from a wind tunnel test after it was observed that a difference between signatures taken at different times was later followed by the complete failure of the model (ref. 3). The basis for flaw detection, therefore, is the observance of differences in signatures.

A past study under the Federal Highway Administration (FHWA) and NASA Headquarters (ref. 4) investigated the two fundamental requirements for a successful technique of this type. The first requirement is that a flaw produces a significant change in the signature and the second is that natural variations in the environment do not produce a signature change that would prevent the detection of a flaw. The detection of fatigue cracks was demonstrated in the laboratory where the cracks were

induced in a test beam with welded cover plates and signatures were obtained at various stages of crack growth. Changes in signatures were apparent at stations about 0.2 m. to 1 m. from the cracks with crack growth on the order of 0.25 cm. to 2 cm. In addition, a relatively new steel girder bridge was instrumented and monitored over a period of about eight months under normal variations in weather and traffic to determine the repeatability of the signatures versus environmental conditions. The repeatability remained very good throughout the study. Thus, the basic feasibility of the method was established, although its usefulness as a practical and economical monitoring system remained unproven.

The objective of this study was to determine the signature characteristics versus variables that are important in developing the method into an operational system for detecting flaws. Although there are many types of flaws, cracks in structural members were of primary interest in this study. The variables considered were:

1. Analytical basis for signature interpretation.
2. Signature characteristics for different types of structures.
3. Similarity of signatures for similar structural members.
4. Sensitivity of signatures to crack size and distance between transducer and crack.

SCOPE OF WORK

The overall program was divided into an analytical study, field work on bridges, and a laboratory study. The scope of each of these studies is discussed below.

Analytical Study

The analytical study examined the mathematical basis of the Randomdec method to determine the relationship between signatures and the physical systems from which they were obtained. The following topics were investigated.

1. Dependence of signatures on the Fourier response spectrum of the time history.
2. Relationship between signatures and the free vibration response of linear systems.

3. Signature accuracy versus record length for a linear two-degree-of-freedom system.
4. Effects on signatures of filtering the time history.

For those cases involving the computation of signatures from a random record, the digital computer at Ames Research Center was used to generate random excitation, system response and resulting signatures.

Field Study

The field work was conducted on different types of bridges containing a variety of structural members. Of the following five bridges that were studied, the first four are in the San Francisco Bay Area and the fifth is in Missouri.

1. Highway 85-101 Separation Bridge - A multiple simple span, steel girder overcrossing of noncomposite construction. This structure was previously monitored (ref. 4) and was monitored in this program primarily to check the repeatability of signatures after the intervening nine months between the study of reference 4 and the present study.
2. Signal Bridge - A welded steel Warren truss spanning the San Francisco Bay Bridge Toll Plaza. This 60 m. span supports signal lights for the traffic passing under the structure. The bridge carries no traffic itself so its excitation is transmitted through the air and its foundation. This all welded structure is lightly damped and contains many structural connections of identical construction. The purpose of this task was to study this excitation and to compare signatures of similar joints to see if it would be feasible to detect a faulty joint by comparing signatures taken at one time. This capability would be useful for evaluating new structures since it would not be necessary to monitor each location over a period of time.
3. West Carquinez Bridge - A double cantilever structure across the Carquinez Straits with a span of 1,100 m. This bridge was built about 50 years ago and has forged eyebar tension members (from two to ten bars per member) and riveted, laced compression members. The eyebars are similar to the one that caused the

collapse of the Point Pleasant Bridge in West Virginia in 1967 and were of concern to engineers of the State of California. The signature characteristics of these eyebars were of primary interest both from the standpoint of individual bars and the similarity between bars in a group comprising a given member.

4. East Carquinez Bridge - A double cantilever structure similar in appearance (but not construction detail) and parallel to the West span. The 1,100 m. span was built about 20 years ago and has welded, high strength steel box members with high strength bolted field connections. This bridge was used for flaw simulation work using traffic as excitation.
5. Missouri Bridge - A 72 m. three-span continuous steel girder bridge of composite construction which has been removed from service. A destructive test of this bridge was sponsored by the Missouri State Highway Commission and conducted by faculty members of the University of Missouri. The bridge was dynamically excited at its resonance to produce fatigue cracks in the girders. Several techniques were used to monitor the deterioration of the bridge. This represented a rare opportunity to obtain vibration data of an actual bridge with flaws. As a part of this program, suspected crack locations at the ends of welded coverplates were instrumented and vibration records for Randomdec analysis were obtained before and during the cyclic loading.

Laboratory Study

A study was conducted in the laboratory to determine the sensitivity of signatures to cracks of different lengths in welded specimens. Both fillet and butt weldments were cyclically loaded to produce fatigue cracks. Vibration records of the specimens were recorded at different stages of cracking. The experimental work was done at the University of Maryland with data recorded onto magnetic tape and the analysis was done at the Nielsen Engineering & Research, Inc. (NEAR) facility.

BACKGROUND OF RANDOMDEC ANALYSIS

The Randomdec technique is a general method of analysis that is particularly well suited to the class of problems in which characteristics are desired of a structure that is in service and subjected to unknown random excitation. Only the measurement of the dynamic response of the structure, and not the excitation, is required for the analysis. A bridge carrying traffic is a good example of an application for the method.

The analysis of a time history (displacement, strain, acceleration, etc., versus time) of the response at some location on the bridge gives a signature that is dependent on structural properties such as natural frequencies and damping and is relatively independent of the excitation.

Having a signature sensitive to changes in the structural properties allows the detection of changes in those properties. Hence, the detection of flaws is possible and can be done by either of two methods. One is to establish a standard signature for a given location on a structure and monitor this station periodically over a period of time. A change in the signature indicates that a change in structural properties has occurred in the intervening time. The other method is to establish a standard signature for many similar components that are in acceptable condition. A signature with significant differences would then indicate a component which had different characteristics. This method would be valuable in detecting a defective structural member among a group of similar members. However, it requires that acceptable members have signatures that are similar enough to establish a standard.

The procedure for obtaining a signature is shown in figure 1. A typical time history is divided into segments of length τ_{\max} with each segment starting at the same amplitude y_s (or \ddot{y}_s if the time history is in terms of acceleration). One-half of the segments are chosen with initial positive slopes and the other half with negative slopes. These segments are then ensemble averaged to give a signature of length τ_{\max} which starts with an amplitude of y_s and an initial slope of zero.

In addition to the above signature, other signatures called Cross-Randomdec signatures can be obtained and are useful for determining the dependence of one station on another. One signature (the primary signature) is determined as described above and the cross-signatures are

obtained from additional simultaneous records by starting each segment at the same time as the corresponding segment in the primary record. Using this procedure, for example, two identical records will yield identical signatures whereas two records that are independent of each other will yield a cross-signature of zero. Records that are dependent but not identical, say from locations close together, will show nonzero signatures.

One of the main advantages of the method is the freedom to choose the bias level y_s . Often the time history will be nonstationary and contain periods of low vibration and a resulting low signal-to-noise ratio. The amplitude y_s can be chosen above this low-noise level to exclude those sections of record. Intermittent traffic on a bridge is an example where this property is advantageous. For linear systems, the signature shapes will be the same for different values of y_s . Nonlinear systems, therefore, can be detected by comparing signatures using different values of y_s . Conversely, using the same value of y_s in different tests makes the signatures for nonlinear systems relatively independent of changes in the intensity of the excitation.

Depending on the excitation, the time history will contain a certain bandwidth of frequencies. Traffic on a bridge produces a wide range of frequency, say 0-10KHz, which allows the analysis of various effects. The low frequency range is of interest for measurement of damping and natural frequencies. The detection of small flaws, however, requires the high frequency characteristics, say greater than 1 KHz, since flaws will not affect low frequencies until the integrity of the structure is threatened. These different frequency-ranges can be isolated by bandpass filtering the time history before the record is analyzed.

In order to measure system properties such as damping and natural frequencies or to interpret changes in signatures as to their causes, the relationship between a Randomdec signature and the physical system must be known. In reference 5, a valid intuitive argument is given to show that the signature of a linear, single-degree-of-freedom system is the free vibration response of the system to an initial displacement. This relationship allows calculation of the damping and natural frequency of such a system from the signature. A change in the signature can be related to the mass, stiffness or damping mechanism depending on the type of change introduced. Systems encountered in practice, however,

are more complicated and the resulting signatures are more intricate and more difficult to interpret. Relationships between signatures and more complicated systems are the subject of the next section.

ANALYTICAL STUDY

Randomdec analysis has been developed over the last few years with the emphasis being on the application of the method rather than its analytical foundation (although reference 6 contains some recent work of an analytical nature). In the following, results are given of various analytical studies which are relevant to the successful application of the method to practical problems.

Randomdec and Fourier Series Representations of Time History

The most common way of analyzing a random time history is to obtain the frequency content of the record by the use of Fourier analysis techniques. Therefore, it is useful to obtain the Randomdec signature in terms of the frequency content. To do this, consider a time history of length $2T$ such as the one shown in figure 1. This record can be represented by the Fourier series

$$y(t) = \sum_{m=0}^{\infty} A_m \cos \left(\frac{m\pi t}{T} + \phi_m \right) \quad (1)$$

where ϕ_m are phase angles.

The Randomdec signature of this record is obtained by choosing segments with initial amplitudes of y_{sn} . The n^{th} segment is represented by

$$y_n(\tau) = \sum_{m=0}^{\infty} A_m \cos \left[\frac{m\pi (\tau + t_n)}{T} + \phi_m \right] \quad (2)$$

where t_n is the discrete value of time such that $y(t_n) = y_{sn}$ and τ is the time variable measured from t_n . This gives

$$y_n(\tau) = \sum_{m=0}^{\infty} A_m \cos \left(\frac{m\pi t_n}{T} + \phi_m \right) = y_{sn} \quad (3)$$

Assuming $y(0) = y(2T)$, equation (2) can be differentiated term by term to give

$$\dot{y}_n(\tau) = \frac{\pi}{T} \sum_{m=0}^{\infty} -m A_m \sin \left[\frac{m\pi (\tau + t_n)}{T} + \phi_m \right] \quad (4)$$

Therefore, the initial slope V_{sn} is

$$\dot{y}_n(0) = \frac{\pi}{T} \sum_{m=0}^{\infty} -m A_m \sin \left(\frac{m\pi t_n}{T} + \phi_m \right) = V_{sn} \quad (5)$$

The signature $\delta(\tau)$ is obtained by ensemble averaging $y_n(\tau)$ and is,

$$\delta(\tau) = \frac{1}{N} \sum_{n=1}^N \sum_{m=0}^{\infty} A_m \cos \left[\frac{m\pi (\tau + t_n)}{T} + \phi_m \right] \quad (6)$$

This can be expanded to give

$$\begin{aligned} \delta(\tau) = \frac{1}{N} \sum_{m=0}^{\infty} A_m \left[\cos \frac{m\pi \tau}{T} \sum_{n=1}^N \cos \left(\frac{m\pi t_n}{T} + \phi_m \right) \right. \\ \left. - \sin \frac{m\pi \tau}{T} \sum_{n=1}^N \sin \left(\frac{m\pi t_n}{T} + \phi_m \right) \right] \end{aligned} \quad (7)$$

For stationary records where the phase angles ϕ_m and the summed effect of t_n (i.e., N is sufficiently large) are independent of the amplitude coefficients A_m , the relation equating the mean-of-the-products to the product-of-the-means can be used. This relation, for independent variables, is (ref. 7)

$$\frac{1}{Q} \sum_{q=1}^Q X_q Y_q = \frac{1}{Q^2} \sum_{q=1}^Q X_q \sum_{p=1}^Q Y_p \quad (8)$$

Equation (8) is satisfied for $Q = 1$ but, generally, implies the limit as $Q \rightarrow \infty$. For a finite value Q , a certain error is present but Q is assumed to be sufficiently large to make the error negligible. Using equation (8), equation (7) becomes

$$\begin{aligned} \delta(\tau) = \frac{1}{(M+1)N} \sum_{m=0}^M A_m \left\{ \cos \frac{m\pi\tau}{T} \sum_{p=0}^M \left[\sum_{n=1}^N \cos\left(\frac{p\pi t_n}{T} + \phi_p\right) \right] \right. \\ \left. - \sin \frac{m\pi\tau}{T} \sum_{p=0}^M \left[\sum_{n=1}^N \sin\left(\frac{p\pi t_n}{T} + \phi_p\right) \right] \right\} \end{aligned} \quad (9)$$

The initial amplitude and slope of the signature are obtained from equations (3) and (5) and are

$$\delta(0) = \frac{1}{N} \sum_{n=1}^N Y_{sn} = \frac{1}{N} \sum_{m=0}^M A_m \sum_{n=1}^N \cos\left(\frac{m\pi t_n}{T} + \phi_m\right) \quad (10)$$

$$\dot{\delta}(0) = \frac{1}{N} \sum_{n=1}^N V_{sn} = \frac{\pi}{TN} \sum_{m=0}^M m A_m \sum_{n=1}^N \sin\left(\frac{m\pi t_n}{T} + \phi_m\right) \quad (11)$$

Using equation (8), equations (10) and (11) become

$$\frac{\bar{Y}_S}{A^*} = \frac{1}{N(M+1)} \sum_{p=0}^M \left[\sum_{n=1}^N \cos\left(\frac{p\pi t_n}{T} + \phi_p\right) \right] \quad (12)$$

$$\frac{\bar{V}_S}{V^*} = \frac{-1}{N(M+1)} \sum_{p=0}^M \left[\sum_{n=1}^N \sin\left(\frac{p\pi t_n}{T} + \phi_p\right) \right] \quad (13)$$

where

$$(\bar{}) = \frac{1}{N} \sum_{n=1}^N ()_n$$

$$A^* = \sum_{m=0}^M A_m$$

$$V^* = \frac{\pi}{T} \sum_{m=0}^M m A_m$$

Substituting equations (12) and (13) into equation (9), the signature becomes

$$\delta(\tau) = \frac{\bar{Y}_S}{A^*} \sum_{m=0}^M A_m \cos \frac{m\pi\tau}{T} + \frac{\bar{V}_S}{V^*} \sum_{m=0}^M A_m \sin \frac{m\pi\tau}{T} \quad (14)$$

Usually, the initial amplitude of each segment is chosen to be y_s so $\bar{Y}_S = y_s$. Also, half the samples are chosen to have a positive initial slope and half have a negative initial slope. Assuming these slopes average to zero ($\bar{V}_S = 0$), equation (14) becomes

$$\delta(\tau) = \frac{Y_S}{A^*} \sum_{m=0}^M A_m \cos \frac{m\pi\tau}{T} \quad (15)$$

For equation (15), the maximum value occurs at $\tau = 0$ and is $\delta(0) = y_s$. Equations (14) and (15) are useful representations of $\delta(\tau)$ because they allow one to calculate the signature from a known amplitude spectrum. Several cases are discussed in a later section.

Although equation (14) and (15) were derived for $\tau \geq 0$, it is interesting to note that the assumptions should be equally valid for $\tau \leq 0$. Equation (15) should be a symmetrical function about zero. In order to verify this, a particular data set from reference 5 was reversed and a new signature was calculated. The result is compared with the signature from reference 5 in figure 2. It will be seen later that the differences fall within the expected variance for the number of points in the time history. Equation (14) gives the shape of the signature with an initial slope \bar{V}_s . If the negative value of \bar{V}_s is used and $\tau \leq 0$ (a negative \bar{V}_s appears positive when viewed backwards), equation (14) retains the same form. Therefore, the signature converges to the same shape when the record is analyzed either backwards or forwards provided the initial slope converges to the same apparent value. This symmetry has been observed when actual experimental records are analyzed backwards. This result is of practical significance with records stored on magnetic tape. Additional independent segments can be obtained to enhance convergence by analyzing the data played backwards.

Signatures of Linear Oscillatory Systems

In vibration analysis, it is common to represent the motion of a linear system in terms of its natural modes. To see the connection between Randomdec signatures and the modal representation, consider a multi-degree-of-freedom system subjected to a random excitation, $F(\tau)$. Representing the system by a finite number of masses ($i = 1, 2, \dots, I$), the equations describing the motion during the n^{th} time segment are

$$\begin{bmatrix} L_{11}(\) & L_{21}(\) & \dots & L_{I1}(\) & \dots \\ L_{1i}(\) & \dots & \dots & L_{ii}(\) & \dots \\ L_{1I}(\) & \dots & \dots & \dots & L_{II}(\) \end{bmatrix} \begin{Bmatrix} y_{1n} \\ y_{in} \\ y_{In} \end{Bmatrix} = \begin{Bmatrix} F_{1n}(\tau) \\ F_{in}(\tau) \\ F_{In}(\tau) \end{Bmatrix} \quad (16)$$

where the linear operators are, typically,

$$L_{ij}(y) = m_{ij} \frac{d^2 y_i}{dt^2} + c_{ij} \frac{dy_i}{dt} + k_{ij} y_i$$

In addition to equations (16), initial conditions on y and \dot{y} exist. If the beginning of each segment ($\tau = 0$) begins when y_i has an amplitude of y_s with alternating samples having a positive and negative slope, the initial constraints on $y_i(\tau)$ will be

$$y_{in}(0) = y_s \quad n = 1, 2, 3, \dots$$

$$\dot{y}_{in}(0) \geq 0 \quad n = 1, 3, 5, \dots$$

$$\dot{y}_{in}(0) \leq 0 \quad n = 2, 4, 6, \dots$$

with no constraints on the remaining y_j or $\dot{y}_j (j \neq i)$.

The signatures of the masses are found by ensemble averaging their time histories. The equations satisfied by the signatures, for a linear system, are obtained by averaging equations (16) over n which give

$$\begin{aligned} \frac{1}{N} \sum_{n=1}^N \left\{ L_{11} [y_{1n}] + L_{21} [y_{2n}] + \dots L_{i1} [y_{in}] + \dots \right\} &= \frac{1}{N} \sum_{n=1}^N F_{1n}(\tau) \\ \vdots & \\ \frac{1}{N} \sum_{n=1}^N \left\{ L_{1i} [y_{1n}] + L_{2i} [y_{2n}] + \dots L_{ii} [y_{in}] + \dots \right\} &= \frac{1}{N} \sum_{n=1}^N F_{in}(\tau) \end{aligned} \quad (17)$$

For linear operators with coefficients independent of time, the summation and differential operation can be interchanged to give, for example,

$$\frac{1}{N} \sum_{n=1}^N L_{11} [y_{1n}] = L_{11} \left[\frac{1}{N} \sum_{n=1}^N y_{1n} \right]$$

Also, the right hand sides of equations (17) represent the ensemble average of independent random variables. Assuming the forces acting on a given

mass have a white noise distribution with a zero mean value, the right hand sides average to zero. Actually, the limit as $N \rightarrow \infty$ should be used when summations are assumed to vanish. The use of a finite N admits the existence of an error but it is assumed that sufficient samples are taken such that the error is negligible.

Using the definition of Randomdec signatures, the governing equations become

$$\left. \begin{aligned} L_{11} [\delta_1] + L_{21} [\delta_2] + \dots + L_{i1} [\delta_i] + \dots &= 0 \\ L_{1i} [\delta_1] + L_{2i} [\delta_2] + \dots + L_{ii} [\delta_i] + \dots &= 0 \\ L_{1I} [\delta_1] + L_{2I} [\delta_2] + \dots + L_{iI} [\delta_i] + \dots &= 0 \end{aligned} \right\} \quad (18)$$

Equations (18) are seen to be identical to the equations governing the free vibration of the system. For the signature of the i^{th} mass, the initial conditions on $\delta_i(\tau)$ are

$$\delta_i(0) = y_s$$

$$\dot{\delta}_i(0) = 0$$

The remaining initial conditions on δ_j , $j \neq i$, have to be established before the shapes of the signatures are unique. The average initial velocities $\dot{\delta}_j(0)$ of the remaining masses can be taken to be zero since their mean value is zero and they are sampled at $\tau = 0$ when $\dot{y}_i(0)$ is both positive and negative. The average displacement $\delta_j(0)$ of each mass when $\delta_i(0) = y_s$ is the position about which that mass is equally likely to deviate a positive or negative amount when $y_i(0) = y_s$. It is hypothesized that this position is one of minimum energy and, since the velocities are zero at $\tau = 0$, is one of minimum potential energy. This corresponds to the static equilibrium position when the mass δ_i is displaced an amount y_s . The signature, therefore, has the same shape as the free vibration response of the system when the point at which the measurement is taken is displaced to y_s , the remaining masses maintain

static equilibrium with no external constraints, and the system is then released. For a single degree-of-freedom system, for example, the signature is the damped cosine wave starting at an amplitude of y_s . For a multiple mode system such as a beam, the signature at a point is the response of the beam when the necessary static force to deflect the beam to y_s is applied to the point of measurement and then suddenly removed. This assumes that the excitation is such that all modes will be excited. Clearly, if the excitation is supplied to a beam just at the center point, only even modes will be excited and the signature at any point on the beam will contain only the even modes.

It has been assumed that constraints have only been imposed on $y_i(0)$ and $\dot{y}_i(0)$. It is possible to impose additional constraints. For example, the segments could be chosen to start only when a number of y_j 's have some prescribed displacement. The signature then would represent the free vibration decay of the system subjected to prescribed initial displacements at the points y_j . Obviously, the record length required to furnish the same number of segments would increase as the number of constraints increased.

The above assumes that the time history is a measurement of displacement. However, it is often more convenient to measure acceleration and treat the acceleration time history directly. The expected shape of the acceleration signature can be derived as follows. If we differentiate equations (18) twice with respect to time and use the relation

$$\frac{d^2}{dt^2} \left[L_{ij} () \right] = L_{ij} \left[\frac{d^2}{dt^2} () \right]$$

we get equations of the form

$$L_{11} [\ddot{\delta}_1] + L_{21} [\ddot{\delta}_2] + \dots + L_{i1} [\ddot{\delta}_i] + \dots = 0$$

which show the acceleration signature satisfies the same free vibration equations as the displacement. The initial conditions

$$\ddot{\delta}_i(0) = \ddot{y}_s$$

$$\dddot{\delta}_i(0) = 0$$

are imposed (this is not the same as differentiating the displacement signature twice). The values of $\ddot{\delta}_j(0)$, $j \neq i$, are taken to be zero because the mean values of $\ddot{y}_j(\tau)$ are zero and they are independent of $\ddot{y}_i(0)$ since the forces acting on each mass are assumed to be independent. The values of $\ddot{\delta}_j(0)$ are also taken to be zero because of their independence. the signature of an accelerometer trace \ddot{y}_i , therefore has the same shape as the free vibration curve for the displacement y_i when the mass y_i is subjected to an initial displacement y_s and the remaining masses have zero displacement. This type of initial constraint (i.e., displacement of one point) will usually yield a free vibration response accenting the higher modes of the system compared to the constraint of a prescribed displacement of one point with the remaining points displacing so as to maintain static equilibrium.

It is interesting to note that an accelerometer is basically a spring-mass system and that the acceleration measurement output is actually a voltage proportional to the displacement of the spring. Thus, if we think of this as simply an addition to the structure and apply the argument in which displacement is measured, the signature may be thought of as the response obtained by displacing the accelerometer mass and then suddenly letting it go. It is quite apparent, that, to keep interaction between instrument and structure small, the force to displace the accelerometer spring must be small compared to the force to displace the structure. Thus, this is essentially equivalent to an initial condition of the accelerometer mass displaced and the structure undeflected.

It has been assumed in the above that the excitation is white noise. No significant problems are encountered if the excitation is not white but still has a relatively flat spectrum over the frequency bandwidth of interest. This is discussed in reference 5 for a single mode system where the effects of filtering the time history are studied and are seen to be small as long as the frequency cutoff is not near the natural frequency. Filtering of a two-mode system is discussed in a later section.

One effect that can influence the signature is the input spectrum containing a significant peak; that is, a sinusoidal component in the excitation. If the motion is strongly dependent on this component (forced sinusoidal vibration), the right-hand sides of equation (17) will not be zero since $f_n(\tau)$ will have nearly the same sinusoidal form for each value of n . Therefore, a strong sine wave in the excitation will appear in the signature. However, if the sinusoidal component is small compared to the level of excitation, its effect will be averaged out because the sampling, nearly independent of the sinusoidal component, will occur in a random fashion with respect to the sine wave.

Numerical Examples For A Two-Mode System

In order to study several aspects of multiple degree of freedom systems analytically, a two-degree-of-freedom model was used as a basis for analysis to calculate exact results such as the step and impulse responses and, also, it was used to perform experiments on the digital computer. This was done by first calculating the response of the system to a set of random impulses. The resulting random time history was then analyzed in the same manner as a record measured on an actual structure. Figure 3 shows the two-mode model and lists the numerical cases studied. Appendix A shows the details of the analytical work.

The first problem considered was the substantiation of the hypothesis that the exact displacement signature of a point is the free vibration response of that point upon release of the system from the initial conditions of the point displaced an amount y_s and the remaining points in static equilibrium. Considering case 1 of figure 3, there are two signatures, one of each mass point. The corresponding initial conditions are, for δ_1 :

$$y_1(0) = y_2(0) = y_s$$

$$\dot{y}_1(0) = \dot{y}_2(0) = 0$$

and for δ_2 :

$$y_1(0) = y_s/2$$

$$y_2(0) = y_s$$

$$\dot{y}_1(0) = \dot{y}_2(0) = 0$$

Figure 4 shows a comparison of the exact signature for δ_1 with experimental values computed from the system response to independent random excitation acting on each mass. It is seen that the experimental signature is basically the same as the exact step response. Figure 5 shows a similar comparison for δ_2 . The initial conditions for this case closely approximate the modeshape of the lower mode so the signature resembles a damped cosine wave at the lower natural frequency.

Next, a verification of the signature for a time history where acceleration has been measured is desired. To obtain an acceleration record from the computed displacement record $y_1(i)$, $i = 1, 2, \dots, M$, the least square fit of a cubic equation to five adjacent points of $y_1(i)$ was used and had the form

$$\ddot{y}(i+2) = \frac{1}{7} [2y(i+4) - y(i+3) - 2y(i+2) - y(i+1) + 2y(i)]$$

$$i = 1, 2, \dots, M - 4$$

Using the analogy between acceleration and displacement, the initial conditions for this case are

$$\delta_1(0) = y_s$$

$$\delta_2(0) = 0$$

$$\dot{\delta}_1(0) = \dot{\delta}_2(0) = 0$$

Figure 6 shows this comparison. Difficulty existed in obtaining an accurate acceleration time history because the error in the approximation for

acceleration increases with frequency and the time history contained frequencies up to the Nyquist value (two points per cycle). This introduced errors into the computed step response. It is seen in figure 6 that the largest errors occur at the points where the displacement signature, figure 4, has a rapidly changing curvature. The overall comparison is good, however, and shows the validity of the acceleration signature.

Signature Accuracy

In reference 5, the convergence of the signature to the exact value for a single degree-of-freedom system was studied and the following relation was given:

$$F_s = \frac{C\sigma_\epsilon}{y_s \sqrt{(2-r)K}} \quad (19)$$

where $0 \leq r \leq 1$ where $r = 0$ indicates no correlation between segments. The value $r = 1$ indicates each pair of positive and negative-slope segments are dependent. For instance, if both segments were chosen at the top of the same peak, they would be identical.

The standard deviation σ_ϵ was measured at the first peak of the signatures where $\delta/y_s \approx 0.88$ and was $\sigma_\epsilon \approx 0.47$. Since σ_ϵ is a parameter that could depend on the number of degrees of freedom, it was calculated in this present study for ranges of parameters with the present model. Values of damping, frequency ratio of the two natural frequencies and selection level y_s were varied to see if trends in σ_ϵ existed. No significant trends were apparent for these parameters. However, a significant trend was found with the level δ/y_s at which σ_ϵ was measured. Figure 7 shows the results for σ_ϵ/σ_y versus δ/y_s . Although these results include variations in the other parameters, the scatter is not reduced by holding any of their values constant. It is seen that the trend is consistent with the results in reference 5. In reference 6, Chang suggests a curve for σ_ϵ/σ_y dependent on τ which starts at zero for $\tau = 0$ and approaches 1.0. This is consistent with the present results in the sense that $\sigma_\epsilon/\sigma_y = 0$ at $\delta/y_s = 1$ which only occurs at $\tau = 0$ (σ_ϵ at $\tau = 0$ is by definition zero) and $\sigma_\epsilon/\sigma_y \rightarrow 1.0$ as $\delta/y_s \rightarrow 0$ which normally occurs as $\tau \rightarrow \infty$. However, zero crossings occur throughout the range of τ and represent points of maximum error. Also, if $\lim \delta/y_s \neq 0$ (for instance,

if the time history, and therefore the signature, is a single cosine wave) then σ_ϵ/σ_Y would not approach 1.0.

It is useful to apply equation (19) to the present work. Letting

$$C = 1.96 \text{ (95\% confidence level)}$$

$$\sigma_\epsilon/\sigma_Y = 0.8$$

$$Y_S/\sigma_Y = 1.0$$

$$(2 - r)k = 400 \text{ (typical of cases studied)}$$

we get

$$F_S = \frac{1.96(0.8)}{20} \approx 0.08$$

This means that 5 percent of the values of δ/Y_S are expected to differ from the exact value by more than 0.08. This is very useful as it allows one to calculate how many segments are needed for a given accuracy. It is seen that this describes the accuracy that exists in figures 4 and 5. In figure 6, a larger error exists but it is felt that this is due to the error in approximating the acceleration.

Effect of Filtering on Signatures

In a previous section, it was shown that the signature is related to the amplitude spectrum of the time history and is given by equation (15) as

$$\delta(\tau) = \frac{Y_S}{A^*} \sum_{m=0}^M A_m \cos \frac{m\pi\tau}{T} \quad (20)$$

Some simple but illustrative cases can be given. First, if the time history is a cosine wave (or a sine wave, since the phase angles do not influence the signature) such that a single coefficient A_p is nonzero and equals 1.0, the signature is, simply,

$$\delta(\tau) = y_s \cos \frac{p\pi\tau}{T}$$

A second useful example is when the time history is white noise. Then, all the A_m 's have the same value and the signature is

$$\delta(\tau) = \lim_{M \rightarrow \infty} \frac{y_s}{M+1} \sum_{m=0}^M \cos \frac{m\pi\tau}{T}$$

which describes a unit impulse function at $\tau = 0$. Practical cases generally fall in between these extremes of an undamped cosine wave and an impulse function because the amplitude spectrum of a physical system subjected to some random excitation has a finite bandwidth. In addition, filters are usually used to exclude unwanted frequencies so it is important to know the effect of filtering on signatures. The error for a single-degree-of-freedom system caused by various R-c filters is discussed in reference 5. It is also useful to study the signatures of filtered white noise. This can be done easily using equation (20). Figure 8 shows the signature of white noise subjected to an ideal low-pass filter. For this case, equation (20) gives

$$\delta(\tau) = \frac{y_s}{(M_1 + 1)} \sum_{m=0}^{M_1} \cos \frac{m\pi\tau}{T} \quad (21)$$

Equation (21) can be summed to give

$$\delta(\tau) = \frac{y_s}{(M_1 + 1)} \left[1 + \cos(M_1 + 1) \frac{\pi\tau}{2T} \sin M_1 \frac{\pi\tau}{2T} \operatorname{cosec} \frac{\pi\tau}{2T} \right] \quad (22)$$

It is seen that $\delta(T/M_1) = 0$ where $\tau = T/M_1$ is the first zero crossing and also one-half the period of the filter cutoff frequency.

Figure 9 shows the signature of white noise subjected to a bandpass filter. The solid line is the signature, obtained from the digital computer program, of the time history generated by the relation

$$y(t) = \frac{1}{(M_1 + 1)} \sum_{m=M_0}^{M_1} \sin \left(\frac{m\pi\tau}{T} + \phi_m \right)$$

or, in digital form

$$y(i) = \frac{1}{(M_1 + 1)} \sum_{m=M_0}^{M_1} \sin \left(\frac{m\pi i}{I} + \phi_m \right), \quad i = 0, 1, 2, \dots, I$$

where the phase angles ϕ_m were a series of random numbers. And,

$$M_0 = 200$$

$$M_1 = 600$$

$$I = 4098$$

The points are calculated from equation (20). The differences are seen to be of the size predicted by equation (19).

Often, a time history is filtered before a signature is obtained. The purpose usually is to accent certain modes of the system by excluding frequencies outside the range of interest. However, filtering changes the apparent system characteristics and it is important to be aware of the limitation and trade-offs involved.

The bandpass filtering of the two-degree-of-freedom model response to white noise can be considered conceptually. Starting with a filter bandwidth wide enough to include both natural frequencies, the results of reference 5 can be applied. A rule-of-thumb is that the change induced in the signature by a filter will be insignificant if the low-pass setting is at least twice the higher natural frequency and the high-pass setting is less than one-quarter the lower frequency. These limits are relatively independent of damping. As the bandwidth narrows, however, the signature becomes dependent of the filter settings and the filter roll-off characteristics. If the settings are centered on one natural frequency, that frequency will dominate the signature as the bandwidth is narrowed

to exclude the other natural frequency and the signature will appear to represent a single mode. However, if the two natural frequencies are close together, say less than an octave separation, the resulting signature will not represent the response of a single mode of the system but will also reflect the damping of the other mode and the filter settings and characteristics.

In the limit, as the bandwidth of the filter decreases to a single frequency component (assuming an ideal filter and a finite record length), the signature becomes a single cosine wave with the frequency of the filter setting. This signature contains only the information that the time history includes that frequency component. Therefore, a trade-off exists between filter bandwidth and useful information. If no filter is used (i.e., an infinitely wide bandwidth), all of the characteristics of the system are contained in the signature but those of interest may be masked by extraneous information. As the bandwidth is narrowed to accent certain properties, more information is excluded until the bandwidth becomes so narrow that all useful information is excluded. Obviously, the optimum bandwidth will depend on the information desired and has to be determined for each type of application. For applications where the properties of a structure are desired (say, damping) the filter bandwidth has to be wide enough to avoid having the filter characteristics influence the value of the damping measurement. However, for flaw detection, where a comparison of signatures is used, it is not as important to avoid the filter effects of a narrow bandwidth if the same filter characteristics and settings are used for all signatures to be compared.

FIELD STUDY

In the following section, a discussion is first given on operational procedures for measuring vibration records in the field. The results of the studies on individual bridges are then given. Based on analytical and field results, it appeared possible to determine the distance to flaws. Although not one of the original objectives, this important feature was briefly explored and is discussed at the end of this section.

Operational Procedures

The operational procedures for obtaining good data can no doubt still be improved but, based on the present state of knowledge, the following

guidelines are given. The guidelines encompass the entire process from the instrumentation of the bridge to the interpretation of signatures.

Installation of accelerometers - The location of accelerometers relative to likely crack sites has not been well established. Based on the present state of knowledge, however, the maximum distance at which small crack growth, say, a 1 cm. change in length, can be detected is about a meter which means that a single transducer location will effectively monitor a particular joint or localized region in a structure.

The method used to mount accelerometers will depend somewhat on the particular manufacturer and the application and frequency range of interest. In general, careful experimental procedures must be maintained, especially in the harsh field environment, to obtain repeatable data. Particular things to avoid are dirty, loose, or faulty electrical connections.

Some flexibility of mounting technique exists depending on the frequencies being monitored. For frequencies less than about 1500 Hz, the accelerometer can be attached with two sided tape provided good bond to the surface exists, as well as both metallic and nonmetallic (nylon, etc.) cementing studs. For frequencies in the range of 10 KHz, aluminum, steel, or equivalent, cementing studs must be used and a lubricant should be used between the accelerometer and stud. For frequencies higher than 10 KHz, a wrench should be used to tighten the accelerometer beyond finger tightness. In this study, aluminum and steel studs were glued to the structures with epoxy. Studs that are threaded into the structure should not be used primarily because the drilling of holes into the structure may provide sites for future fatigue crack initiation.

Excitation - In most cases, the best excitation to provide records for analysis are the in-service loads of traffic. This provides a distributed input and loads the structure in the manner that will eventually cause the suspected flaws. If traffic is not used, then the normal live load on the localized region being monitored should be statically simulated during the application of the excitation. Examples of other forms of excitation that can be used are sandpaper, for individual components; a dolly with steel wheels; acoustic sources, such as nearby traffic or wind; tapping or dynamic shakers. The main requirement is that the excitation provides a random input that has sufficient level over the frequency range of interest and excites the flaw regions.

Record lengths - To achieve good signature repeatability, 2000 segments of the time history are usually adequate and it would be extremely rare to require over 4000 segments. One factor that should be kept in mind is that the record should contain a representative sample of the input. For example, if 2000 segments could be obtained while a single vehicle passed over a long structure, the signature obtained with a large truck providing the excitation might be different from the signature obtained with a small car. Vehicles so different may produce vibrations with different frequency characteristics. Usually, however, a record should contain 50 to 100 vehicles so a representative sample of traffic is obtained.

Assuming the number of segments and the desired length of the signature is known, one can determine the length of record needed. Obviously, this length does not include the time periods when the vibration is below the bias level and no sampling occurs.

Filter settings - The purpose of filtering a time history before Randomdec analysis is performed is to view the record through a window in the frequency plane which isolates a frequency bandwidth containing useful information and eliminates unwanted frequency components such as accelerometer resonances or electronic noise. The location and width of this window in the frequency spectrum depends on the type of flaw under scrutiny and the characteristics of the structure and excitation. The center frequency must be one affected by flaws and the bandwidth must include resonant peaks of the structure except when the flaw will introduce a resonant peak. The bandwidth should be sufficiently wide to avoid having the filter characteristics dominate the signature. A bandwidth at least equal to the lower filter setting (say, 400-800 Hz, 10-20 KHz, etc.) is a reasonable choice.

The relation between flaw type and frequency bandwidth is not sufficiently understood to outline a specific procedure for determining filter settings for a particular flaw. It is currently a trial and error procedure where different settings are tried until a bandwidth that produces a signature with "character" is found. For flaws in early stages of growth, the higher ranges of frequency produced by traffic are appropriate.

Hardware configurations - The hardware specifications for components such as accelerometers and amplifiers will be determined by the required

frequencies and level of vibration present in the particular application. The system used in this study (see fig. 10) has had more than adequate sensitivity and sufficient frequency response for all applications considered.

There is an order of magnitude difference in price between instrumentation and audio tape recorders. Comparison of results show that a good quality audio recorder operating in the direct record mode with frequency response of about 50- to 18,000 Hz is adequate for good results. Frequency response beyond these limits, requiring the versatility of an instrumentation recorder, would rarely be required in bridge work.

In this program, data tapes were analyzed on NEAR's Randomdec Computer, a special purpose hybrid system. A general purpose digital computer can be programmed to obtain signatures from the recorded data. However, this procedure requires the data to be digitized and in study programs such as this, where a large number of signatures are obtained, the turn-around time can be prohibitive.

Calibration - Since malfunctions in equipment components such as test machines, accelerometer mountings, and tape recorders may cause signature changes which could be interpreted as failures, a calibration test on a standard specimen should be made periodically to test the overall system. For example, a test block of metal, such as a piece of a beam, with a permanent accelerometer mounting could be excited with sandpaper and the signature obtained. Comparison of this signature with previous ones would show the overall accuracy of the system.

Interpretation of signatures - Presently, signatures are compared and differences are detected visually. Although this is a qualitative technique, it works well for research purposes. A quantitative method that has been used to obtain a numerical difference between signatures is to superpose signatures and to measure the separation between the signatures at each peak and valley. These distances are then added to obtain a single number. This is a simplified form of integrating the difference of the signatures. This technique can be used to rate relative differences between signatures of the same length and frequency characteristics. However, a single number difference provides no information on the cause of change. It may be important to know if the difference was caused by a shift in frequency, change in damping or an additional frequency.

It is conceived that for flaw detection a standard signature envelope will be established for a given location. This envelope will include the small variations in repeatability. A future signature that falls outside the envelope at one or more points would be cause for alarm. This comparison could easily be automated into a go or no-go evaluation. A trade-off will exist as to the number of false alarms versus the number of undetected flaws. The number of undetected flaws can be reduced by narrowing the standard envelope which, in turn, will increase the number of false alarms. However, as experience with signature interpretation continues, a catalogue of flaw characteristics will develop that identifies causes of particular signature changes and thereby reduce the number of false alarms.

85-101 Separation Bridge

This bridge is the same one studied in reference 4 and is shown in figure 11. It is a typical welded steel girder overcrossing consisting of five simple spans with four girders in each span and of noncomposite construction. The following variables were studied on this bridge.

1. Similarity and dependency of signatures obtained from different girders.
2. Repeatability of signatures over intervening time period between reference 4 and present study.
3. Suitability of less expensive direct-record tape recorders as opposed to FM systems.

To obtain the desired data, two girders of 2 meter depth in an end span of 17 meters were instrumented at a total of eight stations as shown in figure 12 and Table 1. Stations 1A, 3A, and 4A were placed at the same locations as stations 3, 6, and 5 respectively of reference 4.

Figure 13 shows signatures of the four stations on girder A and figure 14 shows those on girder B. Comparison of corresponding station numbers shows that the signatures are different and that standard signatures would have to be obtained for each girder. One physical difference between the girders is that the roadway is curved, although the girders are straight, so some difference in loading on the girders would be expected.

Figure 15 shows a cross-Randomdec signature of station 1B triggered on station 1A. The signatures are seen to be nearly independent thus indicating that flaws detected at a given location could be assumed to be located on that girder.

In figure 16 the signatures at stations 1A, 3A, and 4A are compared with the corresponding signatures given in reference 4. The signatures in reference 4 had a length of 0.010 seconds which can be compared to the first 0.010 seconds of the present signatures which are 0.0125 second long. The repeatability is good at these stations and covers a period of 20 months. The repeatability remained good despite the use of different instrumentation and replacement of mounting studs. A less expensive direct-record machine was used in the present study and proved to be satisfactory in the kilohertz frequency range. If the lower modes of a bridge were to be monitored at frequencies less than, say, 100 Hz, an FM recorder would be required.

Signal Bridge

The Signal Bridge is a structure about two years old over the roadway at the Toll Plaza of the San Francisco Bay Bridge. It has a span of about 60 m. and consists of two parallel Warren truss structures with a walkway between them as shown in figure 17. The bridge carries no traffic but is a supporting structure for signal lights. Nevertheless, the all-welded, lightly damped structure is excited by wind and the traffic passing below to produce a low-level vibration. It was observed that the excitation from the wind in the frequency range of interest was insignificant compared to that from the traffic and that small cars and motorcycles with loud mufflers can induce about the same level of vibration as induced by trucks.

It was of interest to see if this low-level vibration was suitable for flaw detection on this type of bridge. Also the joints of the structure fall into characteristic groups with each group on each of the four chords having identical construction details. For example, all of the joints on the lower west chord are of the type shown in figure 17. Some variation from the distribution of signal lights on the east chords existed but the structure presented a good opportunity to test if signatures of acceptable components were similar enough to allow the detection of a defective component by a one-time comparison of signatures. This capability would be very useful in finding initial flaws in new structures.

At each of the joints monitored, signatures were obtained from two symmetric stations as shown in figure 17. The joints studied can be divided into three characteristic groups; the lower west chord, the lower east chord which supported the signal lights and the upper west diagonal members. Although each group had somewhat different signatures, a surprising similarity existed between all of the signatures. In figure 18, examples of the lower west chord are shown. The largest difference is seen in the signature at location 16 b. Within the limits of visual inspection, this joint showed no irregularities but a close inspection of this joint and other joints with differences would be useful for correlating cause and effect. Figure 19 shows signatures from the east lower chord and the upper chord. The signatures of the upper diagonal members have a higher frequency than the other joints.

There is enough similarity between these signatures to allow the inspection of a bridge of this type where signatures of similar joints are compared and flaws detected without having to monitor over a period of time.

The excitation level is substantially below that from a bridge carrying traffic but should be sufficient for detecting serious flaws. This low level of vibration may require more sensitive equipment to detect small flaws. Also, the frequency content in the response is adequate up to about 2 KHz but small flaws would no doubt require higher frequencies. Artificial excitation, properly applied, could be used to increase both the level and the frequency range.

West Carquinez Bridge

The twin bridges that carry traffic over the Carquinez straits appear similar in overall configuration but are very different in design detail. Both, shown in figure 20, have a total span of about 1100 m. with two central spans suspended between cantilever arms. However, the old (West) Carquinez bridge is about 50 years old with compression truss members mainly of riveted, built-up construction and tension members in the form of eyebars (a member of rectangular cross section supported on a pin which passes through a hole at each enlarged end). The East Carquinez Bridge is about 20 years old with all welded box members and bolted joints. The work done on this latter bridge was concerned with flaw simulation and is discussed in another section.

On the West Carquinez, the eyebars have been of serious concern to engineers of the Bay Toll Administration of the State of California because a crack in a similar member caused the destruction of the Point Pleasant Bridge in West Virginia. With their cooperation, NEAR instituted a program under this contract to determine the applicability of Randomdec analysis to this problem. At the beginning of the program, the State of California closed the bridge to traffic to remove two eyebars (fig. 21) for metallurgical studies, replace those eyebars and to add additional bars at other locations where only two bars comprised the member. This study was not completed until after the end of the field work on the NEAR program so the bridge could not be monitored under traffic. Vibration records were obtained by tapping with a metal tool on the eyebar pins. Since an impulse contains a wide band of frequencies, the excitation can be considered, to some degree, as random localized excitation. However, this excitation does not simulate traffic and conclusions, therefore, may not apply to traffic conditions.

The first study done on the bridge was to monitor the two eyebars which were to be replaced (Bar No. 10, North and South in fig. 22) and the two adjoining members (Bars 8 and 9 in fig. 22) before the removal, before replacement, and after replacement. An array of ten eyebars formed the entire truss member. The outside eyebar, Bar No. 10, was removed by heating it until it slipped off the pin and a new bar was installed at both locations. Figure 22, which is typical of both locations, shows the joint details and the accelerometer stations.

The signatures of Bar No. 10 at both locations are shown in figure 23. In signatures 1 to 4, the new bars are seen to have different signatures from the old bars and in each case have a higher frequency. Signatures 5 and 6 show superpositions of the old bars and the new bars respectively. The old bars show similar frequency content as do the new bars but differences between bars at symmetric locations in the bridge (i.e., north and south locations) are significant.

The signatures of Bars 9 and 8 adjoining Bar 10 at the south location are shown in figures 24 and 25 respectively, and those at the north location are shown in figures 26 and 27. Changes in Bars 8 and 9 due to the removal of Bar 10 indicate the signatures of the different eyebars are interdependent. After the replacement of Bar 10, Bar 9 (which is next to Bar 10) shows an increase of about 7 percent in frequency at each location. Bar 8 (figs. 25 and 27) shows little or no change in

frequency at each location and shows very little change in shape at the north location. The fact that these bars, after the replacement, did not return to their conditions existing before the removal may be due to stress effects. The member strains were monitored by engineers of the State of California and it was determined that the loads did not return to their original values. It was felt that the bracing between the two sides of the bridge transferred some of the load during the removal process.

Each suspended span on the old Carquinez is supported at each corner by a group of four hanger eyebars as shown in figure 28. The two groups at the north end of the south suspended span were monitored to determine the repeatability with time and the similarity between eyebars. Inspection of typical joints involving several eyebars usually showed that few eyebars in the group have the same physical constraints. For example, the inner and outer bars are constrained by the nut on the outside surfaces and a spacer on the inside, whereas the interior bars have spacers on both sides. Also some of the rivet heads on the connecting member contact the surface of the outside eyebars. The excitation in this case could affect the signature of different eyebars. Since it was applied at one location, on the end of the pin, the modes that are excited in different eyebars may depend on where the eybar is located on the pin.

The signatures of the west group over a period of three months are shown in figures 29 through 32. The repeatability of each station is not particularly good although each eybar appears to have a characteristic shape. These signatures contain sufficiently high frequencies (15-20 KHz) to be sensitive to such things as accelerometer tightness so more careful installation procedures might improve this repeatability. To see if the characteristic shape is related to the position of the individual bar in the group, signatures for the group on the east side of the bridge were obtained. These are shown in figure 33 and comparison with figures 29 through 32 show definite similarities between corresponding eyebars. Therefore, there is more similarity between corresponding eyebars of different groups than eyebars of the same group. One distinctive similarity between all of the hanger bars is the negative peak at $\tau = 0.00022$ seconds of each signature. However, the differences are enough to prevent the use of signatures for detecting a faulty member by comparing its signature to a "standard" obtained from a group of undamaged members. This problem should be studied using traffic as the source of excitation

since it should tend to average out many effects and provide better repeatability than the localized input.

The eyobar is locally a very stiff member near the pin hole at the ends and therefore, has high resonant frequencies. This means that high frequencies (say, greater than 10 KHz) are probably needed to excite modes that would reveal a crack near the pin. Work should be done to determine if traffic provides excitation with sufficient high frequency content to detect cracks.

Missouri Bridge

A destructive dynamic test of a bridge removed from service in Missouri was conducted by faculty members of the University of Missouri under Missouri Research Study No. 73-1, An Investigation of the Behavior of a Three-Span Composite Highway Bridge - Phase II. Reference 8 is a preliminary study of this project. During their test program, vibration records were recorded by NEAR for Randomdec analysis. A brief description of the overall test program and the Randomdec results are given here.

The bridge that was tested is shown in figure 34. It is a three-span continuous girder bridge. The four longitudinal girders have welded cover plates over the two interior supports and bolted field splices at the inflection points in the end spans.

The primary objectives of the overall program were to determine the fatigue life of the bridge and to compare the results with the AASHTO specifications; to determine whether bridge properties are significantly altered by cumulative damage; and to investigate methods of detecting fatigue cracks. The dynamic excitation was provided by an electro-hydraulic actuator which sinusoidally drove the bridge at its 2 Hz fundamental resonance. The actuator was located on the deck at midspan and induced a peak-to-peak amplitude of about 7.5 cm. Dead load ballast loading of 40 kips was applied in each span to reduce the maximum tensile strain in the concrete deck caused by the inertial load. This ballast is seen in the foreground of figure 35 with the actuator at midspan.

A preliminary study in reference 8 indicated that critical locations for fatigue cracks were at the ends of the cover plates in the end spans in the top and bottom flanges. The shear connectors embedded in the concrete deck on the top flange were also considered susceptible to fatigue. These locations were considered critical because of the stress

range imposed by the dynamic response of the bridge to the 2 Hz cyclic loading. Before the test began, an extensive inspection of these locations was made visually and with the aid of ultrasonics and radiograms to ensure that no cracks were present. After the cyclic loading began, the methods used to monitor the growth of cracks included Acoustic Emissions, the Acoustic Crack Detector, ultrasonic equipment, strain measurements, mode shape measurements, and penetrant dye.

Surface cracks in the bottom flange could be monitored visually and with penetrant dyes. During the test, cracks were observed at every location on the bottom flange in the fillet weld material and, at several locations, were observed to penetrate into the base material of the girder flange. Figure 36 shows photographs of cracks in the bottom flange and Table 2 shows pictorially the cracks that were observed and dimensions of crack lengths in the base metal. Internal cracks or cracks under the coverplates could not be directly observed.

The top flange was embedded in the concrete deck so its upper surface which included the weld region around the coverplate and the shear connectors could not be observed. No cracks were observed on the bottom surface of the top flange. From this, it is apparent that the true and complete crack history during the test is not known. This points out the difficulty of this type of test where detection methods under development are being evaluated on the one hand but the true crack history of the bridge on the other hand is unknown since practical, proven detection techniques are not currently available. The results of the Randomdec study are given below with the expectation that more definitive conclusions can be drawn after all the methods have been correlated.

For the NEAR study, separate accelerometer records of the high frequency (kilohertz range) response of the bridge were obtained at intervals throughout the duration of the test. The bridge was instrumented at the 16 locations considered to be the most probable crack locations with a total of 24 accelerometer stations. A layout of the stations is shown in figure 37. Two stations were positioned at each bottom flange location and one station was positioned at each top flange location as shown.

Two types of excitation were used to obtain high-frequency records. A steel-wheeled dolly (weighing about 900 N or 200 lbs) was used in the beginning and at the end of the program. Ballast loading was removed and the actuator was turned off while the dolly was pulled across the

bridge with a forklift. It provided good high frequency excitation but little low frequency excitation or live load on the bridge. Midway through the program, the inspection periods were reduced in number so records were obtained while the actuator was exciting the bridge at its 2 Hertz fundamental resonance. The excitation in this case consisted of very large low frequency motion (7.5 cm. peak-to-peak in the fundamental mode) along with high frequencies generated, most likely, by the frictional forces in the cracked concrete deck, girder joints, and broken guard rail. These two methods of producing vibration represented rather extreme types of excitation in that the dolly did not produce any appreciable live load on the bridge whereas the actuator produced inertial forces at the 2 Hz resonance that far exceeded any normal live load. This resulted in the two methods producing a fundamentally different state of stress in the girders when the records were obtained. Traffic would produce excitation somewhere between the two methods used. The results of each method of excitation are discussed below.

Signatures from dolly excitation - In order to apply the dolly excitation, the actuator was turned off and the ballast loading removed. Under these conditions, the top flange was in a state of tension of about 4,200 N/cm² (6,000 psi) which facilitated the detection of structural changes. The signatures of the top flange stations are shown in figures 38 through 46. The results show changes at all stations with similar changes occurring at several stations. Stations 3, 9, and 24 (figs. 38, 40, and 46) all show similar changes and, at the end of the test, appear to be in the same condition. The gradual development of the high frequency component indicates some gradual change taking place rather than a sudden failure. Stations 6, 18, and possibly 15 (figs. 39, 44, and 43) have undergone a similar but more severe change than stations 3, 9, and 24. It appears as if some component became free to vibrate at its resonance.

Station 12, figure 41, has a different signature from the others in this group and the jagged peaks at 95,000 fatigue cycles indicate higher frequencies are involved. Figure 42 shows a higher filter setting for this data and clearly shows most of the change occurred between 0 and 95,000 cycles with little change occurring after that.

Figure 45 shows the results for station 21 which experienced the most significant change of any of the top flange stations. The dramatic change in the signature between 95,000 and 377,000 cycles indicates that

a substantial change occurred in the region near the transducer. Some possible failures are fatigue cracks in the coverplate region, failure of shear connectors and bond failures between the steel and concrete.

In the bottom flange, without the actuator inertial loads or the ballast loads, the critical region was under compressive stress of about $5,000 \text{ N/cm}^2$ (7,000 psi). Large residual tensile stresses commonly exist in localized zones around welds. Cracks in the weld zones at the coverplates would, therefore, be in a tension field. As the cracks propagate into the base metal, they eventually reach the compressive zone.

The signature of the lower flange under the dolly excitation show evidence of detecting cracks within the weld zone. Figures 47 through 54 show comparisons of signatures of stations that are 15 and 60 cm. away from the ends of the cover plates. On the average, the stations nearest the cracks show more change than those further away. To see this, the difference between the peaks and valleys of two superposed signatures was accumulatively measured. The results are shown in Table 2 where the numbers are a relative measure of the amount of difference between signatures. The near and far stations are each summed and the totals are given in the right column. The near stations have about twice the change as the far stations between signatures taken at 0 and 95,000 fatigue cycles. The amount of change drops on the average between 95,000 and 377,000 cycles which may indicate cracks are more difficult to detect outside the residual tension zone. Some cracks were observed to have propagated into the base metal between 95,000 and 377,000 cycles. Figure 50 shows stations 10 and 11 near the location with the largest observed crack in base material. The crack growth, shown in Table 3, that occurred between 95,000 and 377,000 cycles went undetected as seen in figure 50. One must conclude from this that cracks subjected to compressive stress during the recording of the vibration can escape detection.

Signatures from actuator excitation - The very large motions induced by the actuator caused many failures besides the fatigue cracks. The concrete deck cracked through its entire depth about every 30 cm, the heavy steel channel which served as a guard rail sheared the bolts holding it to the structure and there was visible noncomposite slippage between the girder and the deck at several locations. These large amplitudes suggest considerable nonlinear behavior that was not present with the dolly excitation. This was checked by analyzing the same segment of time history

at different bias levels as shown in figure 55. The bias level of the second signature is about five times the level of the first so only large amplitude motions are included in the second signature. For linear systems, since the initial amplitudes are normalized to the same value, the two signatures would be the same. However, the comparison in figure 55 shows that the two signatures are quite different and, therefore, strong non-linear effects are present. This points out the importance of using the same bias levels on signatures to be compared for detection of flaws. This was possible here because the amplitude of the 2 Hz vibration was maintained at a constant level.

The repeatability of signatures was checked as shown in figure 56. Records only 1,000 fatigue cycles apart (to minimize the amount of structural change taking place) were analyzed and are seen to be quite similar.

Station 10 was frequently monitored since it was near the largest observed cracks. This station showed no crack growth between 95,000 and 377,000 cycles with the dolly excitation. The signatures while the actuator was on are shown in figure 57. A large change is apparent between the first two signatures but a decreasing amount of change occurs until very little difference exists between 360,000 and 365,000 fatigue cycles. This corresponds to the observed crack growth which, in fact, ceased at 360,000 cycles. At this stage the crack had grown through the thickness of the flange and further growth was not apparent.

The last signature on figure 57 is entirely different from the rest and shows the detection of a failure that appeared intermittently at most locations. It appears to be a metal-on-metal slippage and is really a "squeak" that occurs for a short portion of each cycle and appears in the time history as a short burst of almost pure sinusoidal motion. Close to each location is a bolted splice joint in the girder. Under dead load this is located at an inflection point so the bending moment would normally be zero. However, the maximum dynamic bending moment in the end span occurs at this location (ref. 8) so the bolted joint is heavily loaded each cycle when the amplitude is maximum. Slippage may occur in this joint under certain conditions and produce the squeak. Another source may be slippage of the girders on their supports. If the squeak contains sufficient energy and its frequency is within the bandwidth of interest, it can mask the effect of cracks. This is the case in figure 57. Since this type of failure is not of interest here, signatures which contain such results have not been evaluated. Station 11 is 60 cm further from

the crack than station 10 but signature changes are apparent as seen in figure 58.

The signatures of the remaining stations are given in figures 59 through 67. Figures 59 and 60 show major changes in the signatures for stations 1 and 2. Table 2 shows that no visible crack growth occurred during this time. If no crack growth has occurred (say, under the cover-plate or internally), then these changes represent a false alarm caused by a presently unknown source. At other stations, cracks are present and changes exist in the signatures, but of particular interest are cases where substantial crack growth in the base metal occurred during the time the shaker was used for excitation (say, after 245,000 cycles). In Table 2, it is seen that in addition to station 10, the crack near station 19 grew about 0.8 cm (0.3 in) between 287,000 and 347,000 cycles. The signatures of station 19 in figure 65 show a drastic change between 278,000 and 320,000 cycles. Station 20, 60 cm further from the crack, shows changes in figure 66 but they are not as significant as station 19.

Another important observation is that the dolly excitation showed station 21 undergoing a unique and large change between 95,000 and 377,000 cycles (fig. 45). This is also apparent in figure 67 where a severe change occurred between 279,000 and 302,000 cycles. It appears, therefore, that a failure occurred, perhaps suddenly, between 279,000 and 302,000 cycles.

The failure that ended the testing of the bridge was the fracture at about 375,000 cycles of girder No. 2 at its midpoint in the center span under the actuator. The failure in the girder web is shown in figure 68 and the crack shown in the web extended upward to the top flange. The failure was apparently heard but the actual crack was not discovered until several minutes of fatigue testing had elapsed. The only visible effect on the dynamic motion was some torsion of the bridge due to the resulting asymmetric stiffness of the structure.

This failure mode was unexpected. Cracks formed as expected at the critical locations on the outer spans. These did not grow as rapidly as expected, and in some cases ceased to grow, probably because the dead load placed the crack regions in compression much of the time. The girder in the center span apparently suffered a premature failure at its center, since there was no indication of any fatigue cracks in the other three girders, and the predicted fatigue life was considerably in excess of the actual failure time. The midpoint was under large tensile stress which,

no doubt, led to a rapid crack growth and subsequent failure. The mid-point was not considered a critical location so no accelerometers were installed closeby. Stations 19, 20, and 21 were at one end of this girder and stations 7, 8, and 9 were at the other. It is improbable that these signatures would be influenced by a failure at midspan because the failure was about 23 m (75 ft) away from the accelerometer stations and the vibration at a point that far away would be quite independent in the high frequency range considered in these measurements. The effect of a change at one point would be averaged out at the other point. In order to detect this failure from such a long distance, one should monitor the low frequency modes of the girder. The recorder used could only record down to about 70 Hz which is probably not low enough. Also, the accuracy of a signature depends on the number of cycles of data recorded. The length of the time histories recorded were determined on the basis of the frequencies of interest being in the kilohertz range and, therefore, were an order of magnitude too short for accurate analysis of data below 100 Hz.

Simulation of Flaws

Because actual flaws in the Bay Area bridges studied in this program were not apparent, the simulation of flaws was attempted. It proved to be quite difficult to introduce an external effect that would change the signature, because an external signal that is unrelated to the vibration at the transducer location will average out and not affect the signature. However, a device that did yield useful results was used on the East Carquinez Bridge. In addition, a test was conducted at the Ames Research Center on a beam in which a sawcut was introduced and signatures obtained for different lengths of cut. These results are discussed here. This work and other results from the analytical study and field study indicated the possibility of determining the distance to a flaw. This useful capability was explored and these results from the viewpoint of locating cracks are discussed in a separate section.

East Carquinez Bridge - The device used to simulate a flaw on the East Carquinez Bridge produced a local constraint that prevented motion at a point on the girder. A crack allows additional freedom of motion at a point because of the free crack surface. These two effects are opposite in nature but should display the same characteristics concerning

the magnitude of effect versus distance from the flaw. A crack also can produce signals from rubbing of the crack surfaces. This effect was not simulated. The device was simply a bolt that could be adjusted to contact the web of a vertical I beam as shown in figure 69. Records were obtained with and without contact of the bolt on the web while the bridge was under normal traffic.

Figures 70 through 74 show the signatures of the five accelerometers and the comparison of the signatures. Tests 1 and 2 show the effects of the flaw and tests 1 and 3 show the repeatability of the standards which is seen to be very good at all five stations. The signatures were taken over a period of hours so small differences can be attributed to the effect of the simulated flaw. A large change in the first cycle is seen at station 1 in figure 70 which is nearest the flaw. Changes are apparent at all other stations but in a decreasing amount as the distance from the flaw increases. One concludes that this flaw was detected at a distance of about a meter.

Sawcuts in a laboratory beam - A simple test was run in the laboratory to simulate the localized vibration effect of a crack in a beam by introducing a sawcut. The test configuration is shown in figure 75. A sawcut is similar to a crack except the surfaces are not in contact. The local resonance effect should, therefore, be adequately simulated by the sawcut. In this test, three levels of input were used and readings at two locations were obtained. The signatures for the lowest level of excitation are shown in figures 76 through 79. The lowest level was significantly below the level measured on most bridges although the frequency content was more concentrated in the high range as seen in figure 75.

Figure 76 shows the signatures for station I which was 15 cm from the flaw. The top graph shows the repeatability of the standard and the other graphs show the changes for the different size of sawcuts. Corresponding signatures for station 2, 75 cm from the flaw, are shown in figure 77. To clearly see the differences, the signatures are superposed in figures 78 and 79. It is seen that the 0.6 cm cut is barely detected at station I and is not detected at station 2. The 1.2 cm cut produces small changes at both stations and the larger cuts produce drastic changes. There was no significant change in these results with increases in the level of vibration. This is to be expected since the behavior should remain linear. An actual crack, however, may produce nonlinear effects dependent on

amplitude. These results substantiate the conclusion that crack growth on the order of 1 cm can be detected at distances up to about 1 meter. Crack growth of more than 2.5 cm is detectable at greater distances since the degradation of signature change is small between 15 and 75 cm.

Location of Flaws

In the analytical study, the signature of an acceleration time history of a linear multi-degree-of-freedom system was shown to have the same shape as the free vibration displacement response to the initial condition of all points except the accelerometer station having zero displacement and zero velocity and the station having an initial displacement. When such a system is released, no effect of a flaw is felt at the station until a wave (bending wave in most applications) travels from the station, reflects off the flaw and returns to the station. A difference between signatures with and without a flaw, therefore, would not appear in the signature until the travel time to and from the flaw had elapsed. By measuring the time to this change in the signature and knowing the wave speed, the distance to the flaw could presumably be calculated. In actual practice, since all modes of the structure are not excited and the record is filtered, the actual signature is something between an acceleration and a displacement signature. This allows the possibility of changes in the signature occurring sooner although these changes, hopefully, will be small. In order to convert the time of the first significant change to a distance to the flaw the wave speed must be known. The speed of bending waves depends on the frequency which complicates the problem. However, to see if this scheme to locate flaws is feasible, a very simplified analysis can be used to find the order of magnitude of bending wave velocities. These wave speeds can then compare to values from the field measurements calculated on the assumption that the time to the first significant change is indeed related to the distance to the flaw.

Consider a beam typical of a narrow strip of material between the station and flaw, with a sinusoidal wave train traveling down it. This neglects the effect of cylindrical waves propagating in a plate. The well-known beam equation is

$$\frac{\partial^4 y}{\partial x^4} + \lambda^2 \frac{\partial^2 y}{\partial t^2} = 0$$

Take the initial and boundary condition as

$$t = 0 , y = A \sin \beta x$$

$$x = 0 , y = A \sin \omega t$$

Since we are only interested in an approximate wave speed, the beam is taken as semi-infinite in length to avoid having to consider reflections. Therefore, the beam at some instant $t = 0$ has a sinusoidal shape of wavelength $2\pi/\beta$ and one end at $x = 0$ oscillates sinusoidally at a frequency ω . An appropriate solution is

$$y = A \sin \lambda c(x + ct)$$

where

$$\lambda c = \beta , \lambda c^2 = \omega$$

Therefore, the wave speed c , is

$$c = \sqrt{\frac{\omega}{\lambda}}$$

and the wavelength which is consistent with ω is

$$\frac{1}{\beta} = \frac{1}{\sqrt{\omega\lambda}}$$

For a given signature, c can therefore be calculated since the frequency ω most predominant in a signature can be measured and the parameter λ can be calculated for a given member. This will now be applied to the field measurements.

East Carquinez Bridge signatures - Referring to figures 70 through 74, the time from the beginning of a signature to when a significant change occurs appears to depend on the distance between the station and bolt.

(At this stage of development, deciding what is a significant change is a matter of judgement and remains to be quantified.) Assuming, in figures 70 through 74 that τ_c denotes the time it takes a wave to travel from the transducer to the flaw and back, the wave speeds can be calculated since the distances between the stations and flaw are known. These are

Station	Distance cm	Time, τ_c sec	Wave Speed $2(\text{dist})/\tau_c$ m/sec	Wave Speed ft/sec
1	7.5	.0006	250	820
2	15	.0013	230	750
3	25	.0028	180	590
4	41	.0036	230	750
5	69	.0053	260	850

To calculate the expected wave speed in the I beams, λ is (for the web thickness of $h = 1.25$ cm)

$$\lambda^2 = \frac{12(0.0769)}{(1.25)^2 (20 \times 10^6) (386) (2.54)} = 0.30 \times 10^{-10} \frac{\text{sec}^2}{\text{cm}^4}$$

$$\lambda = 0.55 \times 10^{-5} \frac{\text{sec}}{\text{cm}^2} = 0.055 \frac{\text{sec}}{\text{m}^2}$$

The predominant frequency in these signatures is

$$f \approx \frac{14 \text{ peaks}}{0.02 \text{ sec}} = 700 \text{ Hz}$$

or

$$\omega = 700(2\pi) = 4,400 \text{ rad/sec}$$

The expected wave speed is

$$c = \sqrt{\frac{4,400}{0.055}} = 280 \frac{\text{m}}{\text{sec}}$$

This value is in the same range as those values measured from the signatures and shows that the theoretical value is similar to that obtained from the signature by assuming that the elapsed time to a signature change is related to the distance to the flaw.

The filter settings in figure 70 through 74 isolate frequencies that are quite low. An example of higher frequencies using the same simulation device is shown in figure 80. The wave speed is measured in figure 81 to be 720 m/sec. The dominant frequency in figure 80 is $f = 11.6$ peaks/ 0.0025 sec = 4,600 Hz. Using the previous analysis for this frequency, the wave speed is

$$c = \sqrt{\frac{4,600(6.28)}{0.055}} = 720 \text{ m/sec}$$

The exact agreement between the measured and calculated values is no doubt fortuitous but, again, shows the feasibility of locating flaws.

On the other hand, the results of the sawcut beam in figures are confusing from the viewpoint of locating cracks. At station 2, differences appear about the same time in the signatures as at station I. This suggests the change affects just a few modes and the signatures have the characteristics of displacement rather than acceleration.

Another factor to consider is that the signature depends on the location of a single point input (ref. 4) such as a shaker. For example, the location of the shaker may be on a node line of several modes which, therefore, will not be excited. Since the signature will change with changes in the location, it represents neither the acceleration nor the displacement signature of the beam itself but, rather, the signature of the beam with some degree of constraint at the input location. Whatever the reasons, this behavior has to be understood before the location of flaws will be possible.

West Carquinez Bridge - traveling waves - Some additional work to correlate the simple theory with experimental measurement of wave speed versus frequency was done on the eyebars of the old Carquinez Bridge. Two stations were established 1.52 m apart on an eyebar and excitation supplied at the end of the member. The Cross-Randomdec signatures were determined by obtaining the signature of the station nearest the excitation in a normal manner and simultaneously obtaining the signature of the

furthest station by starting each sample at the same time as the corresponding sample for the nearest station. A traveling wave that does not change shape will produce two signatures identical in shape except for a time lag. This time lag can be used to compute the wave speed. In the examples studied here, multiple frequencies are present and wave speed is dependent on frequency (dispersive waves) so the wave form will change as it moves along the member. However, an average value of wave speed can usually be estimated.

The first example, in figure 81, shows the actual time history at two stations. This was obtained by using a near-zero bias level and retaining only the first segment of the record. The eyebars were tapped near the end and the wave arrived at station 10 at $\tau = 0$ and at station 11 about 0.4 m/sec later. It is seen that the wave changes form as it travels down the bar. Taking the wave speed from the times of onset of vibration, one gets $c = 3,300$ m/sec. The calculated value is, for $h = 3.8$ cm, $c = 3,080$ m/sec where an approximate value of frequency was estimated by counting the peaks in the top signature (which has a narrow bandwidth) of figure 81 giving $f = 22.8/0.0025 = 9,100$ Hz.

Under continuous excitation where many samples are averaged, it may be difficult to determine a representative wave speed since the signature shape changes. Examples of how this might be done are shown in figure 82. Here, distinctive features of a signature are traced from station to station. In the top photo, a portion of the signature starting at $\tau = 0.00332$ sec, retains its shape but has a time lag of 0.00093 sec. Using this, the wave speed is $c = 1,640$ m/sec. In the lower photo, the sixteenth peak after the highest peak is used and $c = 2,340$ m/sec. Average values of frequencies for the two cases are 2,900 Hz and 4,300 Hz and the computed wave speed values are $c = 1,730$ m/sec and 2,100 m/sec which, again, are close to the measured values.

These examples show that wave speeds can be easily measured on a given member and this wave speed corresponds quite well to the simplified theoretical value. Once the local wave speed for a given signature frequency range has been determined, it could be used to determine the distance to a flaw detected at that location.

LABORATORY STUDY

A short laboratory study was undertaken to gain information on the sensitivity of signatures to fatigue cracks. The program consisted of cyclicly loading welded specimens to induce fatigue cracks and then recording vibration data at several stages of the fatigue loading for Randomdec analysis. The experimental work was conducted by Professors J. C. S. Yang and C. P. Heins and graduate student D. W. Caldwell at the University of Maryland. Magnetic tapes of the vibration records were sent to NEAR for analysis. A complete description of the test program, written by the above authors, is given in Appendix B.

Excitation of Specimens

Two types of specimens, one a fillet weldment and the other a butt weldment, were tested and are shown in figures 83 and 84. At different stages of crack growth, the vibration of the specimen was recorded while the specimen remained in the test machine under a static stress. The excitation induced by the machine through the grips was used as the source of vibration for most specimens. Preliminary study indicated that a relatively flat spectrum existed between 1 and 10 KHz. However, later analysis indicated that intermittent behavior of the testing machine components introduced strong sinusoidal signals which appeared in the signatures. This behavior, which was sometimes followed by actual component failure, often dominated the signature so considerable data had to be disregarded since machine failures were not of interest in this study.

The typical machine effect was the existence of a strong sinusoidal component (probably from the hydraulic valves) in the frequency bandwidth of interest. Figure 85 shows a set of signatures which occurred over the duration of several specimen tests. The emergence of the strong sine wave is apparent and signature no. 5 shows that the vibration has become purely sinusoidal in the frequency range below 3,200 Hz. After test no. 5 was recorded, a leak in the hydraulic system occurred and a valve was replaced. Signature no. 6 is after the repair and shows a form similar to no. 1 which is typical of wide band random vibration. The last signature is a Cross-Randomdec signature of the bottom accelerometer with the top one for test no. 5. The bottom one has the identical form except for a phase shift. This phase shift, since no damping is apparent, is indicative of traveling waves being introduced into one end of the specimen and taking a finite time to reach the other end. Assuming the bottom

accelerometer leads the top accelerometer (the motion is controlled through the lower grip) by less than one cycle, the wave speed is about 390 m/sec (1,280 ft/sec). This speed is typical of that for bending waves in this frequency range and specimen size.

Toward the end of the program, new grips for the machine were installed and these reduced the transfer of machine vibrations to the specimen. For random excitation, specimen no. 7 was rubbed with No. 400 sandpaper which provided an order of magnitude higher level of vibration.

Crack Histories

The crack histories of the specimens are shown in Table 4. It is seen in Table 4 that the crack growth and the number of cycles to initiate the crack varied over a large range for the different specimens. The results of each specimen are discussed below.

Specimen no. 1 - Figures 86 and 87 show results of specimen no. 1. In figure 86, the top accelerometer shows good repeatability in tests 1 to 3 but shows a change in test no. 4. Test no. 4 has the same number of fatigue cycles but is at a different stress level than test no. 3 so the effect as seen by the top accelerometer probably occurred before test no. 3 but only was detectable at the higher stress. The bottom accelerometer, in figure 87, showed a change in test no. 3 that was detected at both stress levels and continued to change in test no. 5. No cracks were visually detected at this stage but the specimen completely failed below the cover plate sometime later as shown in Table 4. It is highly probable that cracks existed prior to the complete failure and that the bottom accelerometer detected these more distinctly than the top accelerometer.

Specimen no. 2 - Figure 88 shows different frequency bandwidths of two tests on specimen no. 2 which are before and after a large crack was observed. The signature of the higher frequency range in test no. 1 shows an apparent machine effect but, nevertheless, the corresponding signature in test no. 2 shows an additional frequency component. This is clearly seen in the lower frequency bandwidth of test nos. 1 and 2. Test no 1, before the crack existed, shows no dominant frequency whereas test no 2 shows a component appearing after the crack was observed.

Specimen no. 3 - In reference 5, the minimum length of crack growth that appeared detectable was about 0.25 cm (0.1 in.). However, the level of excitation in those tests was higher than the level provided by the machine in the present tests. For these conditions, results for specimen no. 3 appear to give some indication of the minimum size that reliably can be detected. Figure 89 shows the signatures for specimen no. 3 where the crack was first observed between tests 2 and 3. Figure 90 shows these signatures superposed as noted. It is seen that changes were apparent before a crack of 0.25 cm (0.1 in.) was observed but the important point is that little change in signatures occurred between test nos. 3 and 4 when the crack grew 0.75 cm (0.3 in.) in length. This crack was not through the specimen so its depth was probably on the order of 0.25 cm (0.1 in.). If one were comparing test no. 4 with test no. 3, rather than test no. 4 with the standard of test no. 1, the crack could have escaped detection at this stage of growth and the low level of excitation.

Specimen no. 4 - Figures 91 and 92 show the effect of a large crack on the frequencies appearing in the signature. In figure 91, the first two signatures are similar. The third shows the effect of a 1.0 cm (0.4 in.) crack and the fourth is the signature after the crack has grown to 3.8 cm. It appears as if a low frequency component has been removed from the signature so lower filter settings were used to obtain figure 92. The frequency of the first three signatures is identical (although some differences in amplitude are apparent), but the fourth shows a large decrease in frequency which is indicative of a basic change in the system properties.

Specimen no. 5 - The effects of the variation in stress level on the signatures of a cracked specimen were included for the levels of 10,300 and 13,800 N/cm² for most specimens in this study. However, this range was extended on two specimens to see the degree to which the signatures varied with stress level. Figure 93 shows the result of a cracked specimen in which the first two signatures are for the crack condition shown in Table 4 and the last five signatures are for the enlarged crack condition at the given stress levels. The crack growth causes a change in the signatures but, also, the last five signatures show a change with stress level at the same crack configuration. The change is somewhat systematic in that the relative height of the first three peak changes uniformly as

the stress changes from 690 to 10,300 N/cm² (1,000 to 15,000 psi) but practically no change is apparent between 10,300 and 13,800 N/cm².

Specimen no. 6 - Although most of the data of the butt welded specimens were disregarded because of machine failure, one specimen yielded results which show the variation with stress level. Figure 94 shows the standards before cracking and are seen to be very repeatable as shown by the last signature in figure 94. Figure 95, similar to the results in figure 93 for the fillet welded specimen, shows a change in signature with stress level up to 10,300 N/cm², but the signatures become nearly the same for 10,300 and 13,800 N/cm². This dependence on stress level may mean that cracks are most easily detected at some given level.

Specimen no. 7 - Specimen no. 7 was excited with No. 400 sandpaper at the different stages of crack growth shown in Table 4. The signatures are shown in figure 96. A crack was not observed until test no. 5 but changes in the signatures occurred before this. Figure 97 shows a superposition of consecutive tests. Since the crack is close to the transducer (about 8 cm), changes should appear in the first few peaks of the signatures. There are some changes in the first two curves but a major one occurs in curve 3, comparing 15,000 and 211,000 cycles. Curve 5, comparing 414,000 and 444,000 cycles, shows a large change whereas curve 6 shows a relatively small change, although the change is primarily a shift in frequency which is more significant than the amplitude change in curve 1. The observed crack growth between test nos. 6 and 7, from Table 4, was 0.6 cm (0.25 in.). Curve 8 shows the most change and shows the crack penetrating the thickness of the specimen and developing a length of 2 cm on the back side. The fact that changes occurred before cracks were observed should be thoroughly investigated. In a previous investigation (ref. 4), a difference between standards at different stations, taken before fatigue testing was started, seemed to correlate with the later crack growth rates. This with the results of the other specimens tested in the program indicate that conditions in the specimen prior to an observed crack change sufficiently to change the signatures. This could be due to internal cracks or to local yielding.

DISCUSSION OF RESULTS

The results of the different tasks are summarized here in terms of the original test variables considered.

Analytical Basis for Signature Interpretation

The analytical study greatly increased the understanding of the relationship between Randomdec signatures and the dynamic behavior of the physical system. It is common to describe the behavior either in terms of its spectral or its modal content. It is especially convenient to relate the signature to modal behavior since both are in the time plane. Predominant frequencies, damping and beating phenomena can be related to the properties of a multi-mode system. Filtering of white noise indicates a significant effect on the signature only in the first half-cycle or two when the filter bandwidth is of the order of an octave.

From the definition of the signature in terms of the system step response, a possible way to determine the distance to a flaw has emerged. This feasibility of this has been partially verified by experimental work on the East Caruqinez Bridge.

The results of reference 5 on the calculation of signature error for single mode systems in terms of record length was extended to a two mode system and can no doubt be extrapolated to multi-mode systems since the error appears independent of the number of modes.

Signature Characteristics for Different Structures

A variety of structural members were tested on the different bridges and many proved to be similar in their response to the high frequency portion of traffic excitation. Girders and I beams often have flange and web thicknesses of 1-2 cm. This was the case on the 85-101 Separation Bridge, East Carquinez Bridge, and Missouri Bridge. These plate elements have sufficient vibration levels in the frequency range of 1-10 KHz and flaw detection should be a similar process for the many types of bridges constructed of this type of member.

The signal bridge is constructed from 20 cm rectangular tubing which also had a thickness of about 1 cm but is excited indirectly by traffic

passing beneath it. This results in a lower level of vibration which may be marginal for detecting small flaws with the present equipment.

The eyebars on the West Carquinez Bridge were a more massive member of about 4 cm thickness. Only artificial excitation was available on this bridge but it appears that higher frequencies (greater than 10 KHz) will be necessary to detect flaws in the region around the ends of the member. It has to be determined if traffic can supply the necessary excitation.

Similarity of Signatures for Similar Members

The results of the Signal Bridge showed signatures at identical locations relative to symmetric joints had sufficient similarity to isolate a defective joint. These members were welded rectangular tubing which had a high degree of uniformity. On the other hand, the eyebars of the West Carquinez Bridge showed significant differences in their signatures. The variation of signatures within a group of four hanger bars at one location was greater than that between bars at corresponding locations in two different groups. The similarities between corresponding bars of different groups showed that the signature depends on the overall configuration of spacers, pin nuts, position on the pin and other structural details that distinguish each bar of a group. These results show that the use of signatures for detecting a defective component out of a group of similar members would have to be verified for different situations.

Sensitivity of Signatures to Cracks

Evidence to date indicates that from a distance of 15-30 cm the smallest crack growth that can be detected with the present equipment is on the order of 0.25 cm. However, this size of crack cannot be detected with certainty. At present, the crack growth that can be reliably detected is about 0.75 cm. Cracks larger than this can be detected at a distance of a meter or more. This assumes that the excitation excites the crack region. The results on the Missouri Bridge showed that if the crack zone is in compression when the vibration is recorded, crack growth on the order of 2 cm can escape detection. To avoid this, the service loading, say traffic, should be used since this

is the load that will produce the flaws and, therefore, will be exciting the flaw region. If artificial excitation is used, care must be exercised to ensure that suspected flaw regions are excited.

CONCLUSIONS

A good understanding of Randomdec analysis has been obtained from analytical, field, and laboratory studies. The conclusions from these studies are:

1. The excitation that is usually the most suitable for flaw detection is the in-service dynamic loads such as traffic. These are the loads that will produce flaws and, therefore, will provide excitations to the flaw regions. Artificial excitation must be applied in a manner that will excite the flaw regions.
2. Cracks can be detected over a range of tensile stress, but the Missouri Bridge results indicate that compressive stress in the crack zone can prevent detection.
3. Some types of failures cause characteristic signature changes which can allow the identification of the flaw. The most obvious one is a pure sinusoidal signal typical of sliding surfaces.
4. The detection of flaws by comparing signatures between apparently identical members appears possible in symmetric structures containing a high degree of uniformity. Other structures may differ enough in fabrication details, loading or constraints to induce differences between signatures of apparently similar members. Therefore, each application would have to be evaluated before using this procedure.
5. It appears possible to locate flaws by measuring the elapsed time in the signature before a change appears.
6. The repeatability of signatures was good in all cases studied with traffic. In the case of the Carquinez eyebars where localized excitation of relatively high frequency was used, it was not as good.

7. With the present equipment, a change in crack length of about 0.75 cm is detectable at a distance up to about a meter at levels of excitation typical of bridge traffic. Smaller cracks, on the order of 0.25 cm, can be detected, without certainty, at closer distances.

RECOMMENDATIONS

Results to date indicate that Randomdec analysis can be developed into a practical method for use on bridges. In order to complete the development, the following recommendations for additional work are made.

Field Work

The West Carquinez Bridge should be studied under normal traffic to determine the repeatability of signatures for eyebars over a period of time and the similarity of signatures between similar eyebars. Also, the frequency content above 10 KHz from traffic excitation has to be evaluated.

Field measurements of cracks on bridges subjected to traffic are needed. Old bridges with known flaws can be monitored or secondary redundant members with induced flaws could be added to an existing bridge and the flaw growth monitored. Once the existence and location of flaws are known, methods to locate them should be studied.

Laboratory Work

A laboratory study should be conducted to more closely define the sensitivity of signatures to variables that affect flaw detection. These variables include excitation level and frequency content, flaw size, distance and static stress level.

Location of flaws has to be investigated to establish the conditions that would limit the application or lead to ambiguous results.

Analytical Work

For the method to be used by maintenance personnel in the field, a systematic, automated and reliable method of detecting significant differences between signatures has to be developed.

The effect on signatures versus level of external noise or sinusoidal components in the excitation should be studied and is well suited to analytical treatment.

REFERENCES

1. Cole, H. A., Jr.: Method and Apparatus for Measuring the Damping Characteristics of a Structure. United States Patent No. 3,620,069, Nov. 16, 1971.
2. Brignac, W. J., Ness, H. B., and Smith, L. M.: The Random Decrement Technique Applied to the YF-16 Flight Flutter Tests. AIAA/ASME/SAE 16th Structures Conference, Denver, CO, May 27-29, 1975.
3. Cole, J. A., Jr.: Failure Detection of a Space Shuttle Wing Flutter Model by Random Decrement. NASA TM X-62,041, May 1971.
4. Cole, H. A., Jr., and Reed, R. E., Jr.: A Method for Detecting Structural Deterioration in Bridges. NASA CR-137,548, 1974.
5. Cole, H. A., Jr.: On-Line Failure Detection and Damping Measurement of Aerospace Structures by Random Decrement Signatures. NASA CR-2205.
6. Chang, C. S.: Study of Dynamic Characteristics of Aeroelastic Systems Utilizing Randomdec Signatures. NASA CR-132,563.
7. Uspensky, J. V.: Introduction to Mathematical Probability. McGraw-Hill, 1937.
8. Salane, H. J., et al.: An Investigation of the Behavior of a Three-Span Composite Highway Bridge. Missouri Cooperative Highway Research Program Report 71-5.

APPENDIX A
TWO-DEGREE-OF-FREEDOM SYSTEM

The equations for the model shown in the text are

$$\ddot{x}_1 + \frac{C}{m_1} \dot{x}_1 + \frac{(k_1 + k_2)}{m_1} x_1 - \frac{k_2}{m_1} x_2 = f_1(t) \quad (A-1)$$

$$-\frac{k_2}{m_2} x_1 + \ddot{x}_2 + \frac{C}{m_2} \dot{x}_2 + \frac{h_2}{m_2} x_2 = f_2(t) \quad (A-2)$$

The natural frequencies are determined from the equation

$$Q^4 + \frac{2d}{b}(b + e)Q^3 + \frac{1}{b}(1 + a + b + 4ed^2)Q^2 + \frac{2b}{b}(1 + a + e)Q + \frac{a}{b} = 0 \quad (A-3)$$

where $x_1 = R[Ae^{Q\tau}]$, $x_2 = R[Be^{Q\tau}]$

Q = complex frequency

$$Q_{1,2} = R_1 \pm i\omega_1$$

$$Q_{3,4} = R_2 \pm i\omega_2$$

$$\tau = \omega t$$

The step response is obtained by letting the forces $f_1(t)$, $f_2(t)$ be constant, $f_1(t) = F_1$ and $f_2(t) = F_2$. The general solution has the form

$$\begin{aligned} x_1 = & e^{R_1\tau} [(\phi_{R1} A_{1R} + \phi_{I1} A_{1I}) \sin \omega_1 \tau] \\ & + e^{R_2\tau} [A_{2R} \cos \omega_2 \tau + A_{2I} \sin \omega_2 \tau] + \frac{F_1 + F_2}{k_1} \end{aligned} \quad (A-4)$$

$$\begin{aligned}
x_2 = & e^{R_1 \tau} [(\phi_{R_1} A_{1R} + \phi_{I_1} A_{1I}) \cos \omega_1 \tau + (\phi_{R_1} A_{1I} - \phi_{I_1} A_{1R}) \sin \omega_1 \tau] \\
& + e^{R_2 \tau} [(\phi_{R_2} A_{2R} + \phi_{I_2} A_{2I}) \cos \omega_2 \tau \\
& + (\phi_{R_2} A_{2I} - \phi_{I_2} A_{2R}) \sin \omega_2 \tau] + \frac{F}{k_1} + F_2 \left(\frac{1}{k_1} + \frac{1}{k_2} \right)
\end{aligned} \tag{A-5}$$

$A_{1R}, A_{1I}, A_{2R}, A_{2I}$ are constants of integration and

$$\begin{aligned}
\phi_{Ri} &= b(R_i^2 - \omega_i^2 + 2 \frac{de}{2} R_i + \frac{1+a}{b}) \\
\phi_{Ii} &= b(2 \frac{de}{b} \omega_i + 2R_i \omega_i) \quad , \quad i = 1, 2
\end{aligned} \tag{A-6}$$

The initial conditions for the step response are

$$x_1(0) = \dot{x}_1(0) = x_2(0) = \dot{x}_2(0) = 0$$

However, it is more convenient for later use to solve the following equations for the two sets of initial conditions

$$\begin{bmatrix} 1 & 0 & 1 & 0 \\ R_1 & \omega_1 & R_2 & \omega_2 \\ \phi_{R1} & \phi_{I1} & \phi_{R2} & \phi_{I2} \\ (R_1 \phi_{R1} & (R_1 \phi_{I1} & (R_2 \phi_{R2} & (R_2 \phi_{I2} \\ -\omega_1 \phi_{I1}) & -\omega_1 \phi_{R1}) & -\omega_2 \phi_{I2}) & -\omega_2 \phi_{R2}) \end{bmatrix} \begin{Bmatrix} A_{R1} \\ A_{I1} \\ A_{R2} \\ A_{I2} \end{Bmatrix} = \begin{bmatrix} 1 \\ 0 \\ 1 \\ 0 \end{bmatrix} \text{ and } \begin{bmatrix} 0 \\ 0 \\ 1 \\ 0 \end{bmatrix} \tag{A-7}$$

Denoting the first set of solutions by $x^{(1)}$ and the second by $x^{(2)}$, the step response for only F_1 acting is

$$x_1^{(1)} = \frac{F_1}{k_1} \left[x^{(1)} \right], \quad x_2^{(1)} = \frac{F_1}{k_1} x^{(1)} \tag{A-8}$$

and for only F_2 acting

$$x_1^{(2)} = \frac{F_2}{k_2} \left[\frac{k_2}{k_1} X^{(1)} + X^{(2)} \right]$$

$$x_2^{(2)} = \frac{F_2}{k_2} \left[\frac{k_2}{k_1} X^{(1)} + X^{(2)} \right]$$

The impulse response is the derivative of the step response and is defined as

$$y_1^{(1)} = \frac{\dot{x}_1^{(1)}}{w}, \quad y_2^{(1)} = \frac{\dot{x}_2^{(1)}}{w}$$

$$y_1^{(2)} = \frac{\dot{x}_1^{(2)}}{w}, \quad y_2^{(2)} = \frac{\dot{x}_2^{(2)}}{w}$$

letting

$$B_{Ri} = R_i A_{Ri}^j + \omega_i A_{Ii}^j$$

$$B_{Ii}^j = -\omega_i A_{Ri}^j + R_i A_{Ii}^j$$

$$C_{Ri}^j = (R_i \phi_{Ri} - \omega_i \phi_{Ii}) A_{Ri}^j + (R_i \phi_{Ii} + \omega_i \phi_{Ri}) A_{Ii}^j$$

$$C_{Ii}^j = (-\omega_i \phi_{Ri} - R_i \phi_{Ii}) A_{Ri}^j + (-\omega_i \phi_{Ii} + R_i \phi_{Ri}) A_{Ii}^j$$

$i = 1, 2$; $j = 1, 2$ (summations are not implied by repeated indices)

The impulse response functions are

$$y_1^{(i)} = e^{R_1 \tau} \left[B_{R_1}^{(i)} \cos \omega_1 \tau + B_{I_1}^{(i)} \sin \omega_1 \tau \right] + e^{R_2 \tau} \left[B_{R_2}^{(i)} \cos \omega_2 \tau + B_{I_2}^{(i)} \sin \omega_2 \tau \right] \quad (A-9)$$

$$Y_2^{(i)} = e^{R_1 \tau} \left[C_{R_1}^{(i)} \cos \omega_1 \tau + C_{I_1}^{(i)} \sin \omega_1 \tau \right] + e^{R_2 \tau} \left[C_{R_2}^{(i)} \cos \omega_2 \tau + C_{I_2}^{(i)} \sin \omega_2 \tau \right] \quad (A-10)$$

Having the impulse response functions, the response to a random excitation can be calculated from

$$Y_1(t) = \int_0^t \left[P_1(\xi) Y_1^{(1)}(t - \xi) + P_2(\xi) Y_1^{(2)}(t - \xi) \right] d\xi \quad (A-11)$$

For this study, the time history was formed as a digital record where $t = i - 1$, $\xi = j$. This gives

$$Y_1(i) = \sum_{j=1}^{i-1} \left[P_1(j) Y_1^{(1)}(i - j + 1) + P_2(j) Y_1^{(2)}(i - j + 1) \right],$$

$$i = 1, 2, 3, \dots, M$$

where two sets of random numbers with prescribed mean values of 0.0 and standard deviations of 1.0 were used for the random excitations $P_1(j)$, $P_2(j)$. This random time history can then be treated with the Randomdec procedure to obtain signatures of the system.

In summary, therefore, the step response, with appropriate initial conditions represents, according to the hypothesis, the exact signature of the system, and the impulse response can be used to generate a random time history from which the signature can be experimentally (in the case, a digital experiment) obtained.

APPENDIX B

LABORATORY TEST PROGRAM

INITIAL WORK PLAN

Objective

To test a series of steel plate weldments, under constant uniaxial sinusoidal loads, and to measure the signatures of these specimens at various stages of crack growth.

Tests

Two types of specimens will be tested:

1. Fillet weldment, figure 73.
2. Butt weldment, figure 74.

Four specimens of each type will be tested. Initially, the signatures of each specimen will be obtained under a constant dead load stress of 10,300 and 13,800 N/cm². Two accelerometers will be used, located approximately as shown in figure 73 and 74.

Each specimen will then be subjected to a minimum stress $\sigma = 690$ N/cm² and a stress range of $\sigma_r = 20,000$ N/cm². These stresses will be applied cyclically, until a crack of 0.25 cm or less is seen. A signature will then be taken at dead load stresses of 10,300 and 13,800 N/cm².

The cyclic loads will be continued until the crack reaches approximately 0.6 cm. Another signature will be taken.

Cyclic loads will be continued and crack growth versus cycles will be obtained.

SPECIMENS

The grade of steel for all specimens tested was ASTM-A36. The geometry of the specimens is as shown in figures 83 and 84.

One specimen, figure 83, consisted of the attachment of a 3.8×7.6×1.2 cm plate to an 8.8×39.2×0.6 cm coupon plate. The small 1.2 cm plate was attached by means of 0.6 cm continuous longitudinal fillet welds, placed along the 7.6 cm face, with no transverse end welds.

The welds were placed by submerged arc welding process using ASTM class B 70 electrodes. This type of specimen simulates the type of weld used for cover plated beam specimens.

The other specimen, figure 84, consisted of two ends of the basic coupon butt welded together. The welding process also used B 70 electrodes.

All specimens were fabricated from hot rolled ASTM-A36 steel plate of 0.6 and 1.2 cm thickness. Standard tension tests were conducted on parts of the various specimens, giving an average value of 25,000 N/cm² yield of the material and 20.7×10^6 N/cm² for the modulus of the material.

EQUIPMENT

The equipment used for the test series consisted of:

1. The Gilmore Servo Controlled Fatigue Testing Equipment,
2. The Load Frame, and
3. The Vibration Equipment used to tape record signals from the specimen during fatigue crack development.

In the following, a brief discussion of the three components of the system and their capabilities will be given, although not all the features of the machine were utilized. In particular, only constant amplitude fatigue tests were conducted.

Fatigue Testing Equipment

The fatigue testing equipment consists of a closed-loop hydraulic system with a 20 GPM variable volume pumping unit. The actuator has a 222,000 newton (50,000 lb) dynamic rating and an 382,000 newton static rating, with a six-inch maximum stroke. The actuator is equipped with a 222,000 newton fatigue rated cell, a six-inch Linear Voltage Differential Transformer (LVDT) for deflection measurement and control, and a 25 GPM Servo Valve and Flushing block.

The system is capable of loading in tension and/or in compression while controlled by load through a Load Signal Conditioner providing load cell excitation and signal conditioning. Also, the system may be controlled by deflection through a Position Signal Conditioner providing LVDT excitation and signal conditioning. Strain control is also provided through a Strain Signal Conditioner providing excitation and conditioning for a strain gage mounted on the specimen.

A power and switching command module allows the system to be controlled either by a Function Generator, a Curve Follower, or a set of ten Block Programming Modules as the command source.

The Function Generator is capable of producing square, triangle, ramp, sine and cosine waveforms at frequencies between 0.0015 to 1,100 Hertz (CPS).

The Curve Follower, using paper 15 cm in width in loops of up to 1.8 m in length, can designate various mean and dynamic amplitude positions at various frequencies. Any of the signals produced by the Signal conditioner can be imposed on the Curve Follower signals.

The ten Block Programming Modules provide a means for generating a predetermined number of cycles at a certain mean and dynamic amplitude level at various frequencies. Any sequential number of the blocks could be operated and the final block in any sequence can stop the system or return to the first block in the sequence. Again, the waveforms produced by the Function Generator could be imposed on the Block Module signals.

Each of the ten Block Modules is provided with a six-digit counter which records counts in the particular module and also to pre-set a particular cycle count. A six-digit counter gives total counts in the system and has the capacity to shut down the system when a predetermined number of cycles is reached. This counter also gives total counts during Block Programming sequence tests and lists the counts during the use of the Function Generator and the Curve Follower. Also in the system is an oscilloscope which provides the capability of monitoring the output of the Load Cell, the LVDT, or the Strain Control Module.

The load commands to the system are in terms of the percentages of either the maximum loads, the maximum deflection or a given strain, and both the Servo Amplifier and the ten block modules are provided with pots of 1,000 graduations. Thus, the load commands have an accuracy of 0.1 percent. The system can operate at either 100 percent, 50 percent, 20 percent, or 10 percent of its capacity. Thus, in the constant load position, for example, the system when operating at the 10 percent position will have the capacity to apply 22,200 newtons with an accuracy of up to 22 newtons.

The control console is also equipped with failsafe alarms that terminate the loading process in case of a "sudden" increase in the ram movement. Such a situation would be the development of a large crack in the specimen.

The Test Frame

The loading frame is a standard universal testing frame that can accommodate a 100 K load, and has a 100 cm vertical test zone.

Vibration Recording Equipment

The Vibration Recording Equipment consisted of two piezoelectric accelerometers, two Charge Amplifiers, and a two-track tape deck.

A partial list of the equipment specifications is given below.

Accelerometers

Mounted resonance:	35,000 Hz
Frequency response:	Near DC to 10,000 Hz \pm 10 percent
Weight:	13 grams

Charge Amplifiers

Frequency response:	Near DC to 100,000 Hz \pm 5 percent
---------------------	---------------------------------------

Tape Recorder (at 7-1/2 ips)

Frequency response:	40 to 18,000 Hz \pm 2 db
Signal, to noise ratio:	> 58 db (at peak recording level)
Flutter and wow:	< 0.09 percent
Harmonic distortion:	< 2 percent

TESTING PROCEDURE

The object of the testing program was to induce fatigue cracks into fillet and butt welded test specimens and to record the vibration responses at various stages of crack growth.

The desired responses were to be of a random nature with fairly uniform and wider frequency spectrums to which the Randomdec procedure could be applied. To obtain this type of response, three different method of randomly exciting specimens under constant load conditions were tested.

The methods of excitation that were analyzed included:

1. the natural, inherent excitation transmitted through the grips by the fatigue machine;
2. continuously tapping transversely on the specimen with the metal tip of a screwdriver; and
3. rubbing a sandpaper block in the transverse direction along the side of the specimen.

The latter two excitations also included the natural vibrations induced by the fatigue machine. Methods 2 and 3 were considered as possibly convenient methods to excite on-line structures. However, for the purposes of this testing program, the method utilizing only the natural machine vibrations was selected.

The specimens as shown in figure 83 and 84 were clamped by the grips of the fatigue machine and subjected to an initial constant amplitude tensile load applied uniaxially at such a magnitude as to induce a $20,700 \text{ N/cm}^2$ nominal stress on the $6.2 \times 0.6 \text{ cm}$ center section. This loading was the maximum that the specimens were to experience while being sinusoidally stressed. This initial loading tested the capability of the grips to hold each specimen and to allow the specimen to seat firmly in the jaws. It quickly became evident that the grips would not hold the specimens adequately. To solve this problem, beads of weld were placed on the top and bottom ends of the specimens. It was found that the removal of slag from the weld beads prior to clamping the specimens helped to reduce the slippage in the grips during later stress cycling.

Once the specimens were found to be secure in the trips, the removal of slag and rust in the central region of the specimens was accomplished with a wire brush. Further cleaning around the anticipated points of fatigue crack initiation was done with alcohol and a toothbrush. This was necessary to remove microscopic particles which would have obscured the view of the minute cracks. Using a 4.2X American Optical Microscope, the cleanliness of the specimen was checked and the weld joints were analyzed for any initial cracks. This was accomplished under constant tensile load so that any cracks would be opened and more easily seen.

The accelerometers were positioned on the specimens as shown in figures 83 and 84. Beeswax was used for this purpose. They were then connected to the recording equipment.

Now complying with the initial work plan, vibration responses from the specimens were recorded at the constant dead load conditions of 10,300 and 13,800 N/cm². From these responses Randomdec signatures representing the undamaged specimens could be obtained. The specimens were then subjected to a minimum tensile stress of 690 N/cm² and a tensile stress range of 20,000 N/cm², sinusoidally cycling at a frequency of 10 Hz.

The numbers of cycles to failure was estimated from previous studies done on similar specimens. Considerably before these numbers were obtained the fatigue machine was stopped at a constant load condition and the specimens were checked for crack initiation. (Responses were not always recorded when the specimens were checked for cracks.) Continued stress cycling and crack analysis were frequently done in an attempt to obtain responses for crack lengths of 0.25 cm or less. Recordings were made prior to crack initiation and at various times during crack growth at the same constant load conditions of 10,300 and 13,800 N/cm². This process of stress cycling, crack analysis and response recording were repeated until either the specimens failed or very large cracks were present. Along with each vibration response recording, detailed sketches, including crack positions and lengths, were made. The number of accumulated stress cycles at these times were also noted.

In the tests conducted on the last two specimens responses were recorded at the constant load conditions of 690; 3,450; 6,900; 10,300; and 13,800 N/cm². This was done in order to see how the response changes as a function of stress.

COMMENTS ON TEST RESULTS

The major difficulty in visually detecting cracks, equal to or less than 0.1 inch, during these tests was that of being unable to reliably predict a rough estimate of the number of stress cycles at which a crack would initiate. This was particularly true for the butt weld type specimens. Fatigue cracks in these specimens were noted starting at as low as approximately 500,000 cycles. Yet one specimen did not start to crack even though it had over 3,500,000 cycles accumulated. In addition, since the welding process had made the butt weld specimens slightly bent, when the cracks did form, they rapidly spread along one side of the specimen to a long length while the depth remained shallow. These factors made a quick crack detection very difficult. Because of the large

variations in crack initiation times and rapid crack growth, most of the initial crack sizes were larger than called for in the original work plan. In an attempt to correct this situation, more specimens were tested. The fillet weld specimen cracks were somewhat more predictable and would be recommended over the butt weld specimens if further tests were to be conducted.

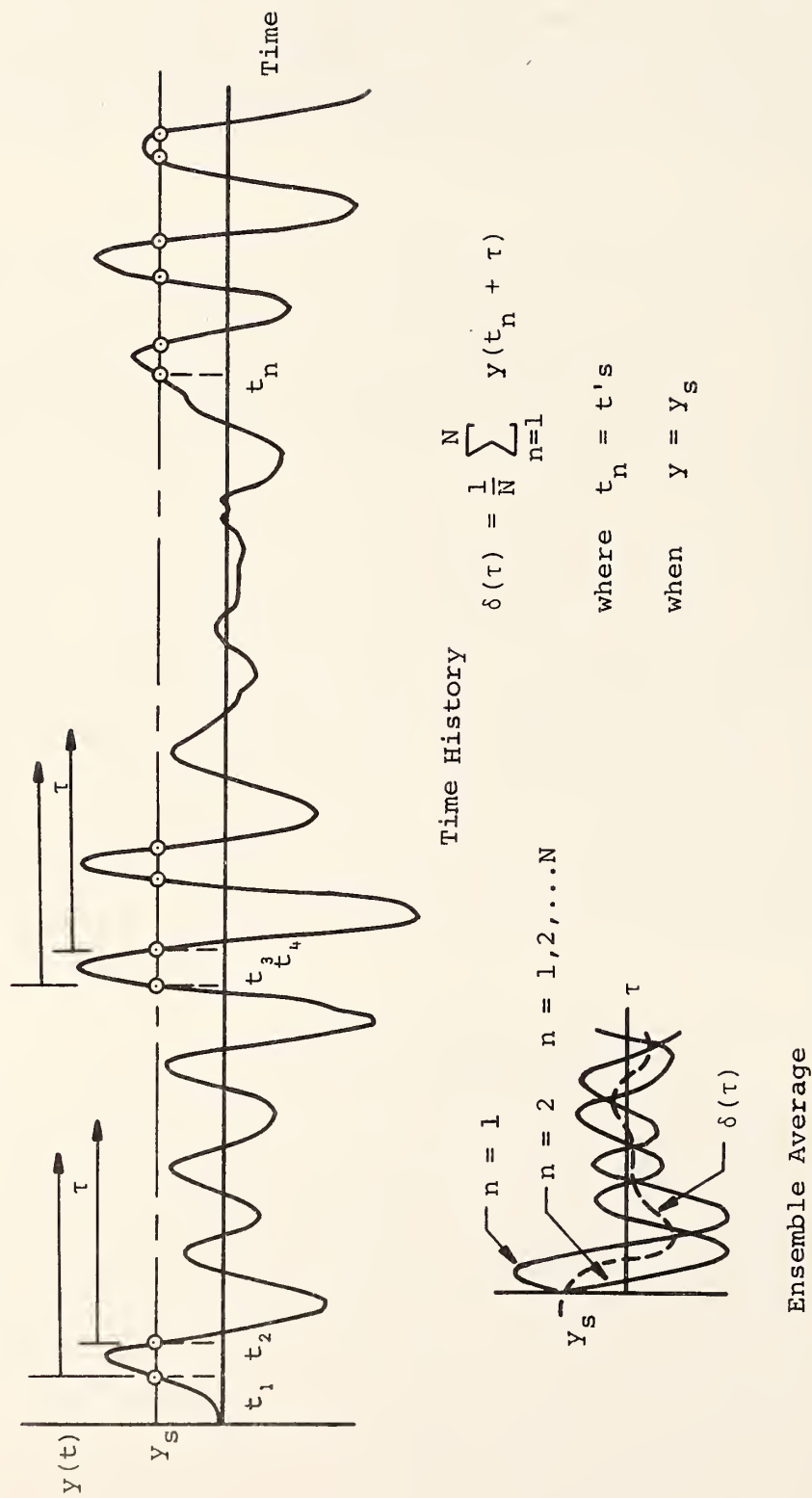


FIGURE 1.- DEFINITION OF RANDOM DEC SIGNATURE.

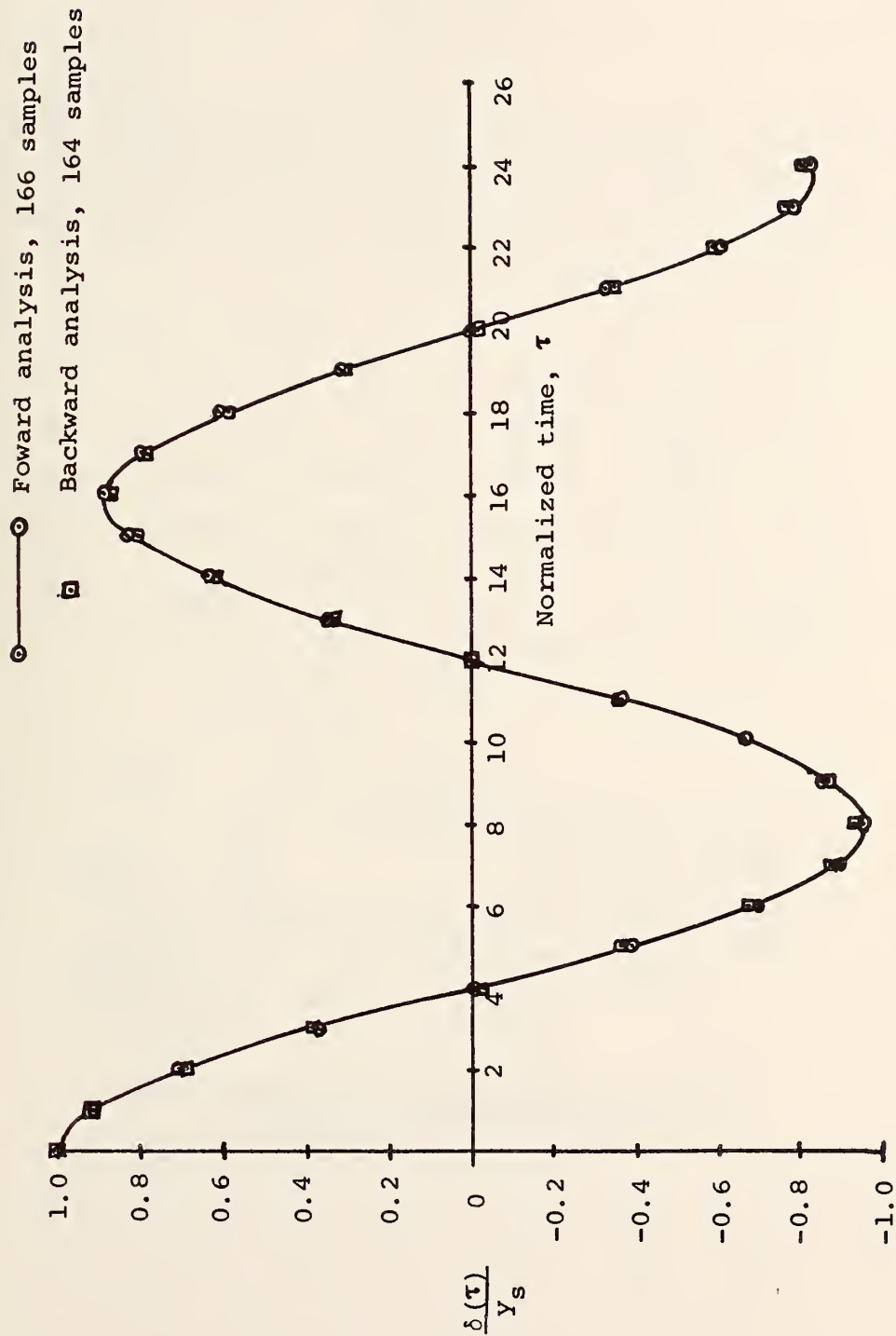


FIGURE 2.- COMPARISON OF FORWARD AND BACKWARD ANALYSIS OF TIME HISTORY.

	Case				
	1	2	3	4	5
a	1.0	1.0	5.0	5.0	50.0
b	1.0	1.0	5.0	5.0	50.0
d	0.02	0.05	0.02	0.05	0.02
e	0.50	0.50	0.50	0.50	0.50
f_1	0.618	0.617	0.801	0.801	0.932
f_2	1.618	1.617	1.248	1.247	1.073
f_1/f_2	0.38	0.38	0.64	0.64	0.87

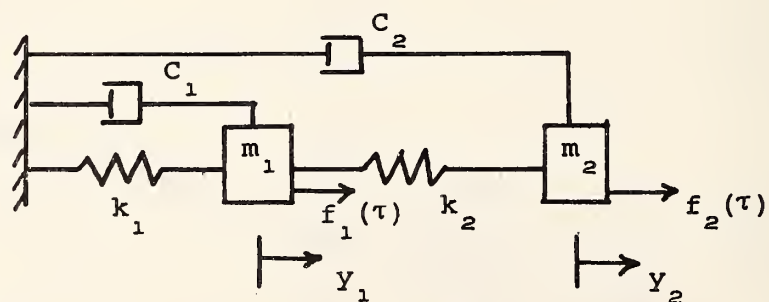


FIGURE 3.- NUMERICAL CASES FOR TWO-DEGREE-OF-FREEDOM ANALYTICAL MODEL.

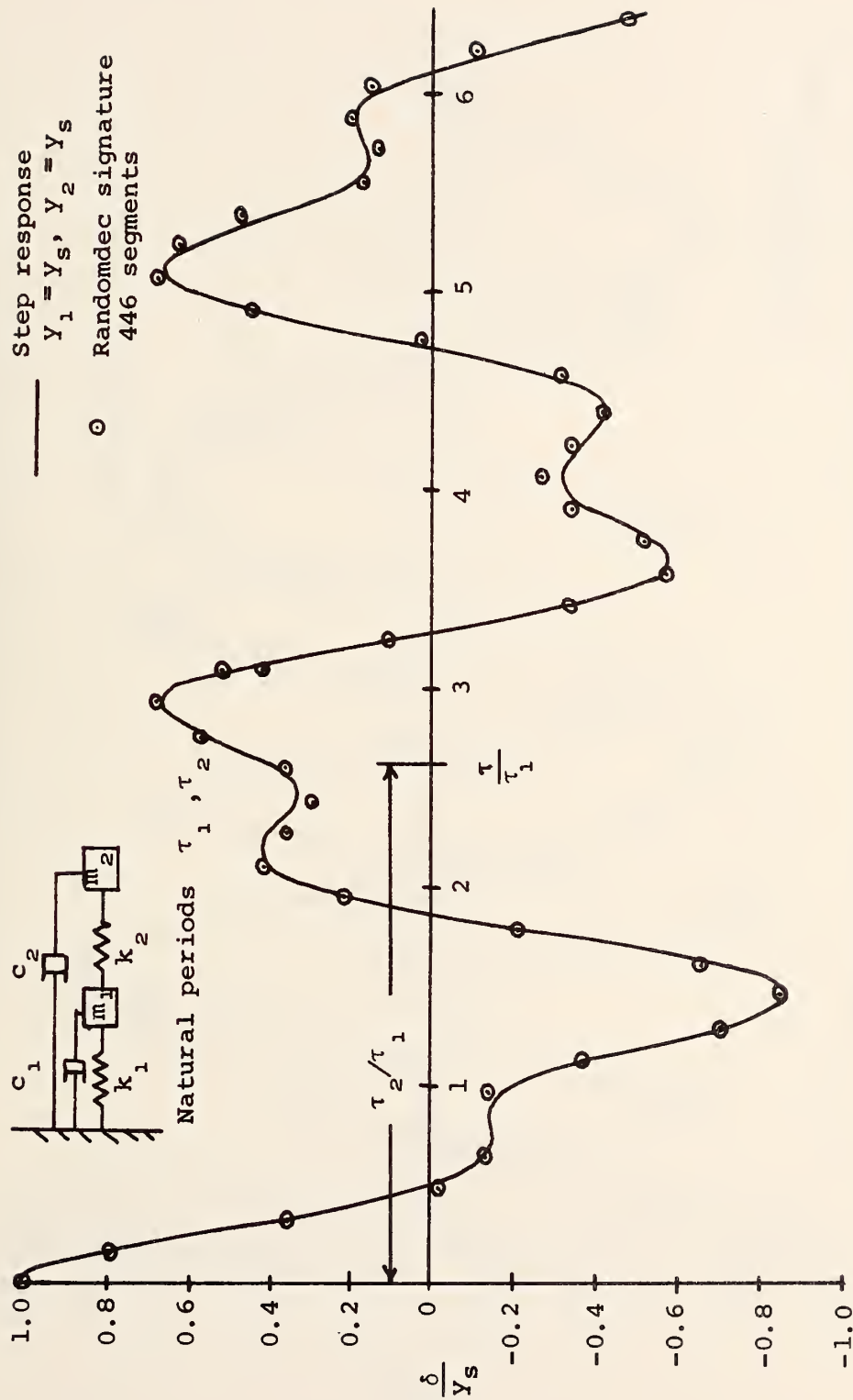


FIGURE 4.- COMPARISON OF SYSTEM STEP RESPONSE Y_1
 AND RANDOMDEC SIGNATURE, CASE 1.

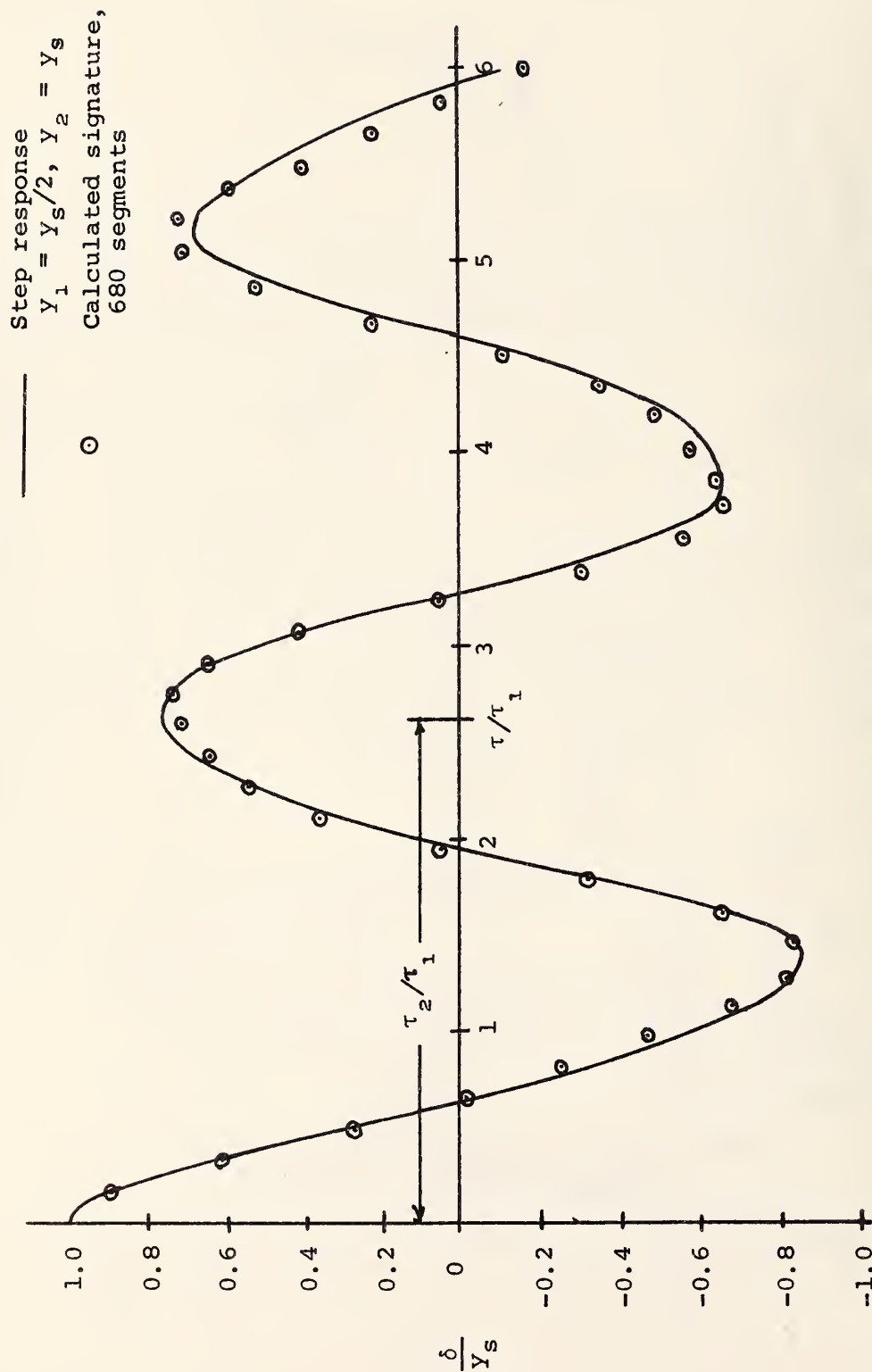


FIGURE 5.- COMPARISON OF SYSTEM STEP RESPONSE Y_2 AND RANDOMDEC SIGNATURE, CASE 1.

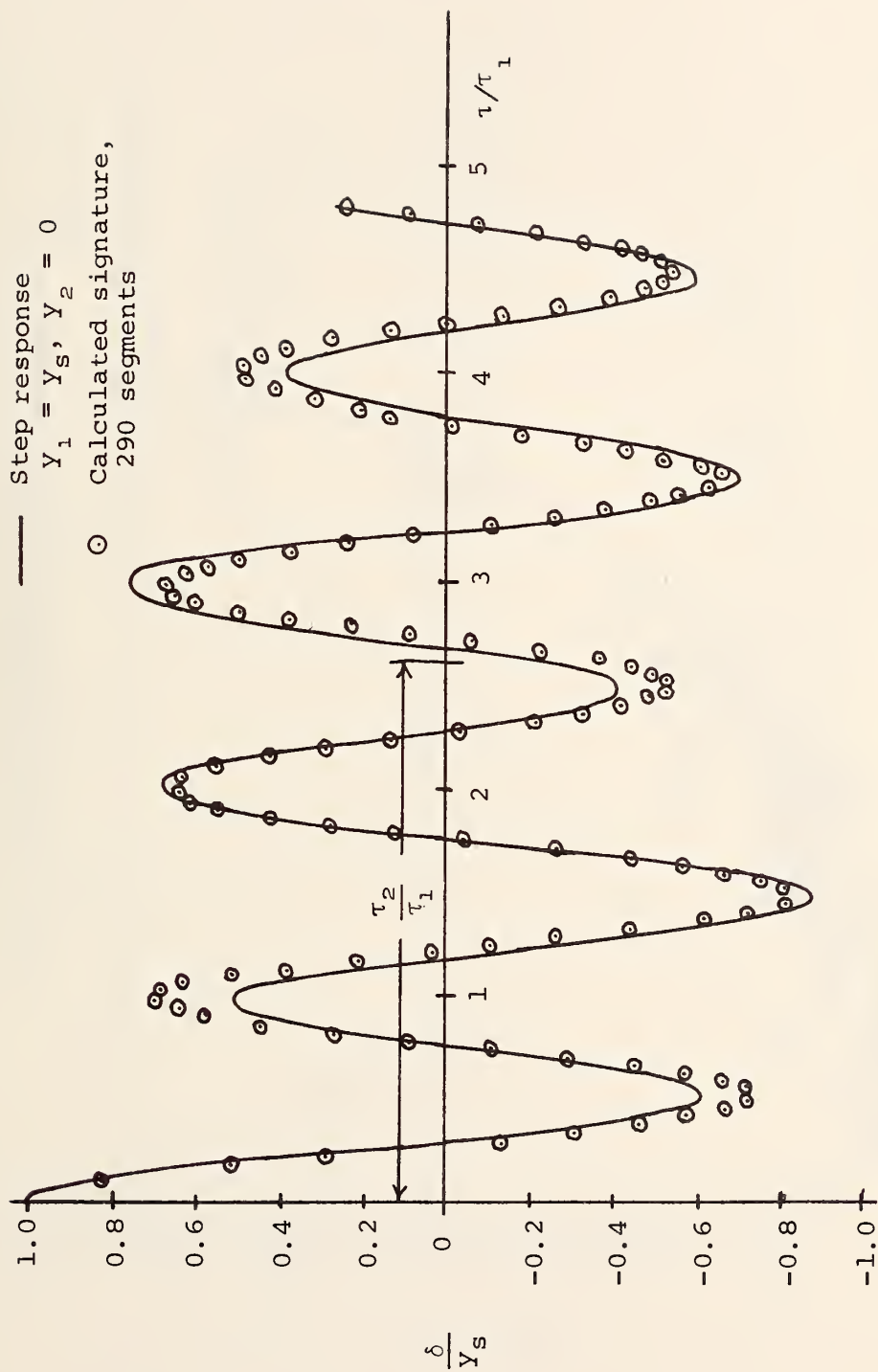


FIGURE 6.- COMPARISON OF SYSTEM STEP RESPONSE Y_1 AND ACCELERATION SIGNATURE, CASE 1.

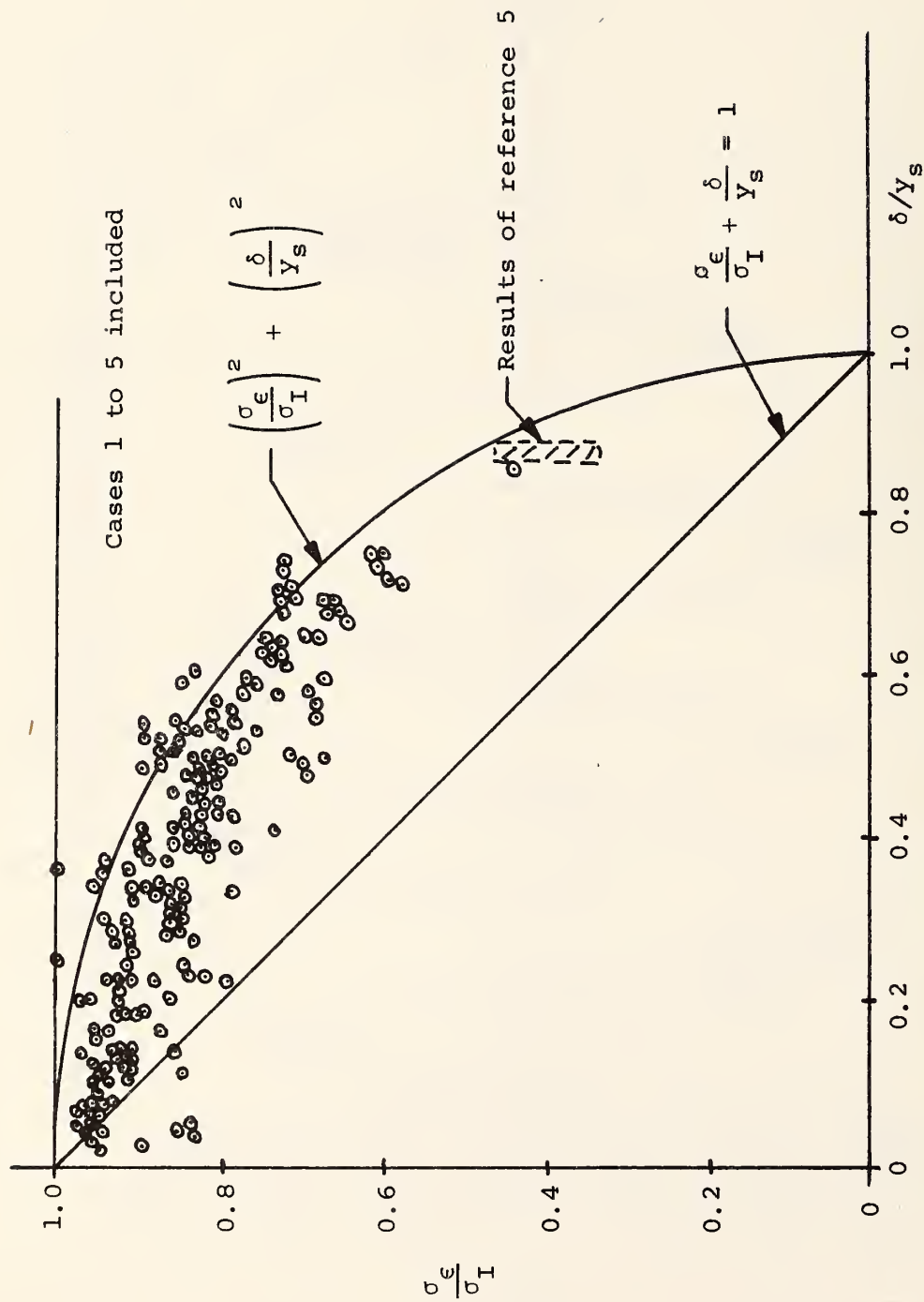


FIGURE 7.- STANDARD DEVIATION OF SEGMENTS
VERSUS SIGNATURE AMPLITUDE.

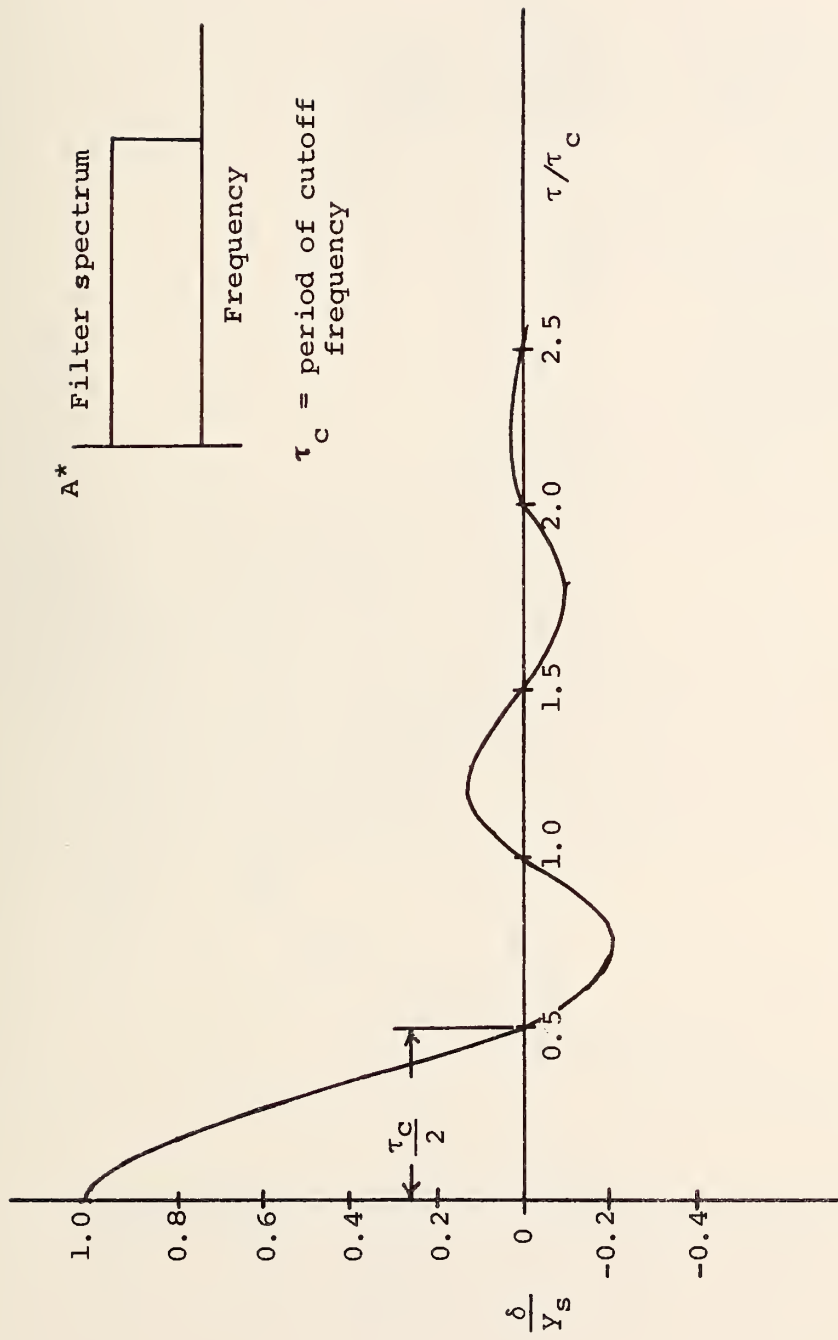


FIGURE 8.- RANDOMDEC SIGNATURE OF WHITE NOISE SUBJECTED TO IDEAL LOW-PASS FILTER.

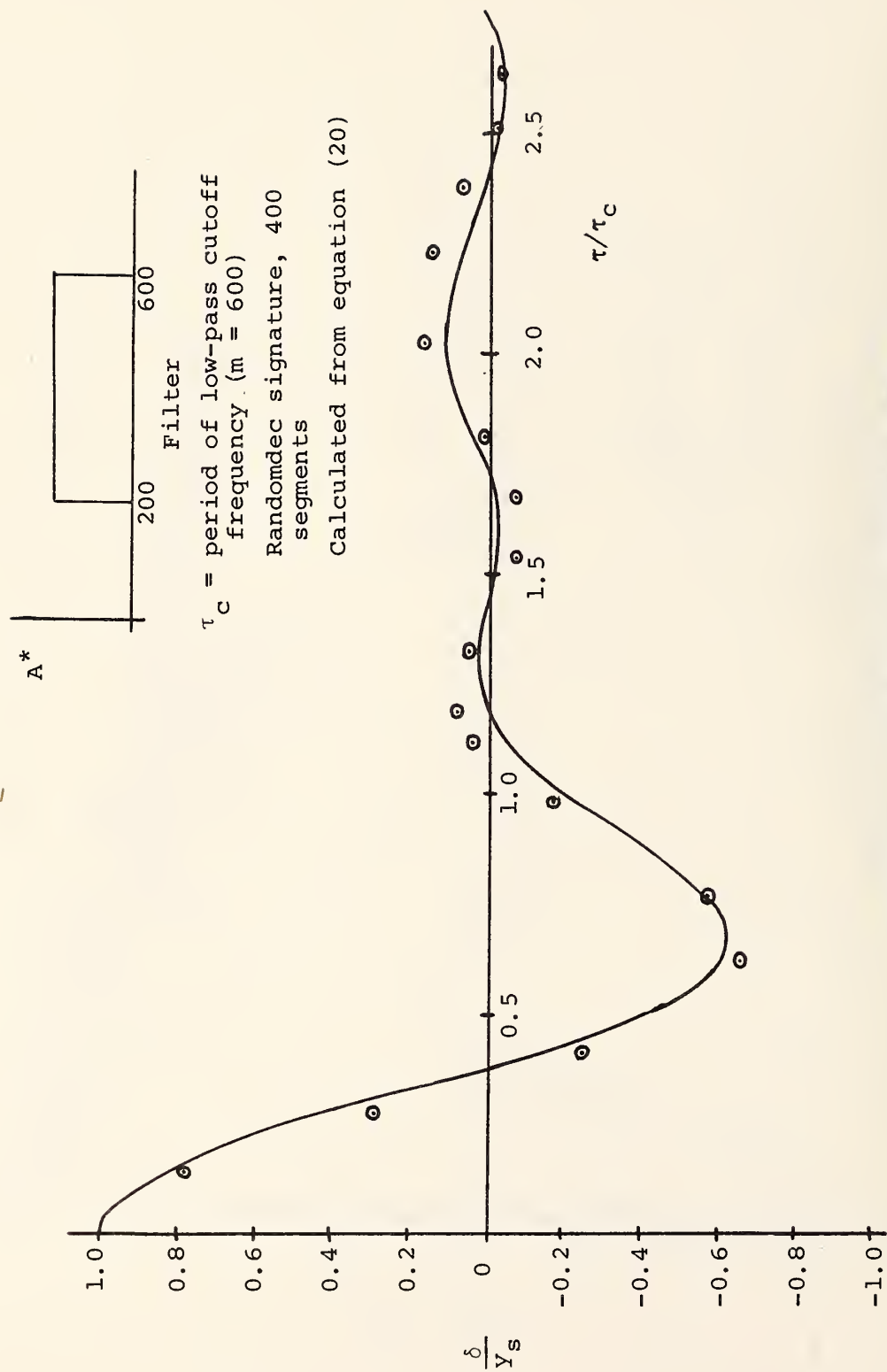


FIGURE 9.- RANDOMDEC SIGNATURE OF WHITE NOISE SUBJECTED TO IDEAL BAND-PASS FILTER.

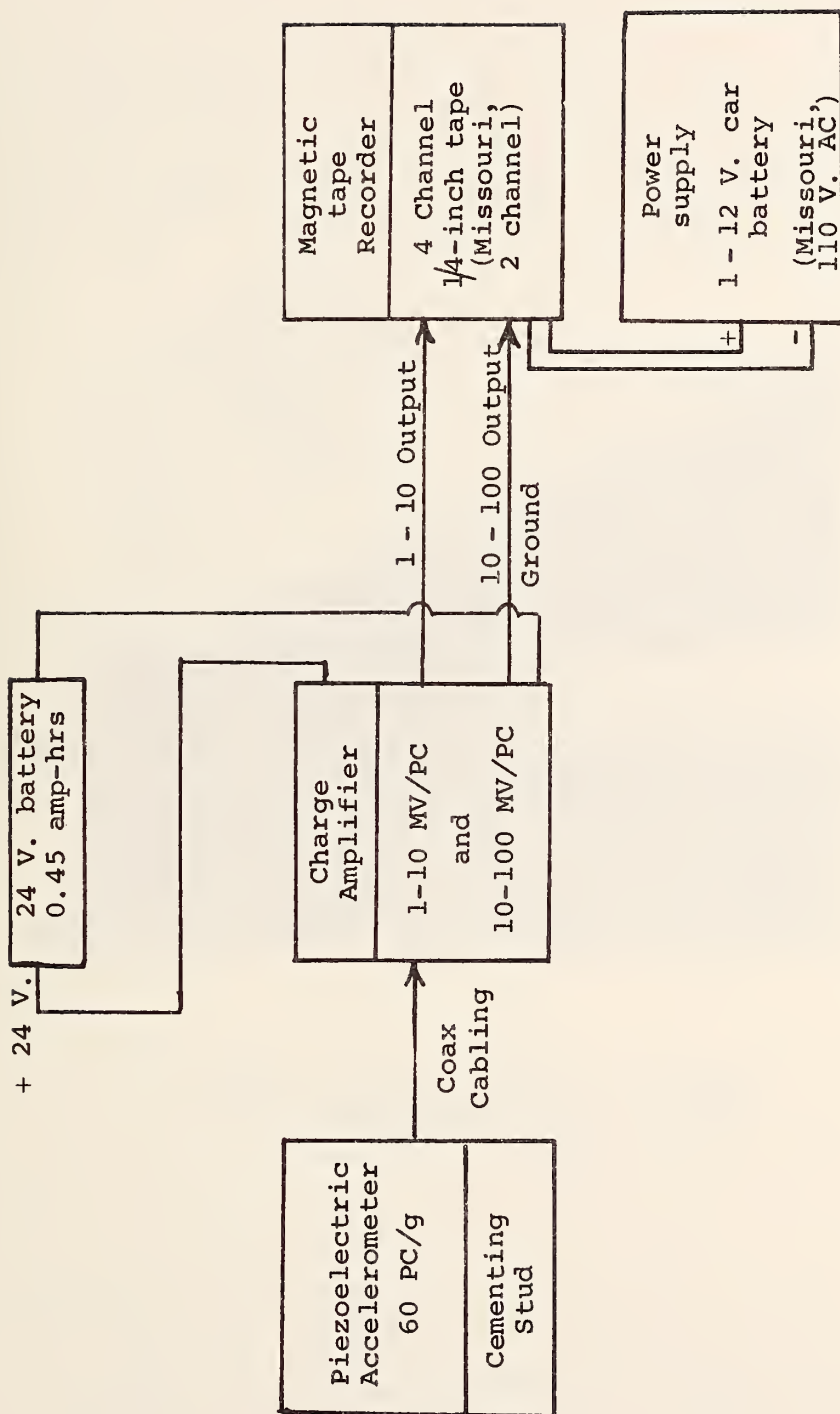


FIGURE 10.- INSTRUMENTATION FOR FIELD MEASUREMENTS.

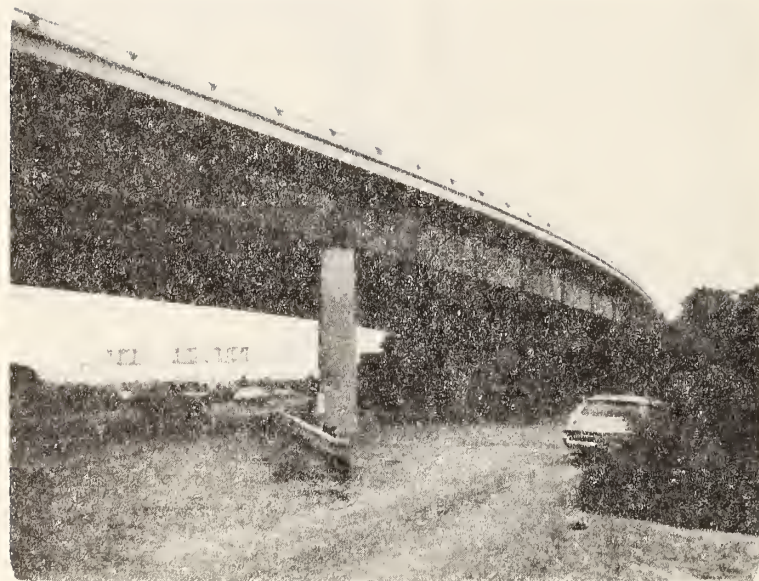


FIGURE 11.- HIGHWAY 85-101 BRIDGE,
LOOKING NORTH ON HIGHWAY 101.

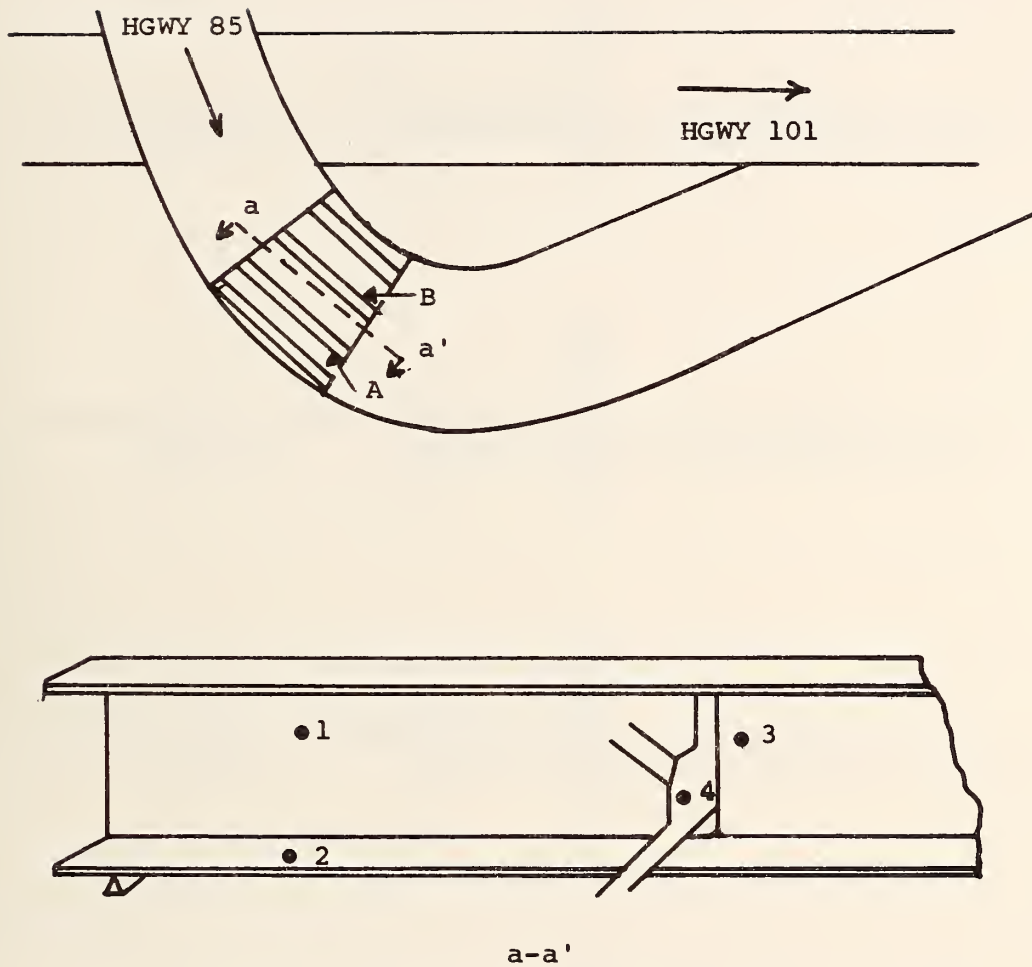


FIGURE 12.- 85-101 BRIDGE ACCELEROMETER LOCATIONS.

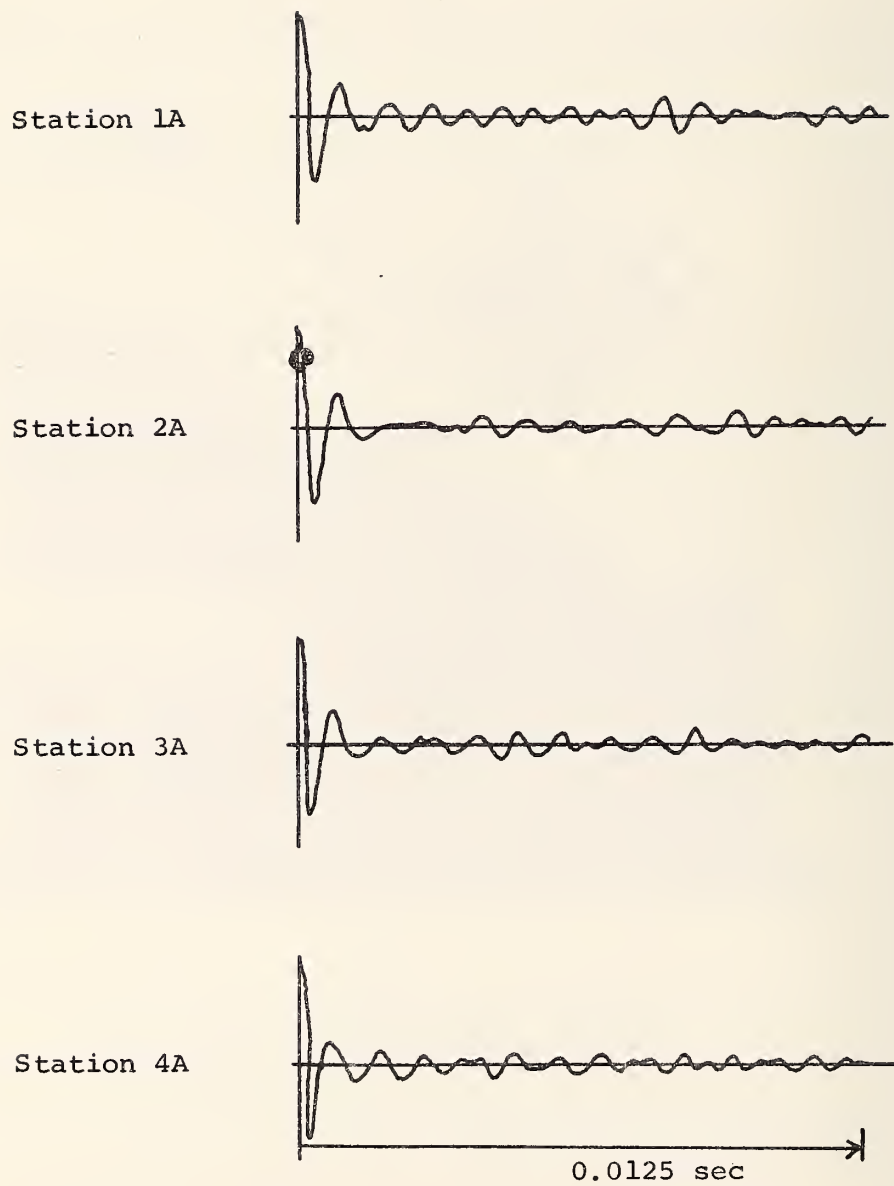


FIGURE 13.- SIGNATURES OF 85-101 BRIDGE, GIRDER A;
FILTER: 1,000 - 6,400 Hz.

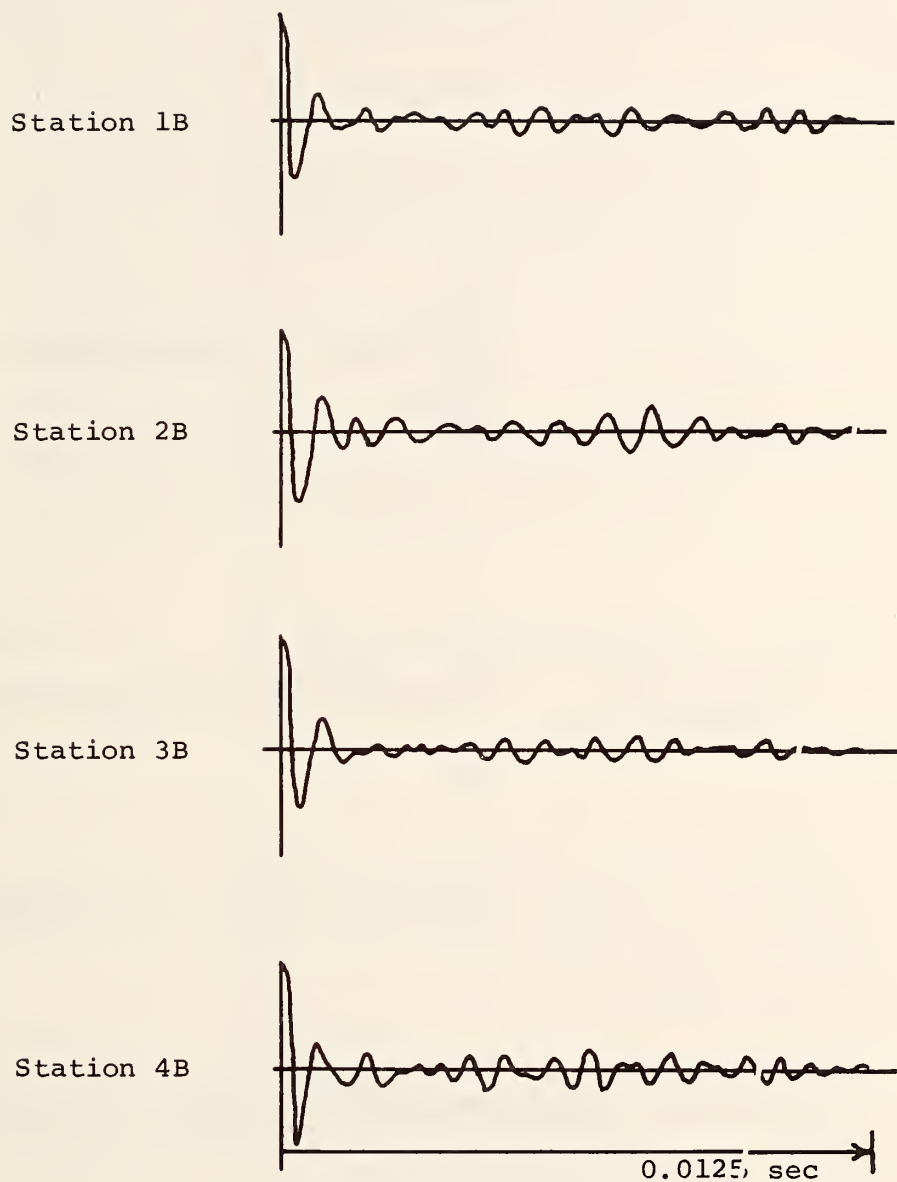


FIGURE 14.- SIGNATURES OF 85-101 BRIDGE, GIRDER B;
FILTER: 1,000 - 6,400 Hz.

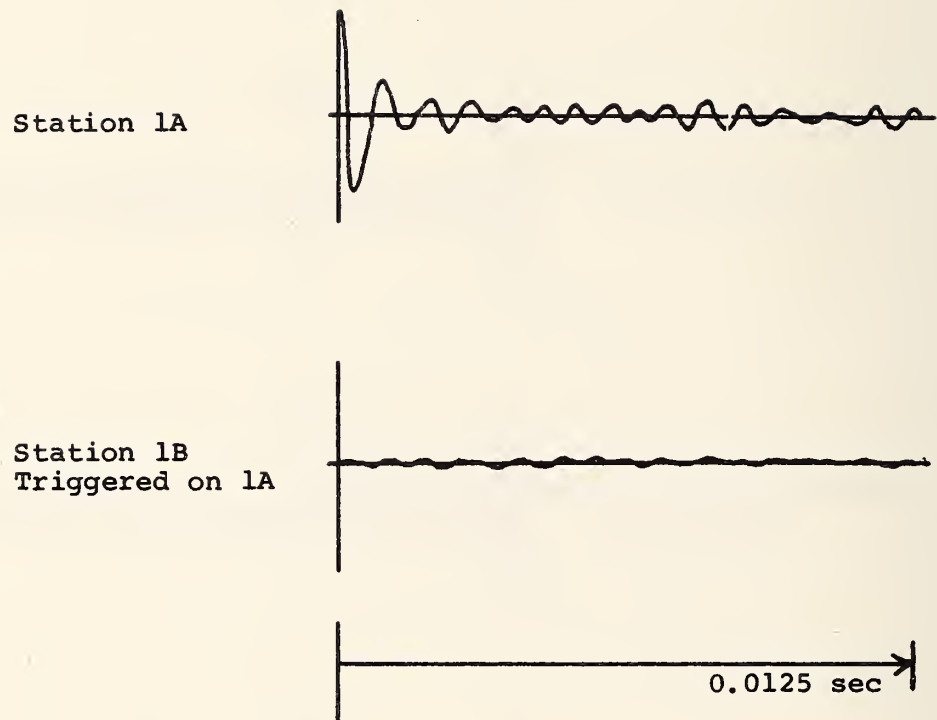
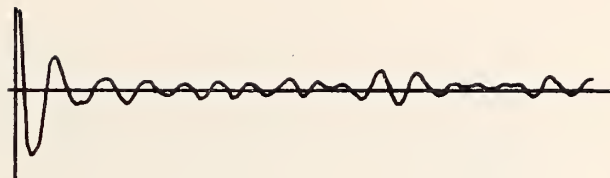
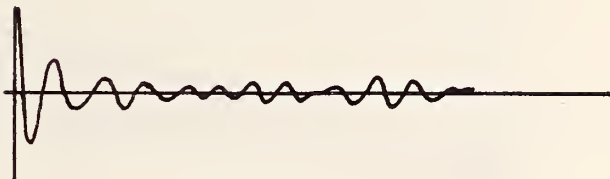


FIGURE 15.- CROSS-RANDOMDEC SIGNATURES, 85-101 BRIDGE;
FILTER: 1,000 - 6,400 Hz.

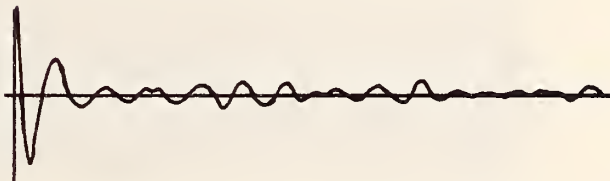
Station 1A
Recorded 4/11/75



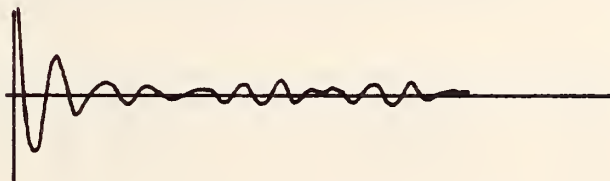
Station 1A
Recorded 8/30/73
(Station 3, ref. 1)



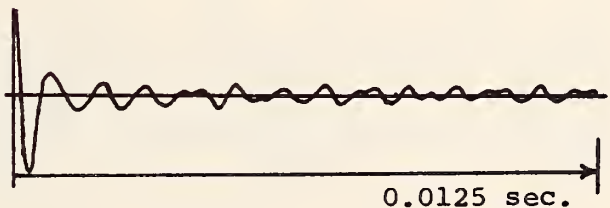
Station 3A
Recorded 4/11/75



Station 3A
Recorded 8/30/73
(Station 6, ref. 1)



Station 4A
Recorded 4/11/75



Station 4A
Recorded 8/30/73
(Station 5, ref. 1)

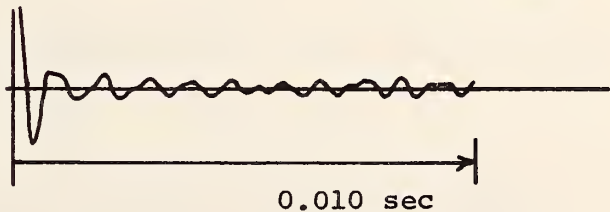


FIGURE 16.- REPEATABILITY OF SIGNATURES ON
85-101 SEPARATION BRIDGE;
FILTER: 1,000 - 6,400 Hz.

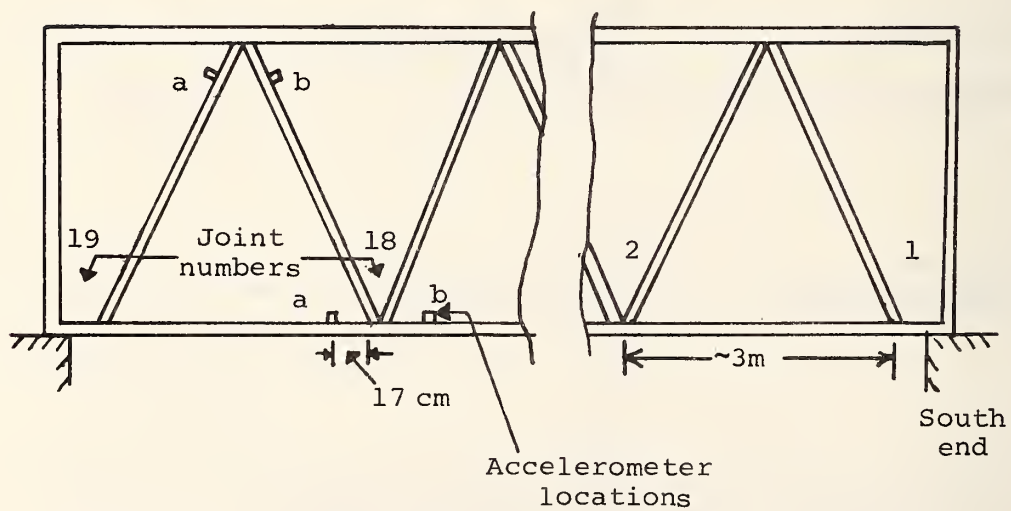
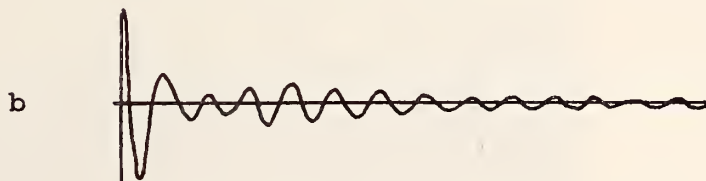
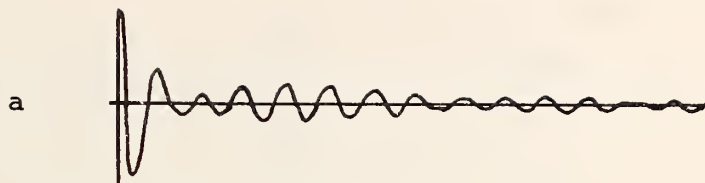
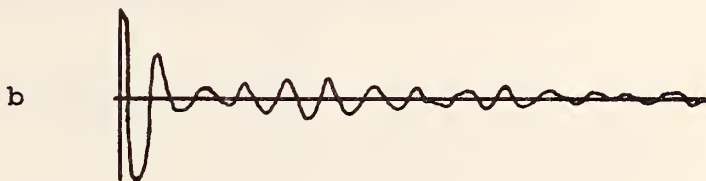
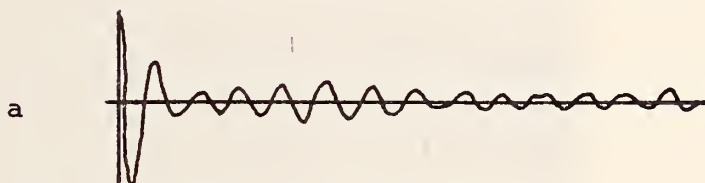


FIGURE 17.- SIGNAL BRIDGE, LOOKING NORTH ACROSS
EAST APPROACH TO SAN FRANCISCO BAY BRIDGE.

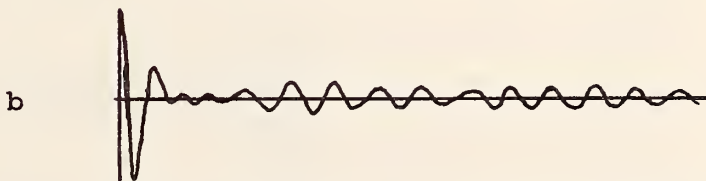
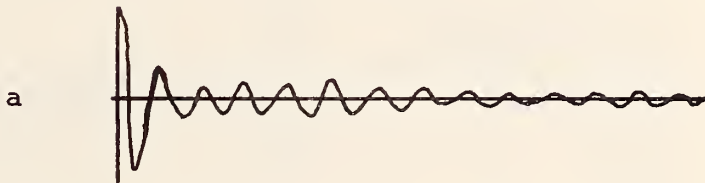
Joint 5



Joint 7



Joint 16



0.00625 sec

FIGURE 18.- SIGNATURES OF LOWER WEST CHORD;
FILTER: 2,000 - 4,800 Hz.

Lower east chord

Joint 7

a

b

Joint 8

a

b

Upper diagonal
member

Joint 9

a

b

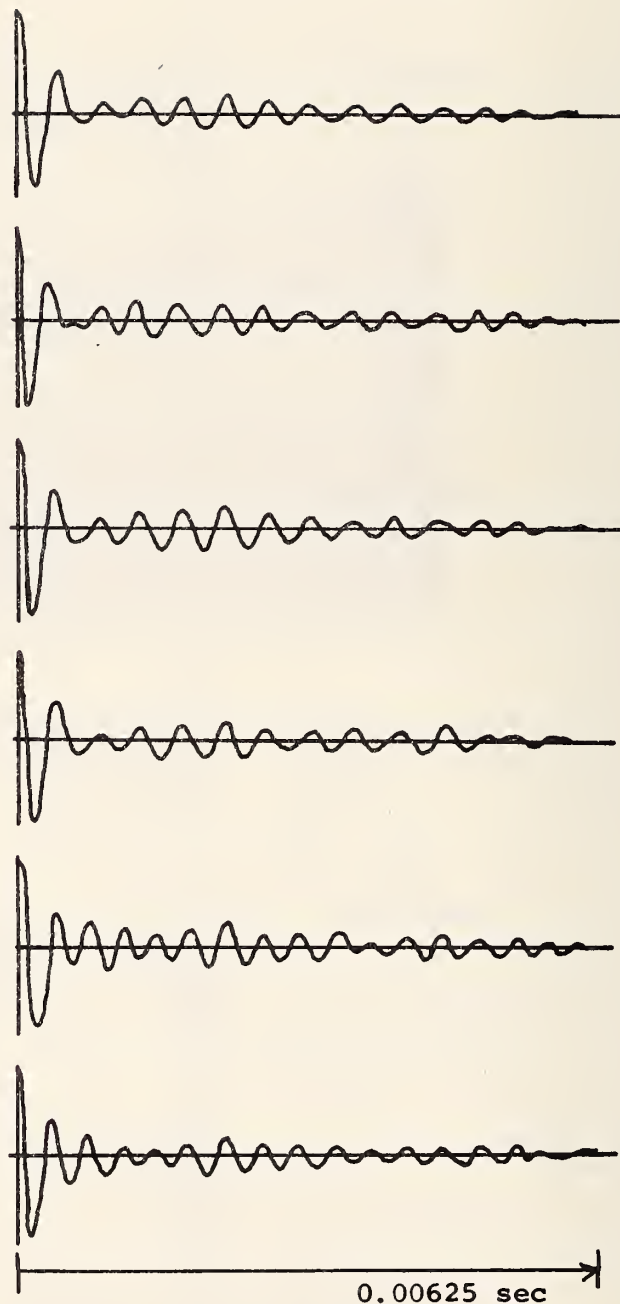


FIGURE 19.- SIGNATURES OF LOWER EAST CHORD
AND UPPER DIAGONAL MEMBER;
FILTER: 2,000 - 4,800 Hz.

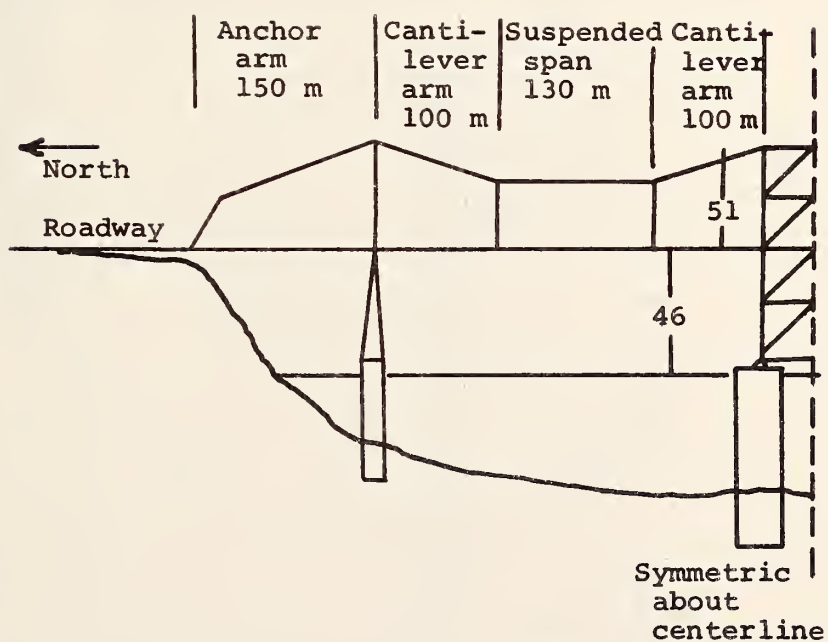


FIGURE 20.- CARQUINEZ BRIDGES, WEST
CARQUINEZ BRIDGE IN FOREGROUND.

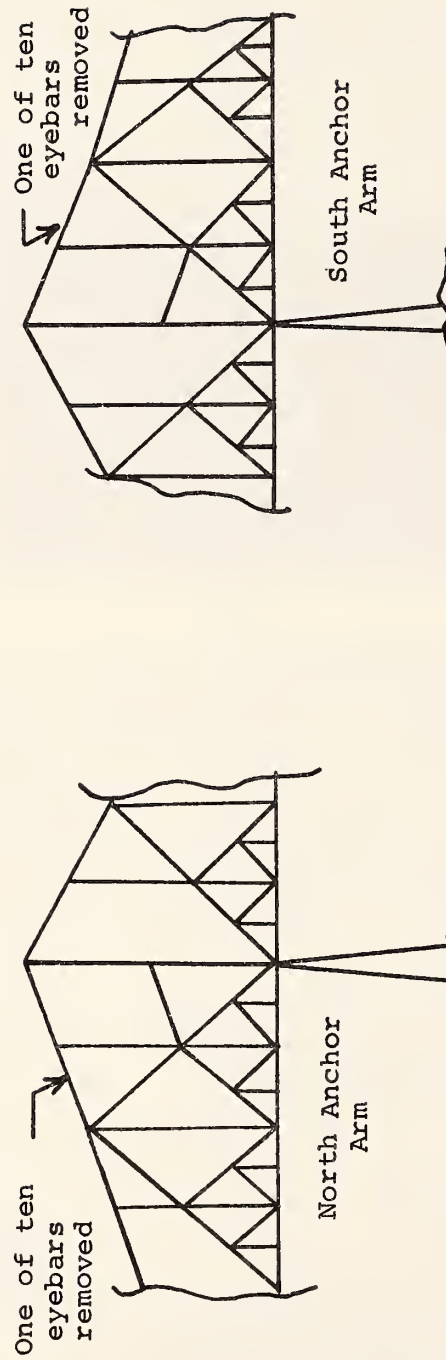


FIGURE 21.- LOCATIONS OF EYEBAR REMOVAL ON
WEST CARQUINEZ BRIDGE.

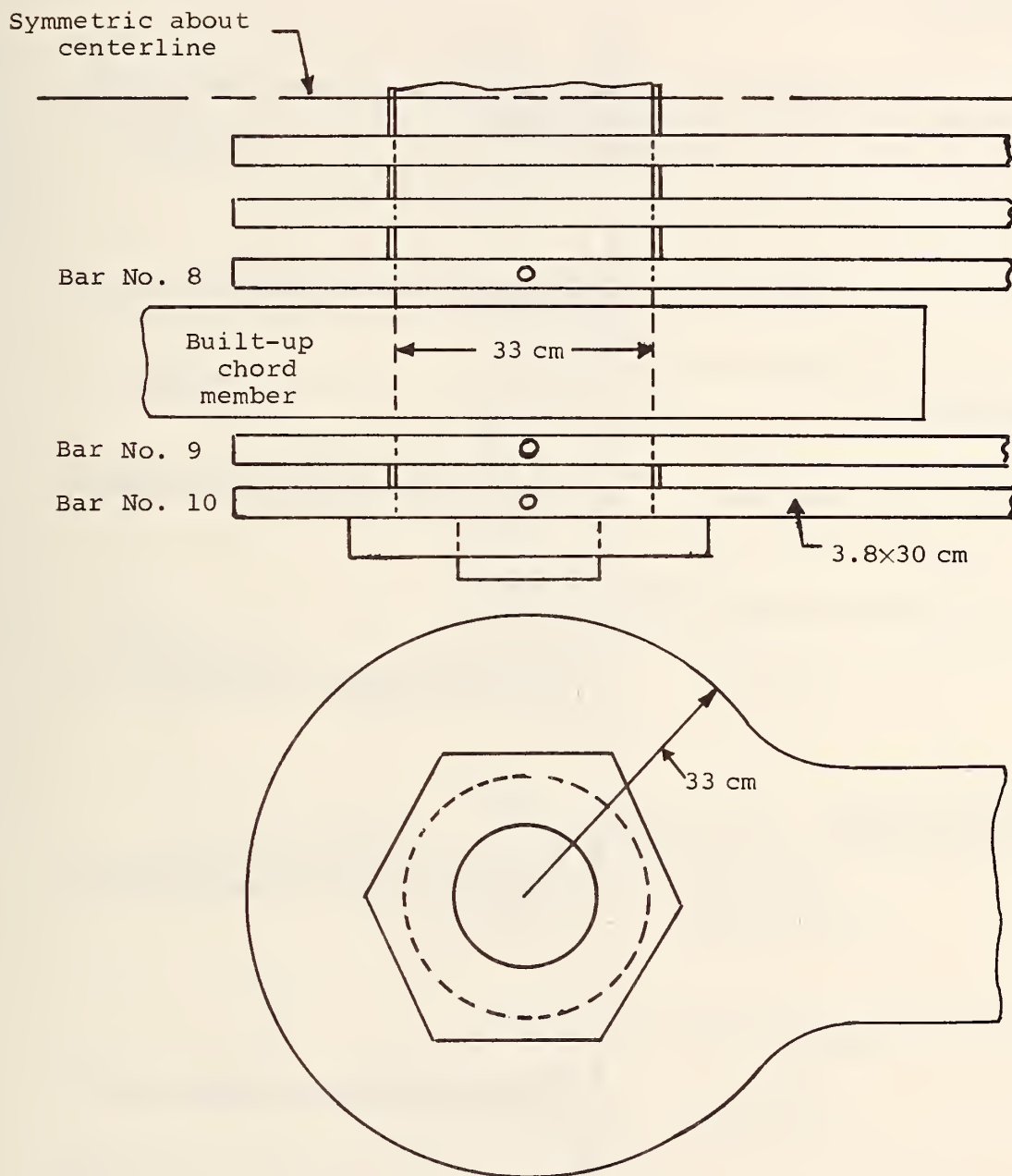
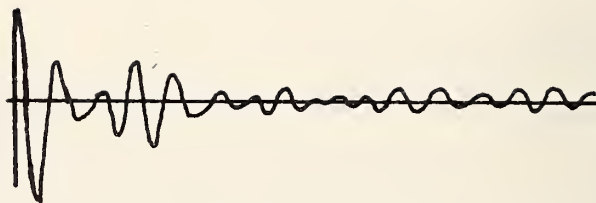


FIGURE 22.- EYEBAR CONFIGURATION AT REMOVAL LOCATION.

South end

Old bar

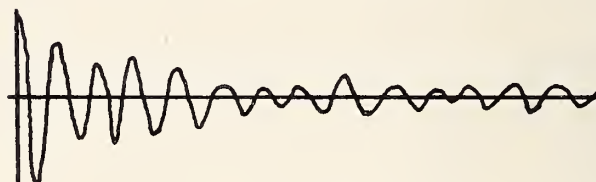


New bar

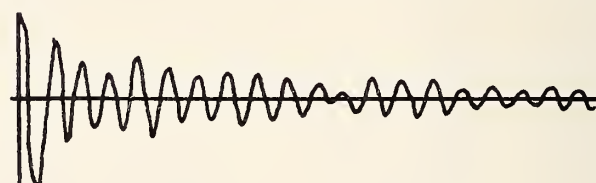


North end

Old bar

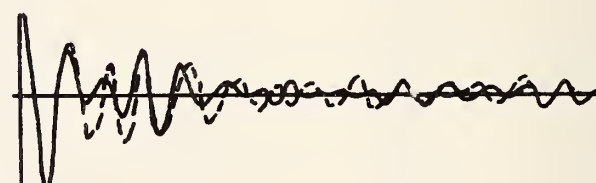


New bar

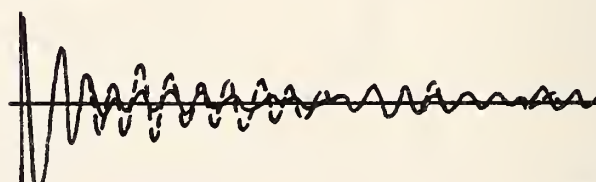


Superposition

Old bars



New bars



0.00125 sec

FIGURE 23.- EYEBAR REPLACEMENT, BAR NO. 10 ;
FILTER: 6,400 - 20,800 Hz.

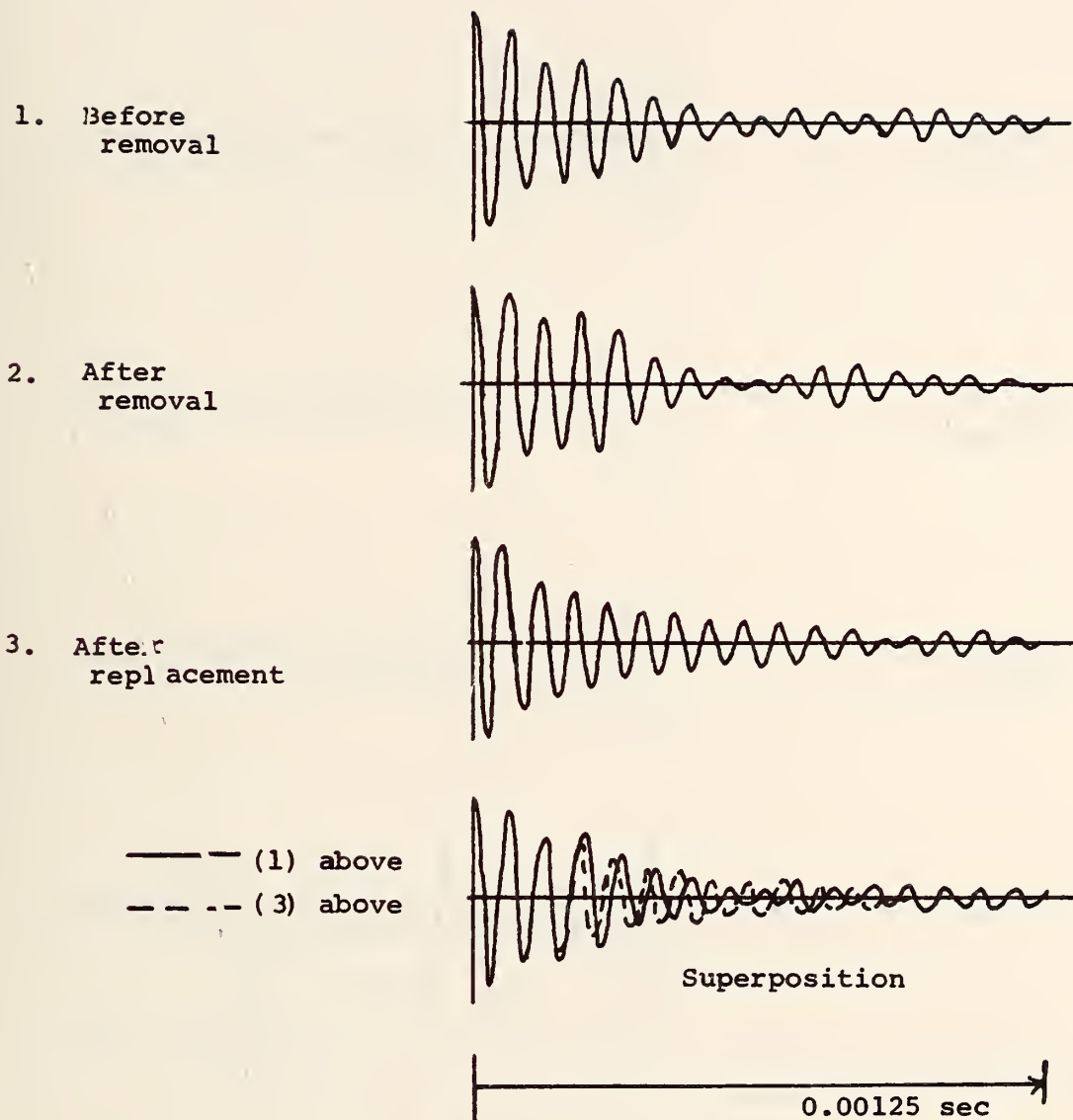


FIGURE 24.-- EYEBAR REPLACEMENT; SOUTH END;
BAR NO. '9; FILTER: 6,400 - 20,800 Hz.

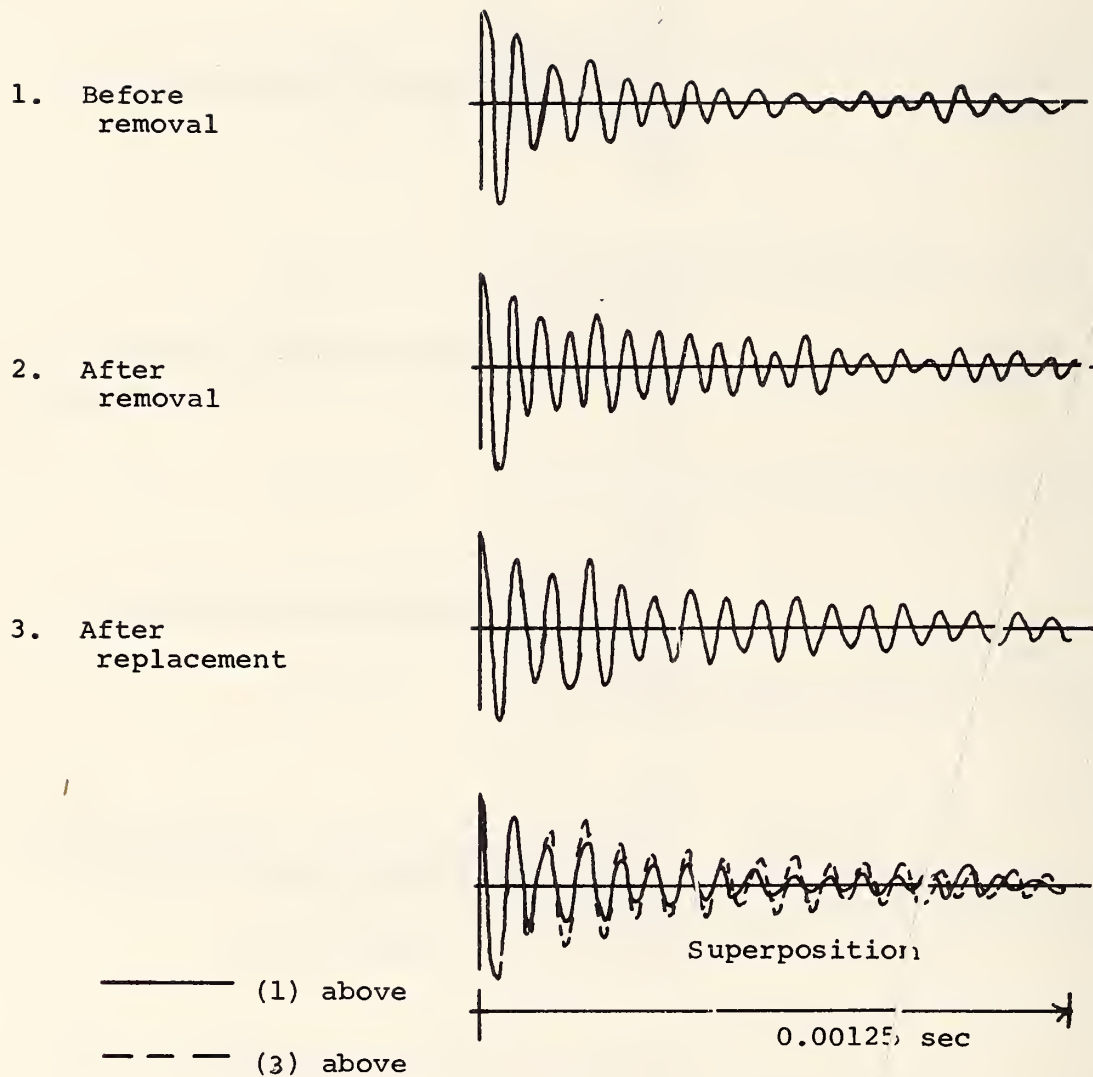


FIGURE 25.- EYEBAR REPLACEMENT; SOUTH END;
BAR NO. 8; FILTER: 6,400 - 20,800 Hz.

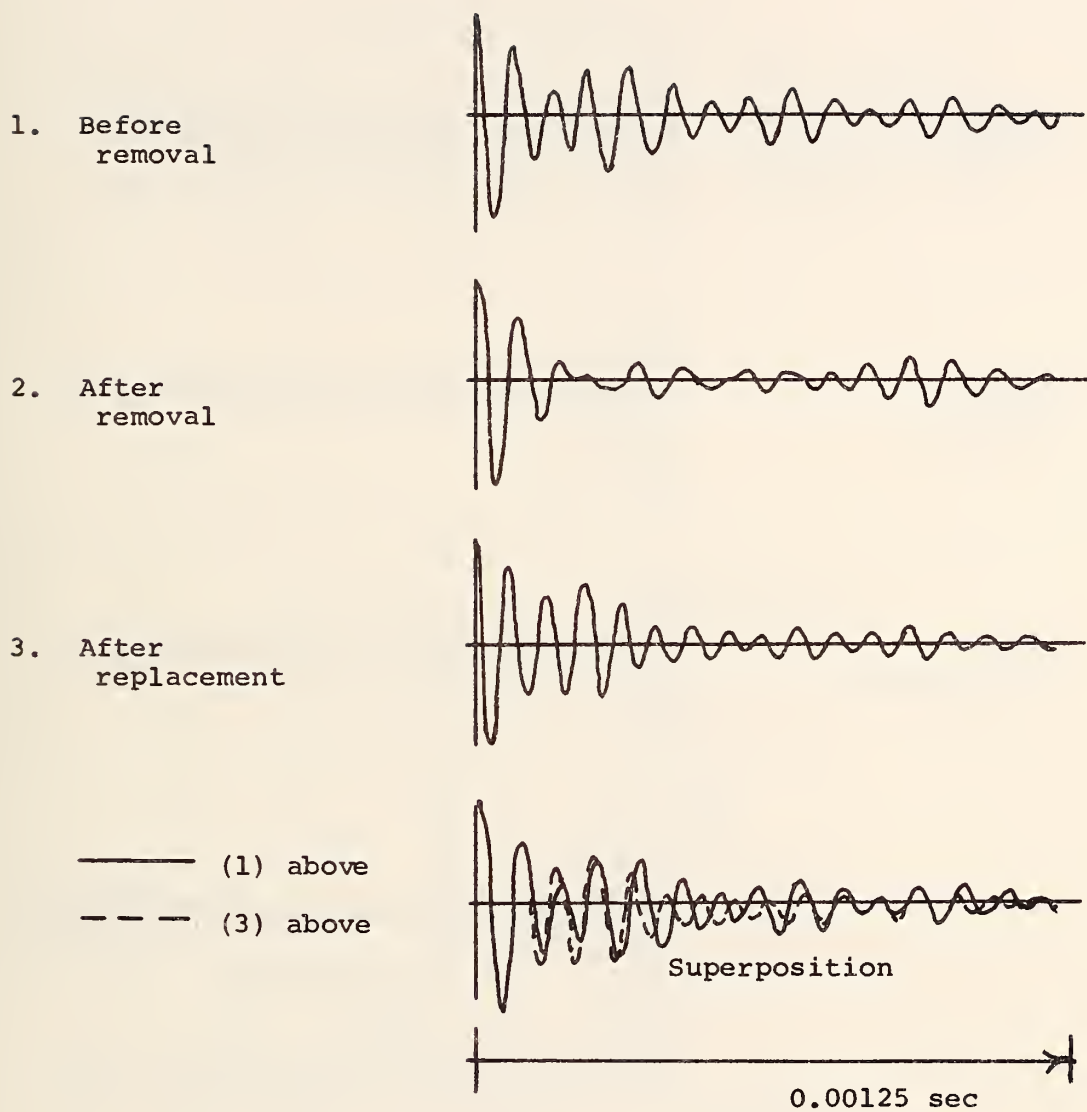


FIGURE 26.- EYEBAR REPLACEMENT; NORTH END;
BAR NO. 9; FILTER: 6,400 - 20,800 Hz.

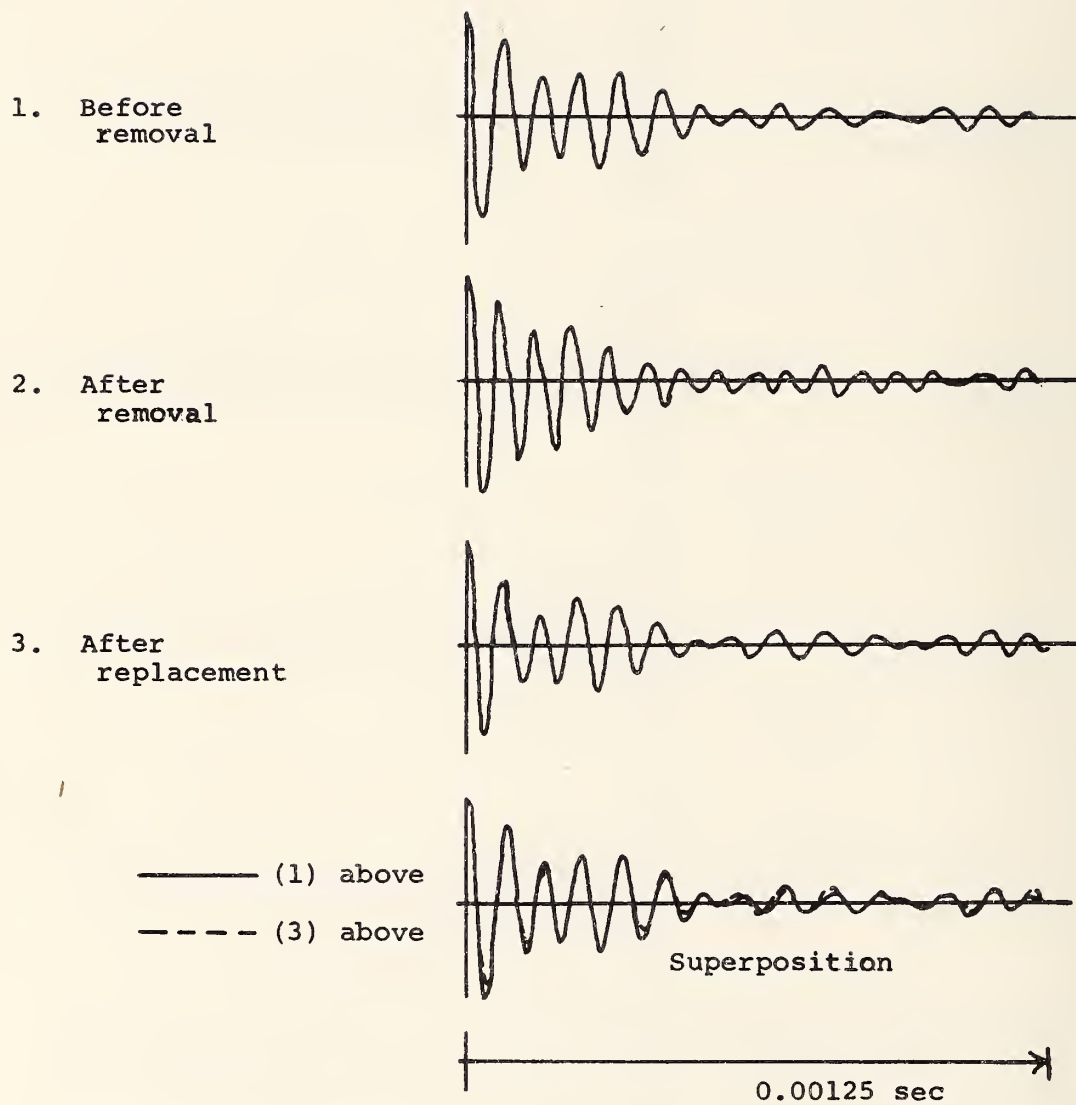


FIGURE 27.- EYEBAR REPLACEMENT; NORTH END;
BAR NO. 8; FILTER: 6,400 - 20,800 Hz.

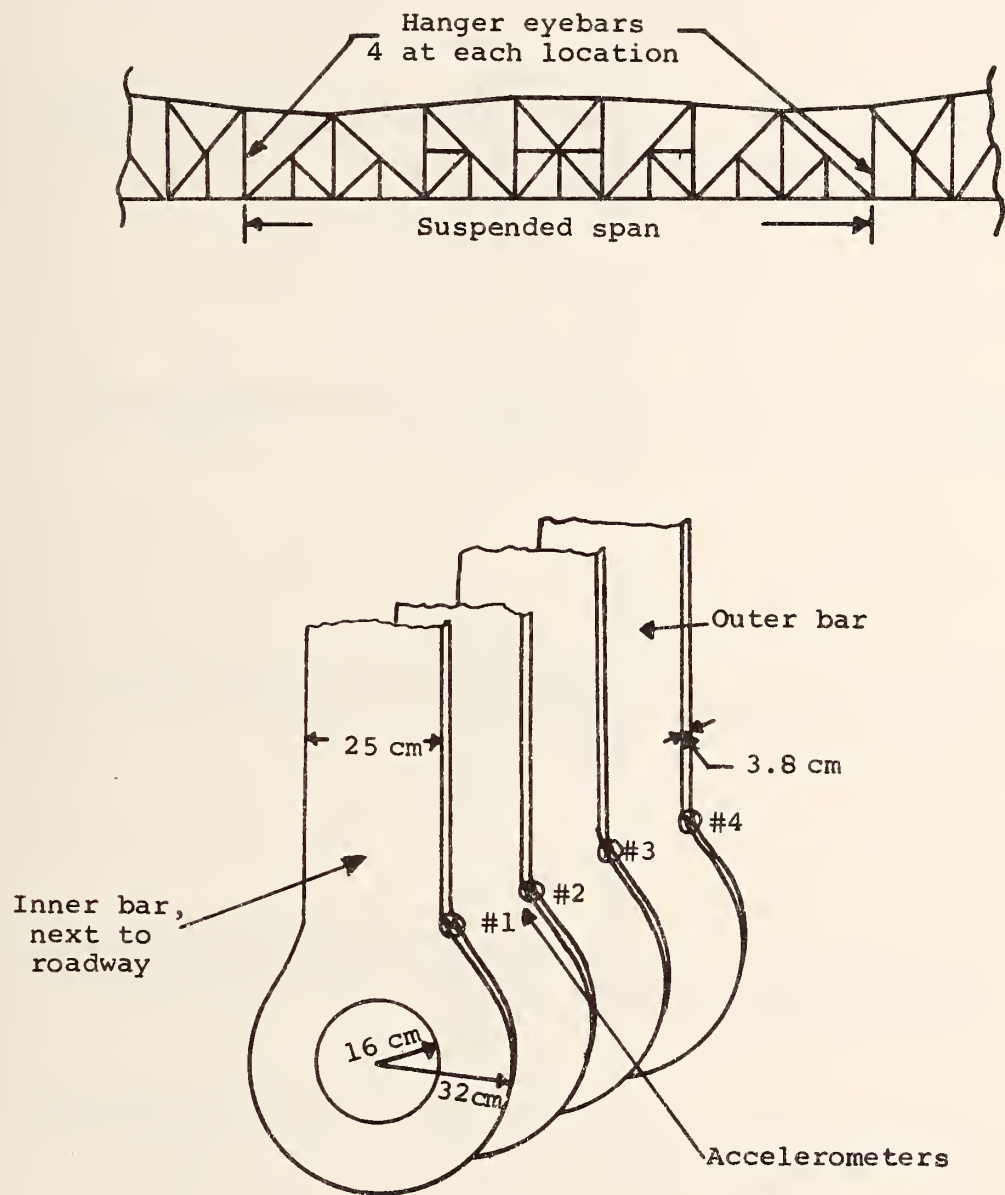


FIGURE 28.- HANGER EYEBAR LOCATIONS.

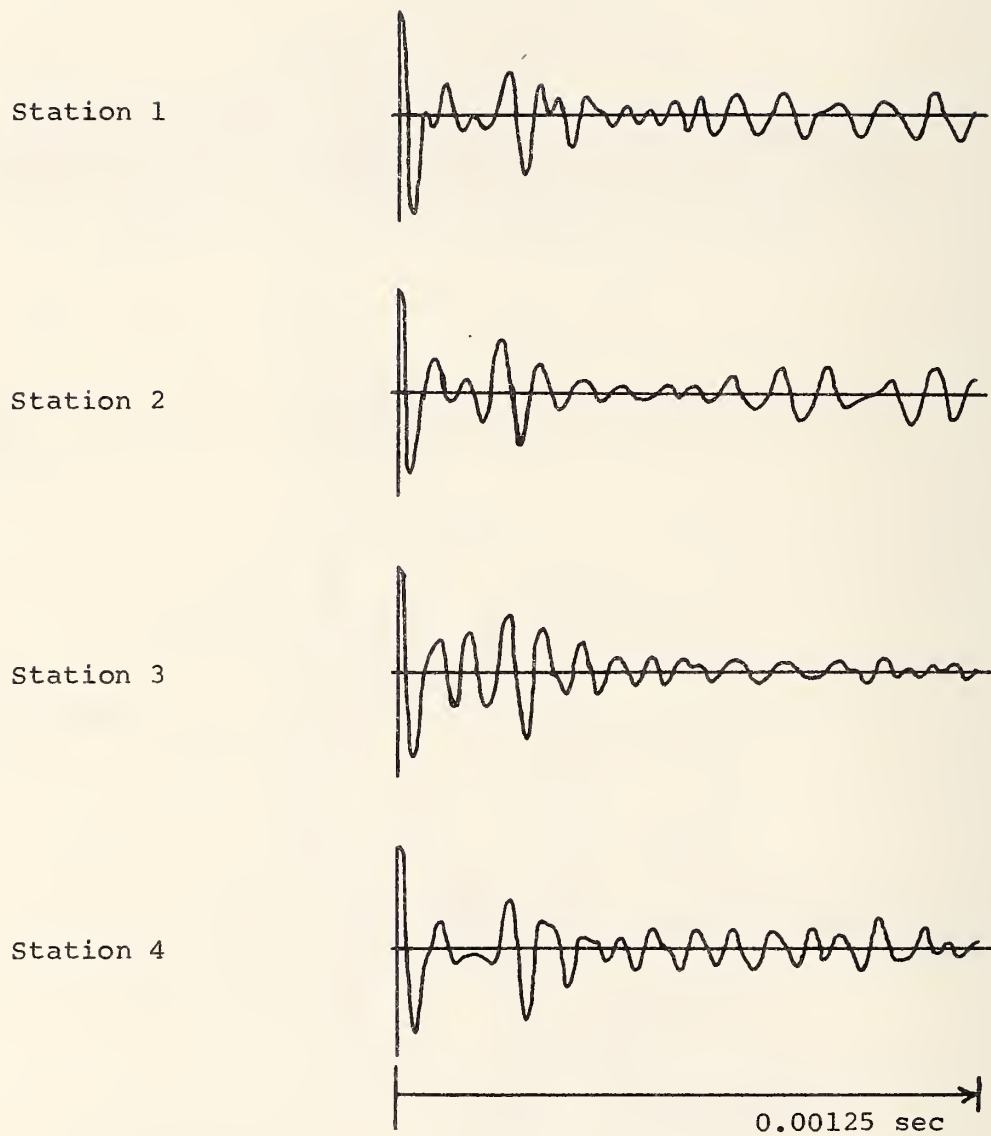


FIGURE 29.- SIGNATURES OF HANGER EYEBARS;
2/22/75; FILTER: 6,400 - 20,800 Hz.

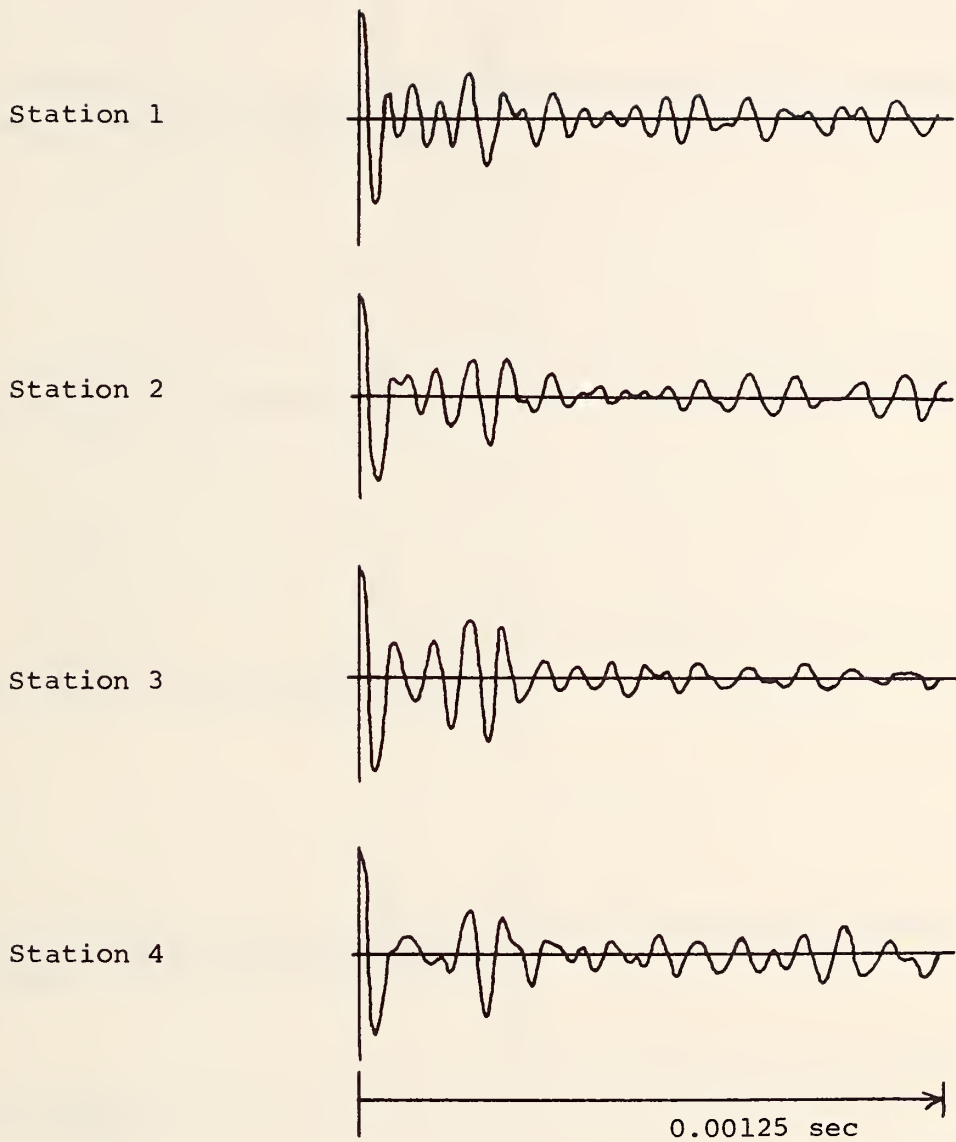


FIGURE 30.- SIGNATURES OF HANGER EYEBARS;
3/4/75; FILTER: 6,400 - 20,800 Hz.

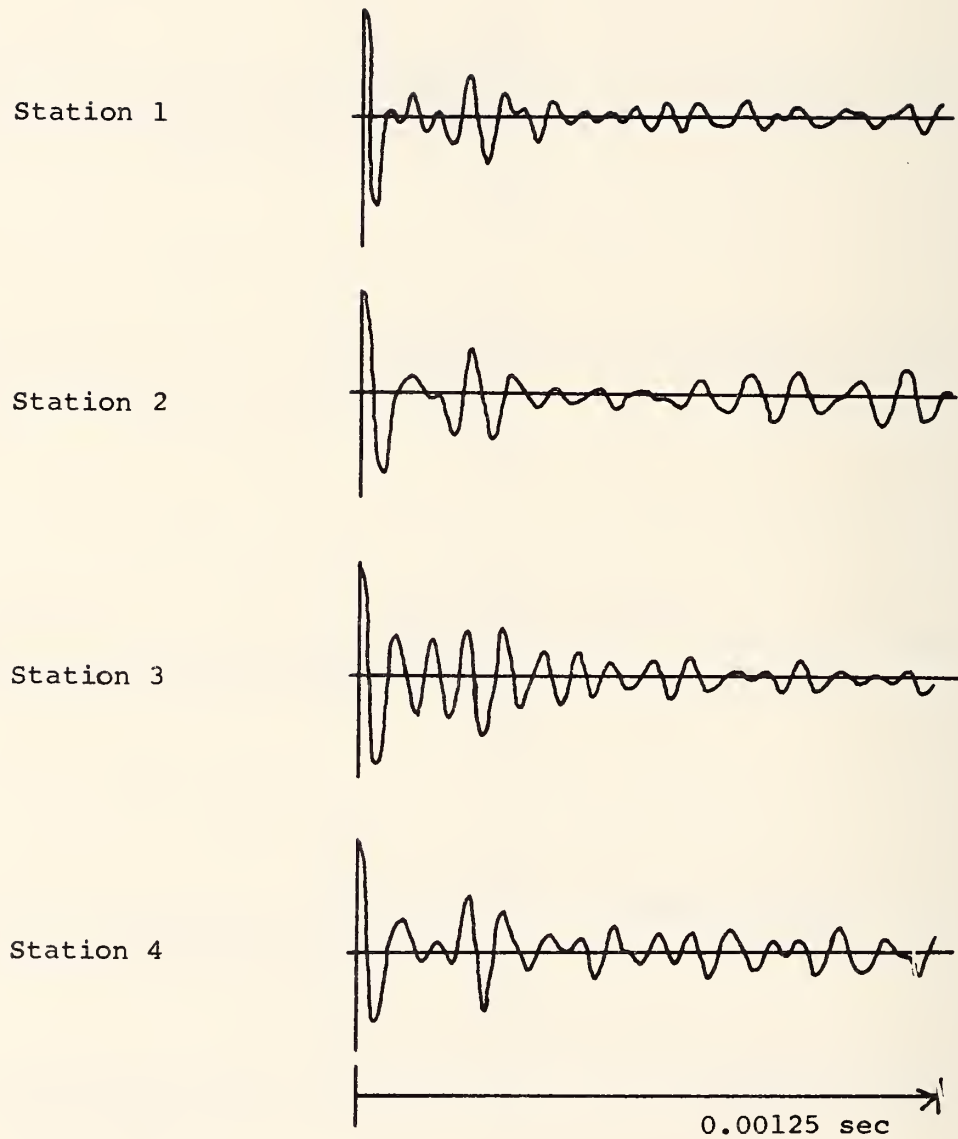


FIGURE 31.- SIGNATURES OF HANGER EYEBARS;
3/20/75; FILTER: 6,400 - 20,800 Hz.

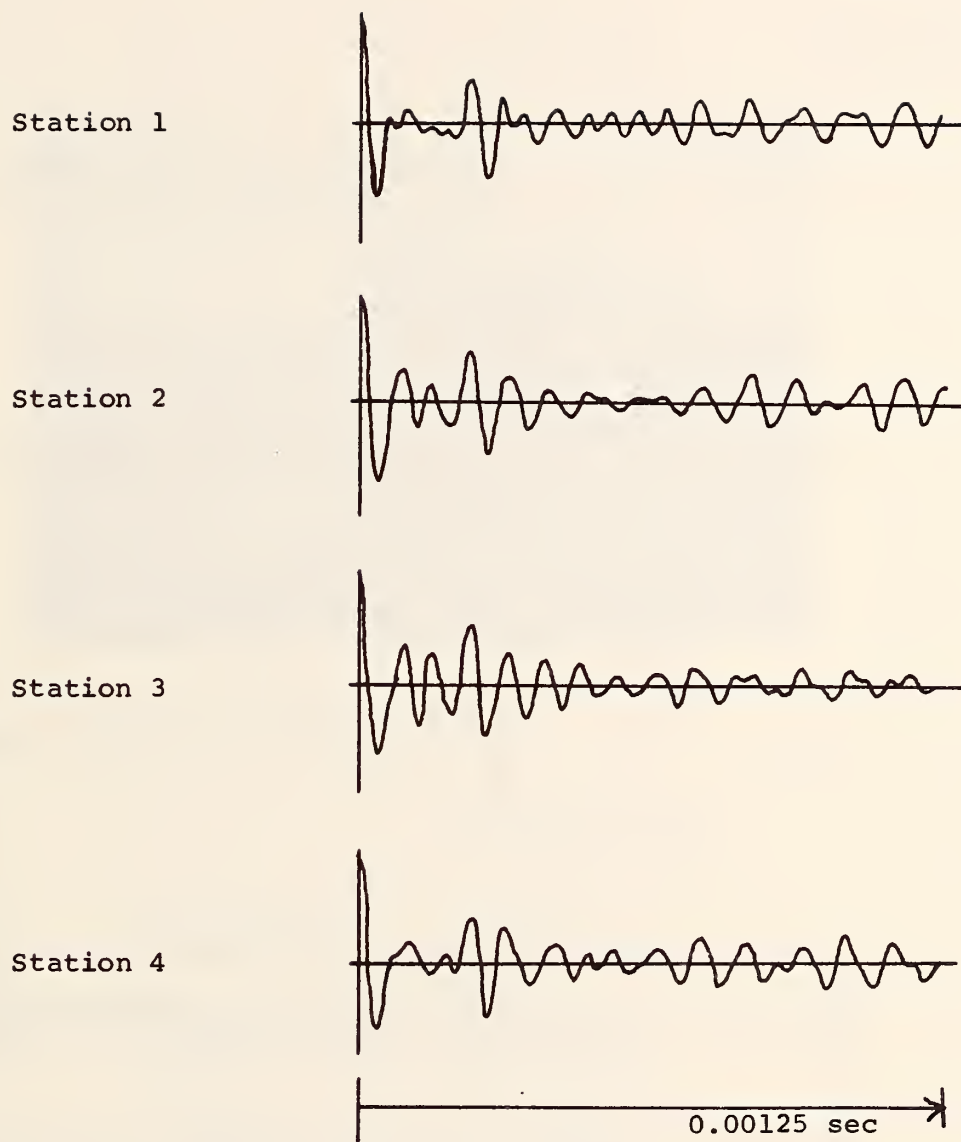
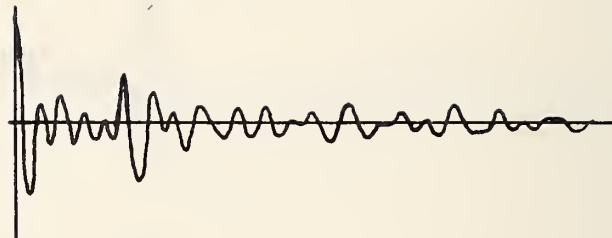


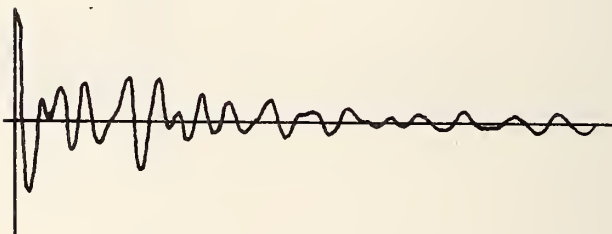
FIGURE 32.- SIGNATURES OF HANGER EYEBARS;
5/20/75; FILTER: 6,400 - 20,800 Hz.

East Side

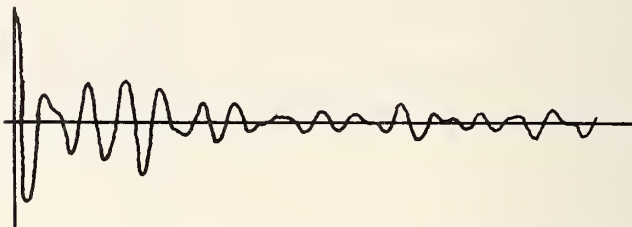
Station 1



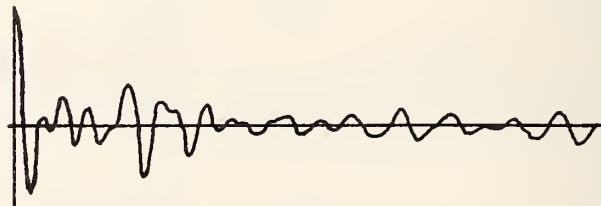
Station 2



Station 3



Station 4



0.00125 sec

FIGURE 33.- SIGNATURES OF HANGER BARS; EAST SIDE;
5/20/75; FILTER: 6,400 - 20,800 Hz.

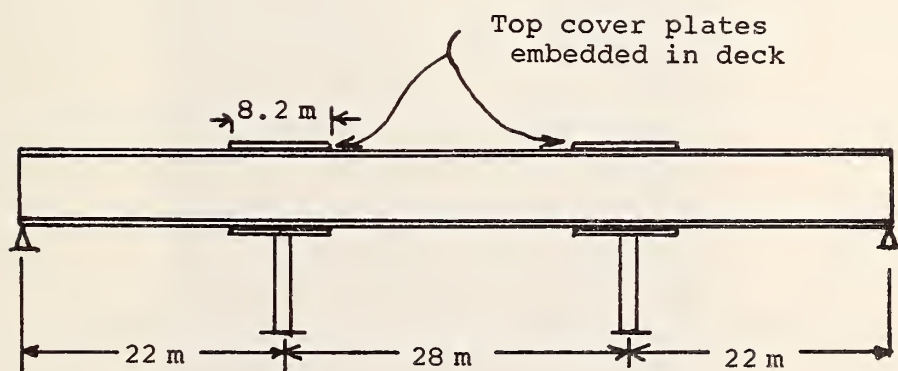


FIGURE 34.- TEST BRIDGE IN MISSOURI FOR
DYNAMIC FATIGUE STUDY.

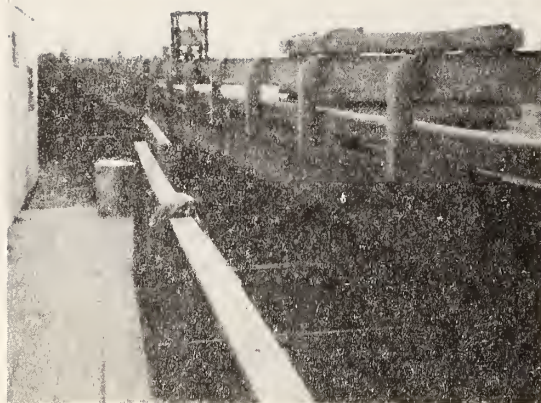
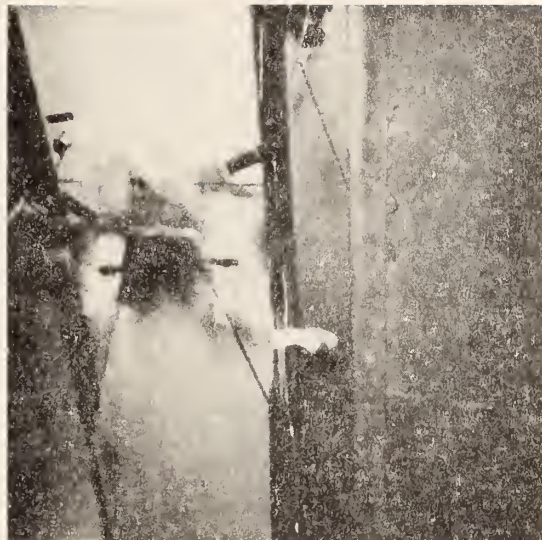


FIGURE 35.- BALLAST LOADING AND ACTUATOR
ON MISSOURI BRIDGE.

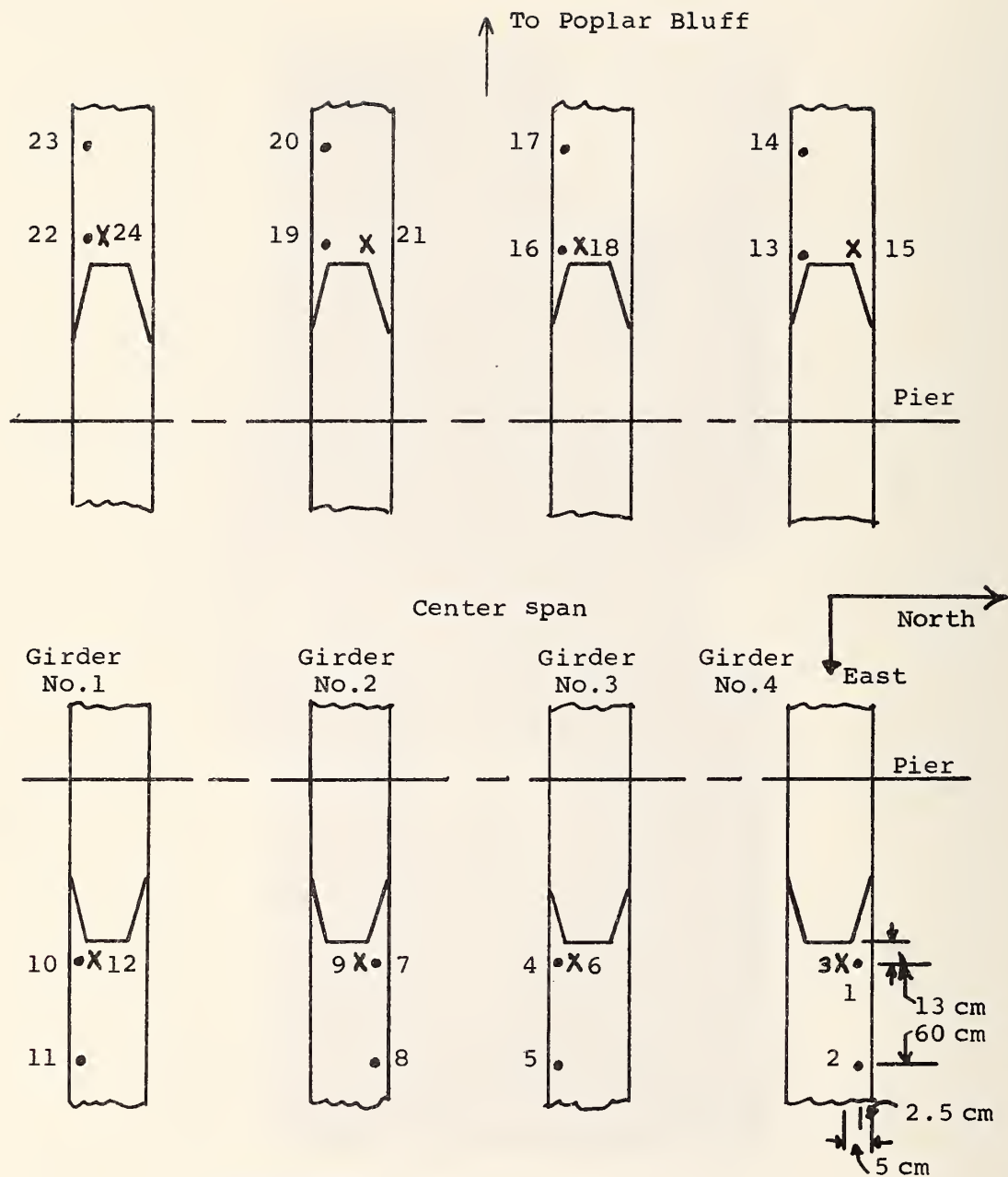


Near Station 10



Near Station 22

FIGURE 36.- CRACKS IN BOTTOM FLANGE
OF MISSOURI BRIDGE.



X = Top flange nos. 3,6,9,12,15,18,21,24

• = Bottom flange

Plan view (looking down on girders)

FIGURE 37.- TRANSDUCER LOCATIONS ON MISSOURI BRIDGE.

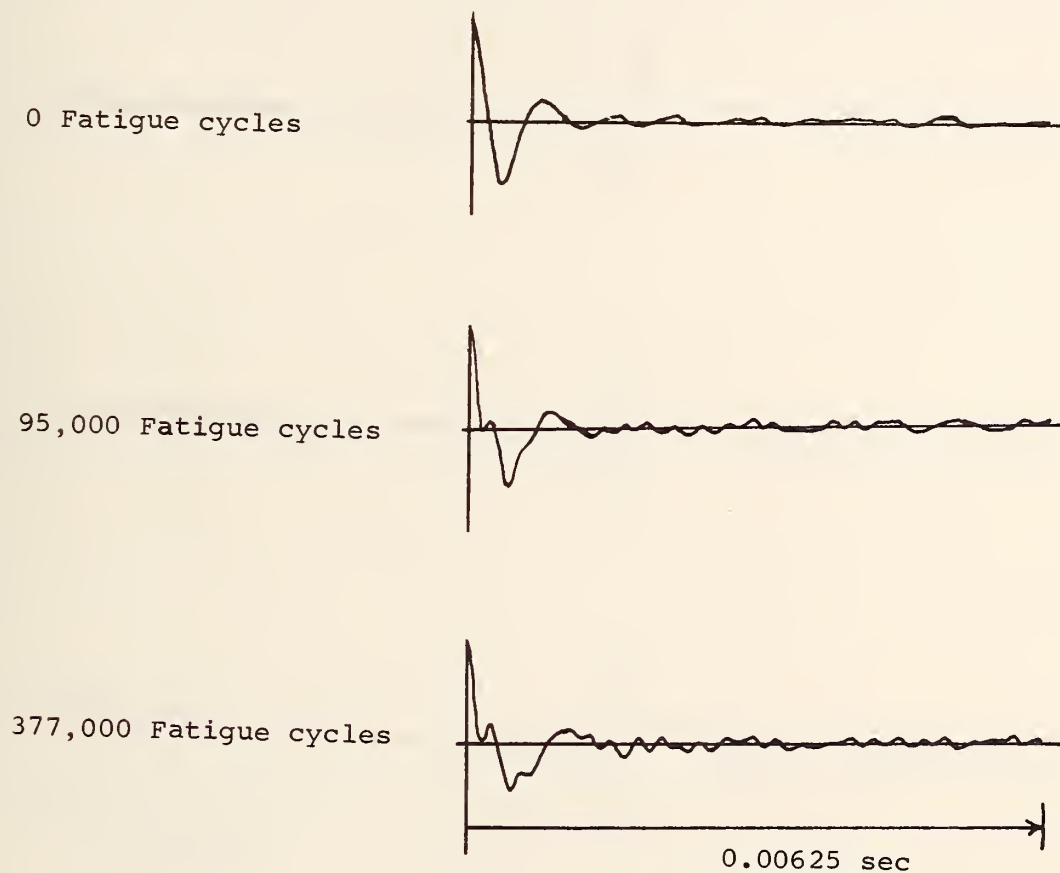


FIGURE 38.- STATION 3; TOP FLANGE; FILTER: 960 - 5,200 Hz;
EXCITATION: STEEL-WHEELED DOLLY.

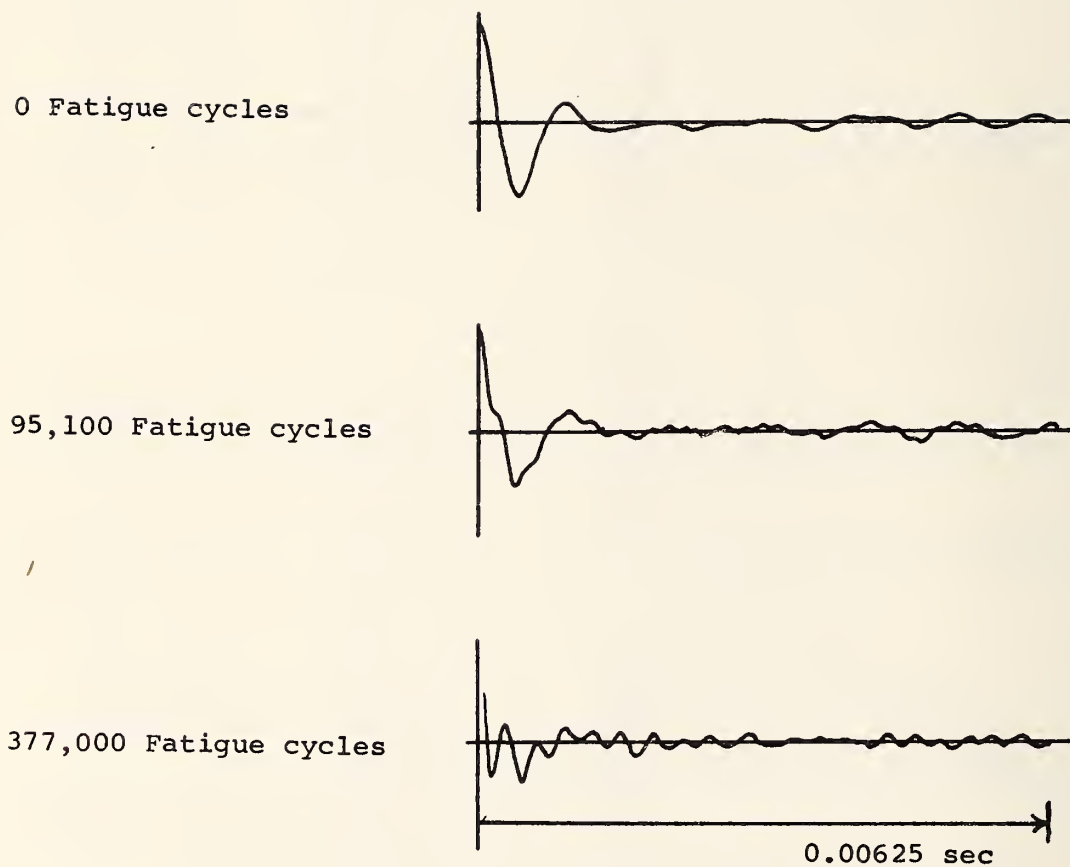
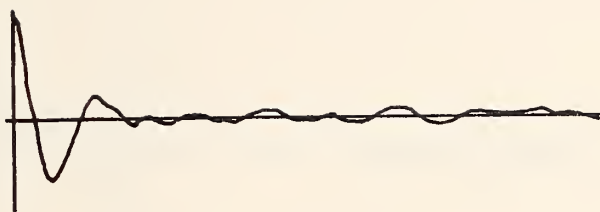


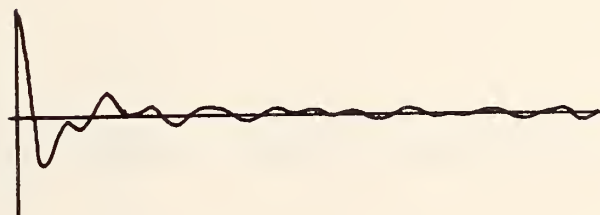
FIGURE 39.- STATION 6; TOP FLANGE; FILTER: 960 - 5,200 Hz;
EXCITATION: STEEL-WHEELED DOLLY.

Standard

0 Fatigue cycles



95,100 Fatigue cycles



377,000 Fatigue cycles

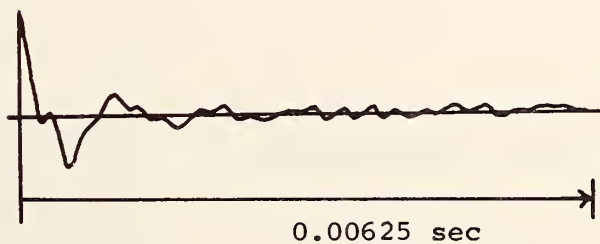


FIGURE 40.- STATION 9; TOP FLANGE; FILTER: 960 - 5,200 Hz;
EXCITATION: STEEL-WHEELED DOLLY.

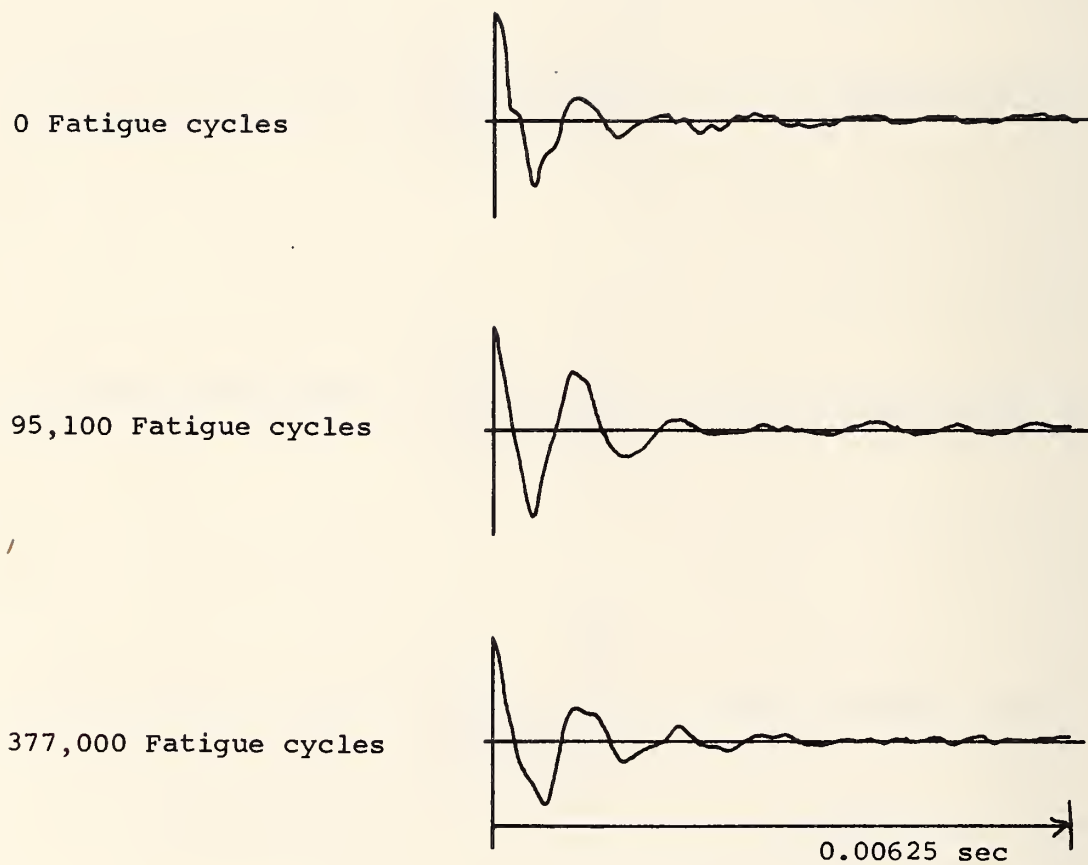


FIGURE 41.- STATION 12; TOP FLANGE; FILTER: 960 - 5,200 Hz;
EXCITATION: STEEL-WHEELED DOLLY.

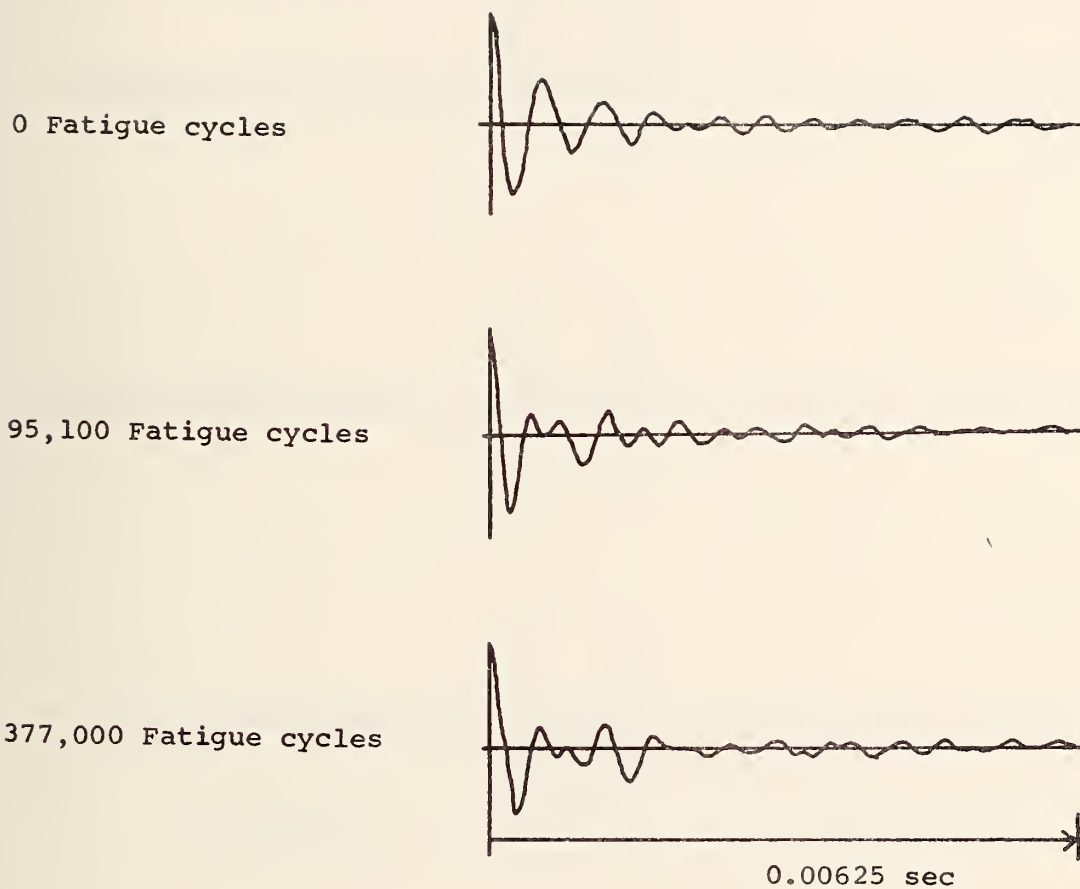
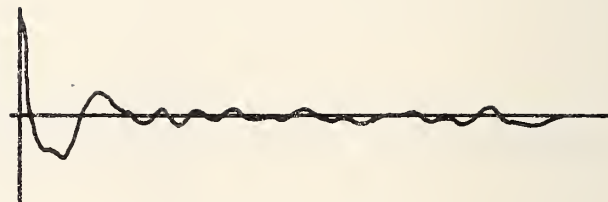
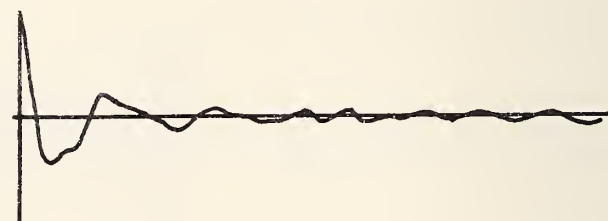


FIGURE 42.- STATION 12; TOP FLANGE; FILTER: 4,000 - 12,000 Hz;
EXCITATION: STEEL-WHEELED DOLLY.

0 Fatigue cycles



95,100 Fatigue cycles



377,000 Fatigue cycles

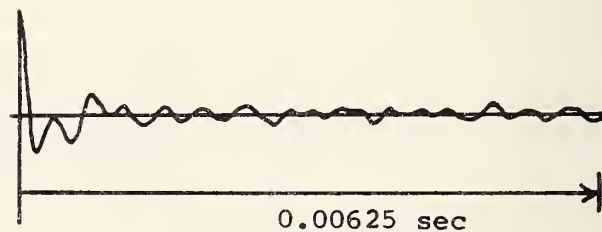
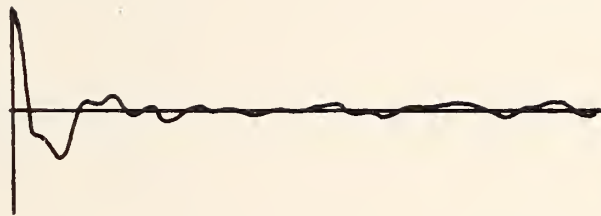


FIGURE 43.- STATION 15; TOP FLANGE; FILTER: 960 - 5,200 Hz ;
EXCITATION: STEEL-WHEELED DOLLY.

0 Fatigue cycles



95,100 Fatigue cycles



377,000 Fatigue cycles

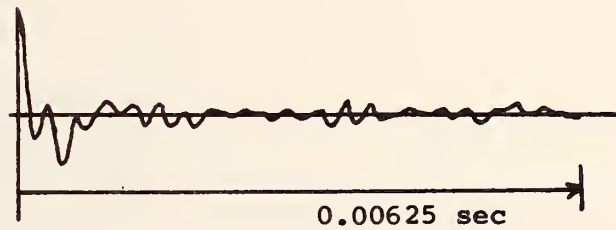


FIGURE 44.- STATION 18; TOP FLANGE; FILTER: 960 - 5,200 Hz;
EXCITATION: STEEL-WHEELED DOLLY.

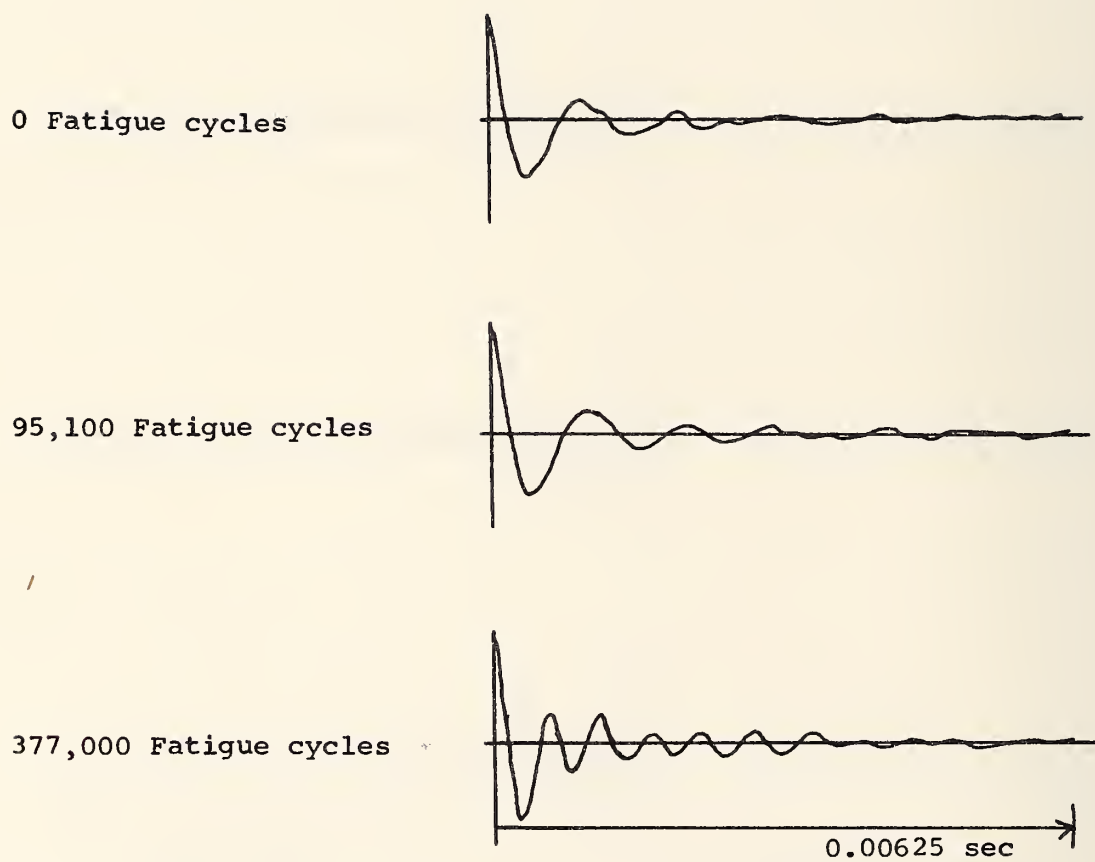
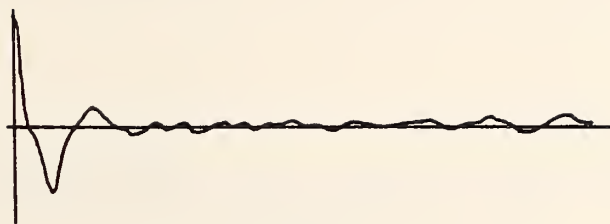
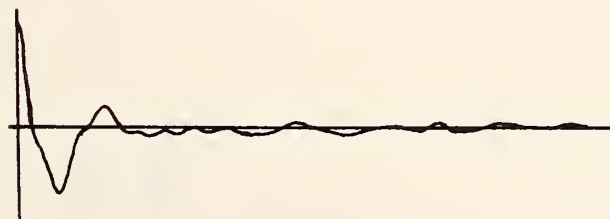


FIGURE 45.- STATION 21; TOP FLANGE; FILTER: 960 - 5,200 Hz;
EXCITATION: STEEL-WHEELED DOLLY.

0 Fatigue cycles



95,100 Fatigue cycles



377,000 Fatigue cycles

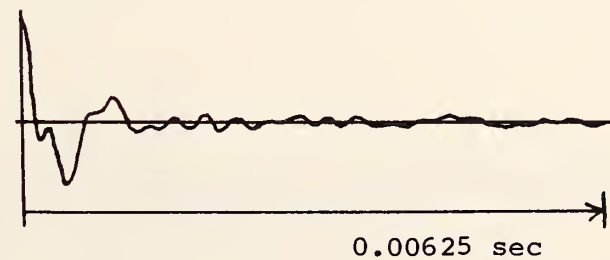
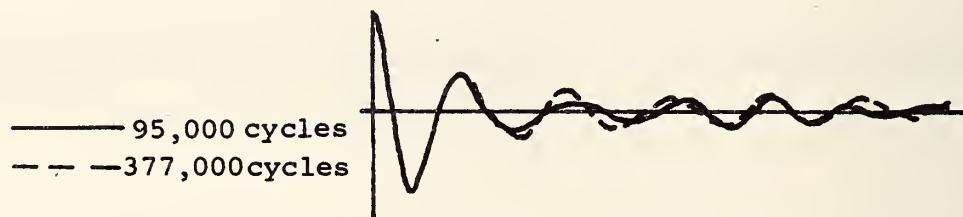
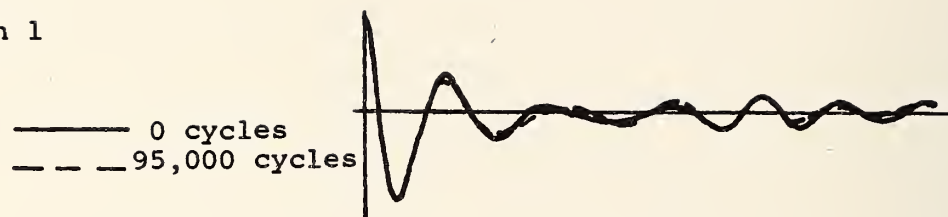


FIGURE 46.- STATION 24; TOP FLANGE; FILTER: 960 - 5,200 Hz;
EXCITATION: STEEL-WHEELED DOLLY.

Station 1



Station 2

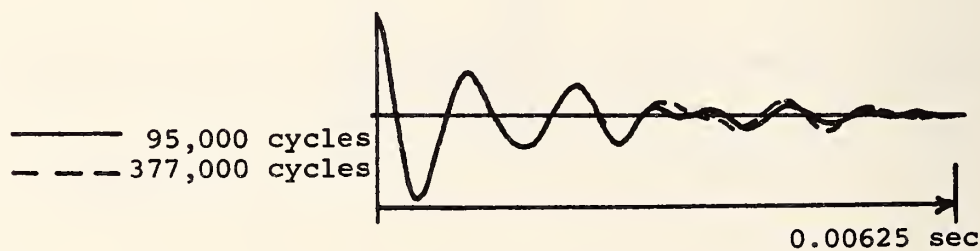
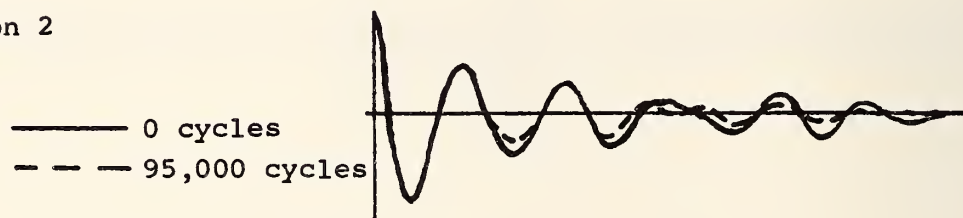
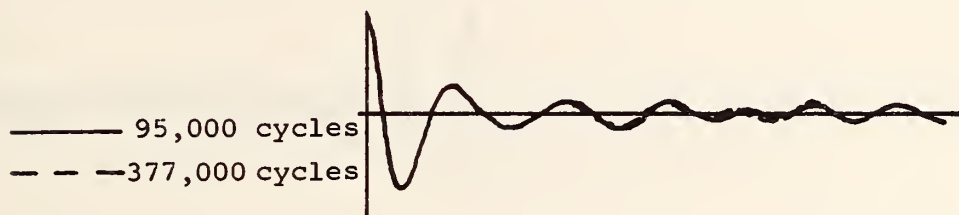
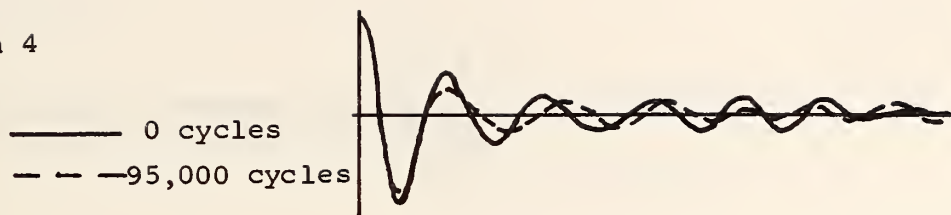
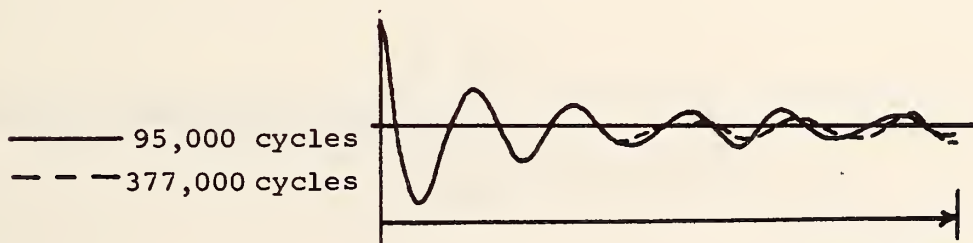
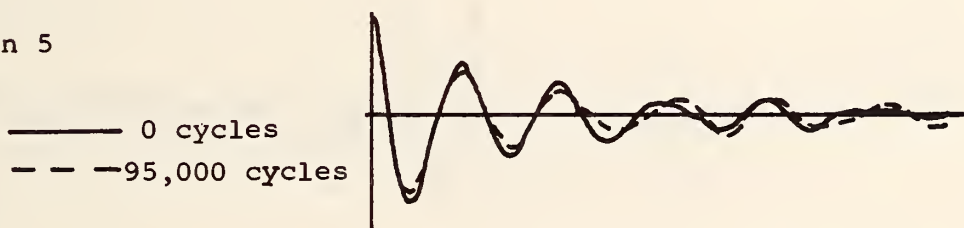


FIGURE 47.- COMPARISON OF BOTTOM FLANGE SIGNATURES,
STATIONS 1 and 2; FILTER: 960 - 5,200 Hz;
EXCITATION: STEEL-WHEELED DOLLY.

Station 4



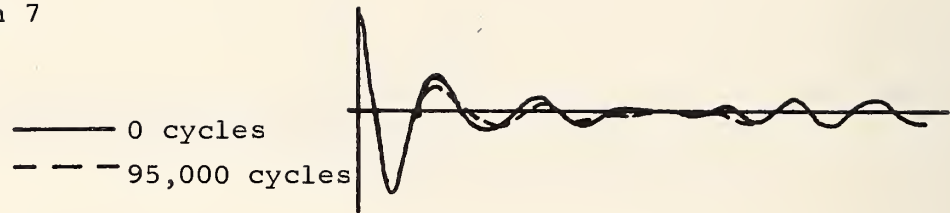
Station 5



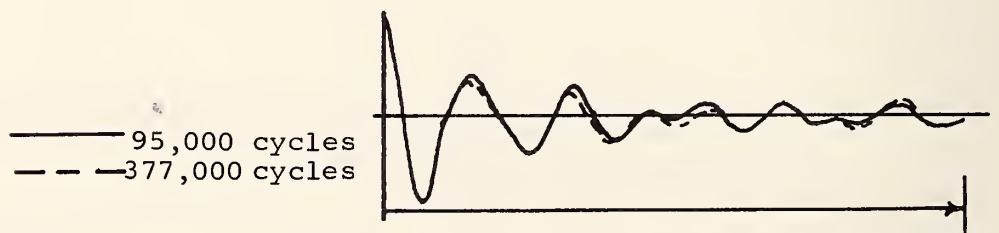
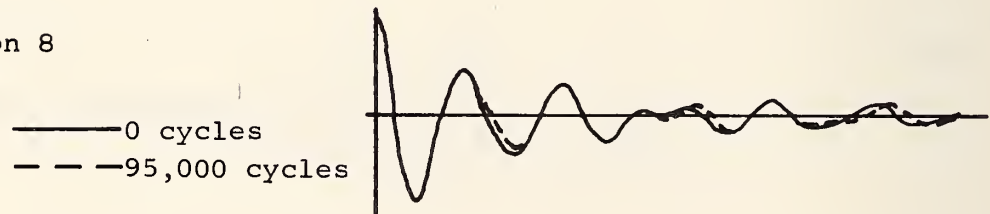
0.00625 sec

FIGURE 48.- COMPARISON OF BOTTOM FLANGE SIGNATURES,
STATIONS 4 AND 5; FILTER: 960 - 5,200 Hz;
EXCITATION: STEEL-WHEELED DOLLY.

Station 7



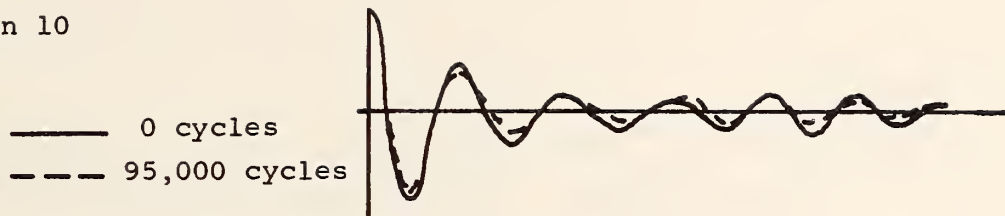
Station 8



0.00625 sec

FIGURE 49.- COMPARISON OF BOTTOM FLANGE SIGNATURES,
STATIONS 7 and 8; FILTER: 960 - 5,200 Hz;
EXCITATION: STEEL-WHEELED DOLLY.

Station 10



Station 11

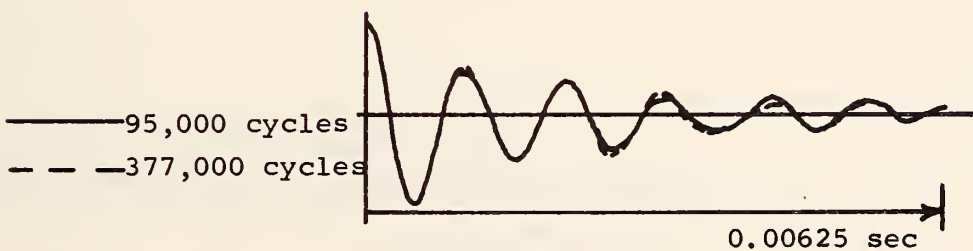
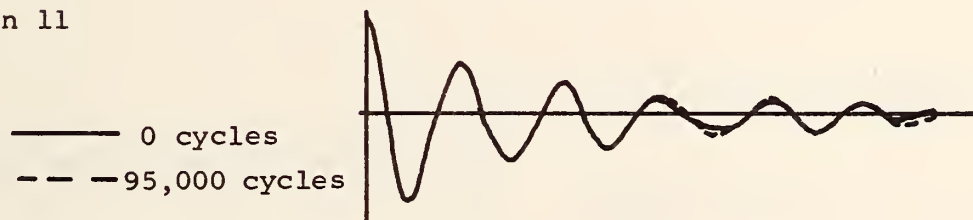
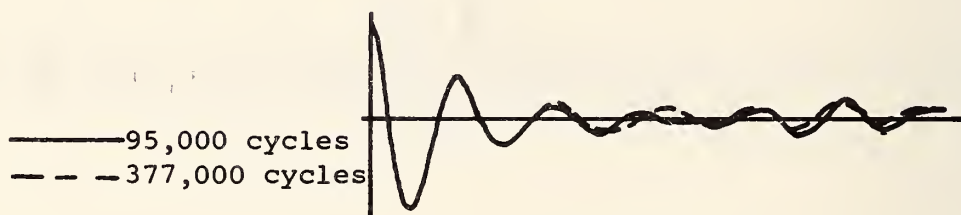
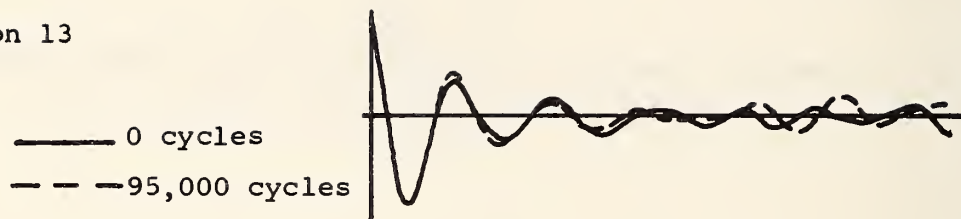


FIGURE 50.- COMPARISON OF BOTTOM FLANGE SIGNATURES,
STATIONS 10 and 11; FILTER: 960 - 5,200 Hz;
EXCITATION: STEEL-WHEELED DOLLY.

Station 13



Station 14

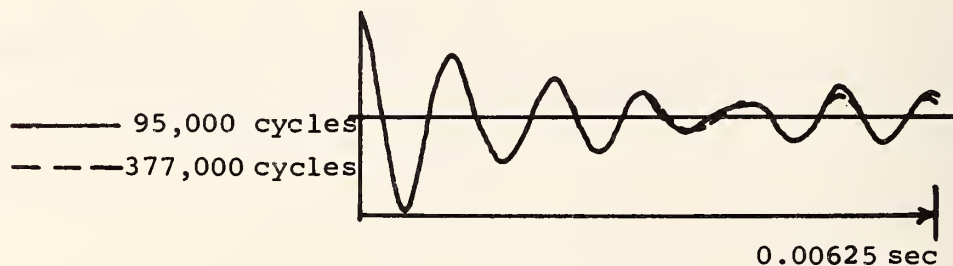
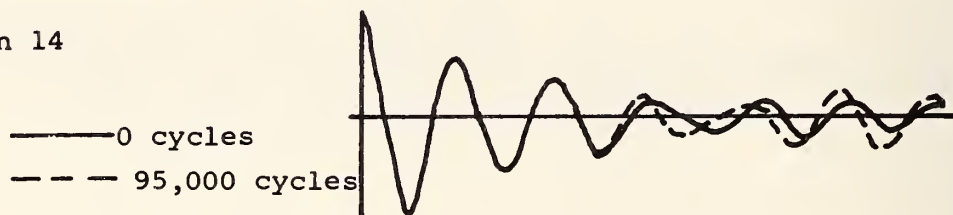
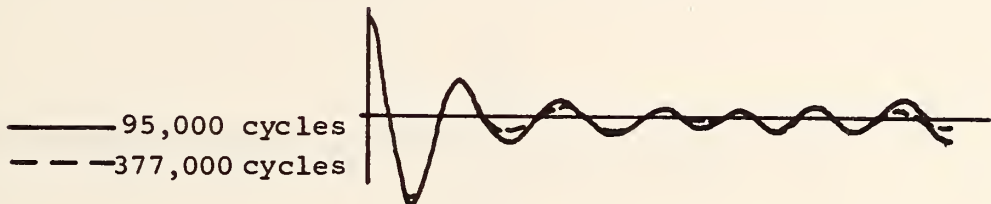
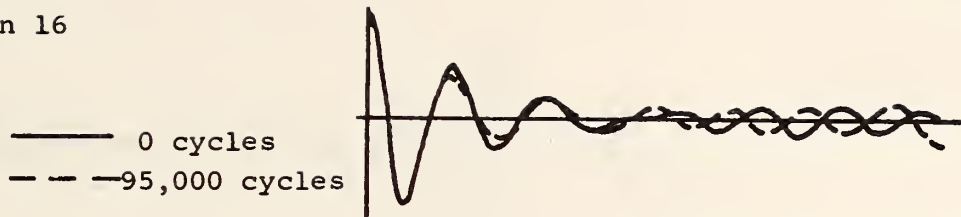
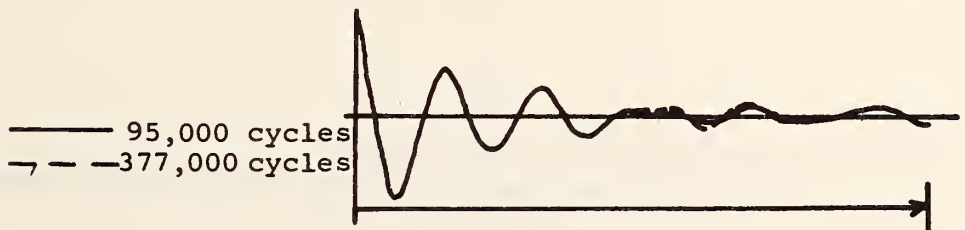
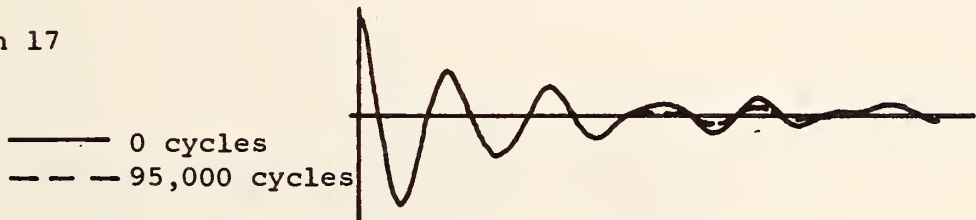


FIGURE 51.- COMPARISON OF BOTTOM FLANGE SIGNATURES,
STATIONS 16 and 17; FILTER: 960 - 5,200 Hz;
EXCITATION: STEEL-WHEELED DOLLY.

Station 16



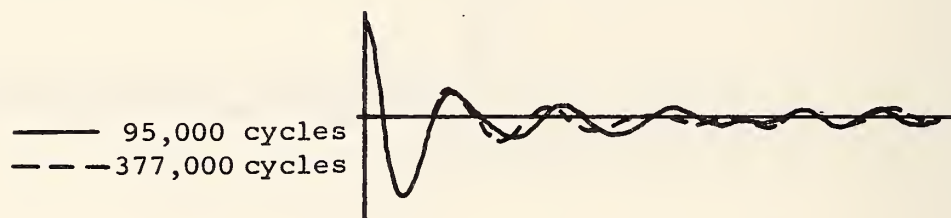
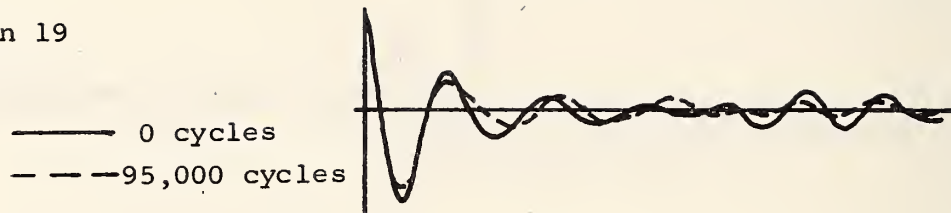
Station 17



0.00625 sec

FIGURE 52.- COMPARISON OF BOTTOM FLANGE SIGNATURES,
STATIONS 16 and 17; FILTER: 960 - 5,200 Hz;
EXCITATION: STEEL-WHEELED DOLLY.

Station 19



Station 20

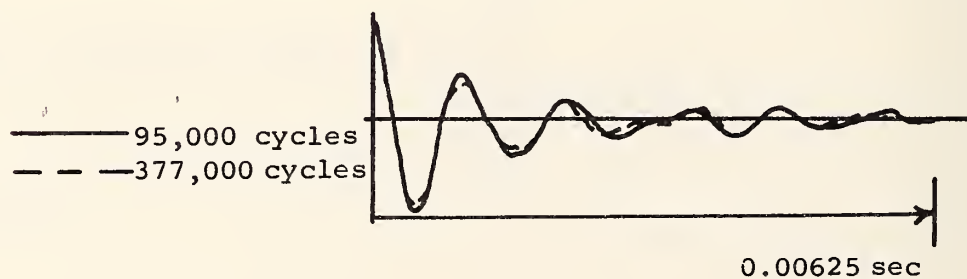
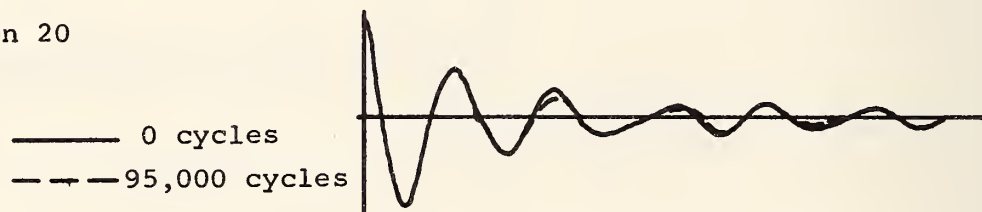
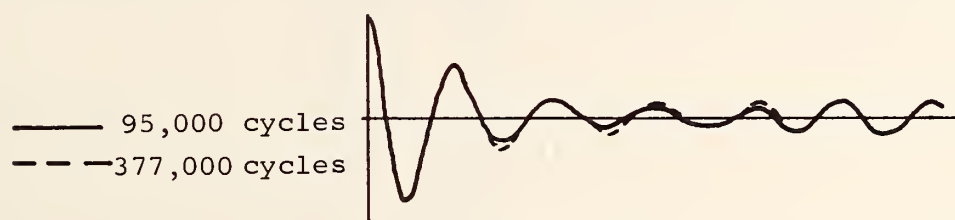
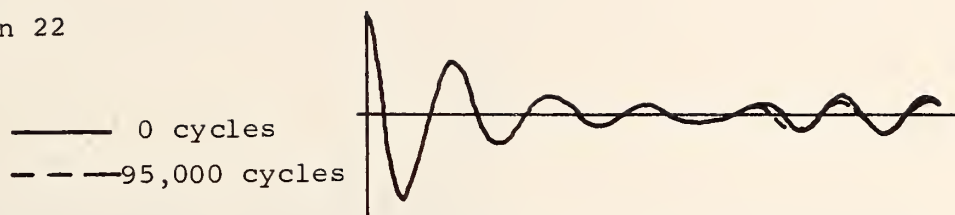


FIGURE 53.- COMPARISON OF BOTTOM FLANGE SIGNATURES,
STATIONS 19 and 20; FILTER: 960 - 5,200 Hz;
EXCITATION: STEEL-WHEELED DOLLY.

Station 22



Station 23

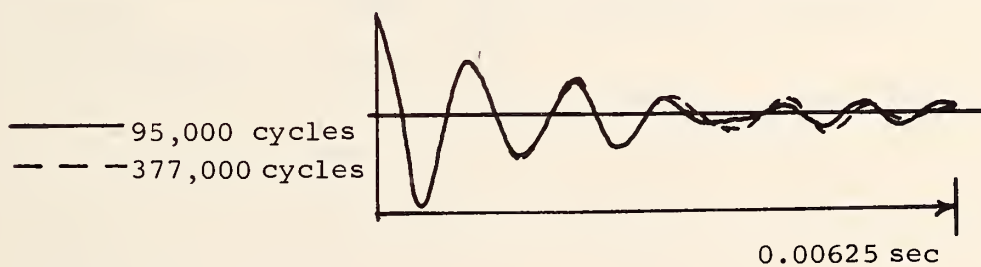
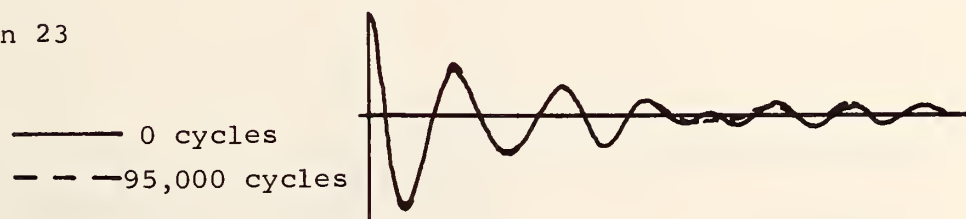
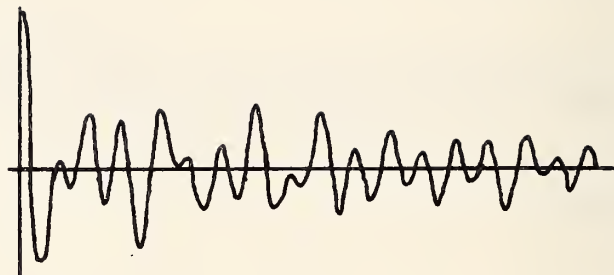


FIGURE 54.- COMPARISON OF BOTTOM FLANGE SIGNATURES,
STATIONS 22 and 23; FILTER: 960 - 5,200 Hz;
EXCITATION: STEEL-WHEELED DOLLY.

Bias level - 1.0



Bias level - 5.0



Comparison

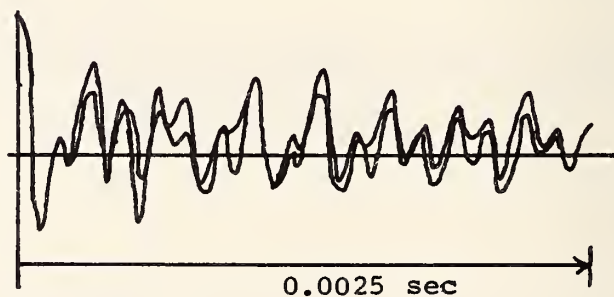
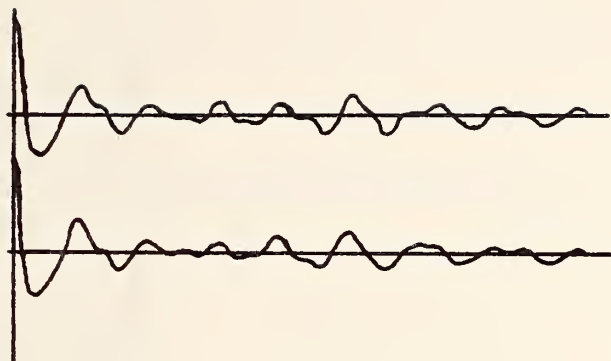


FIGURE 55.- CHECK OF STRUCTURAL LINEARITY;
FILTER: 2,400 - 12,000 Hz;
EXCITATION: ACTUATOR.

Station 10

359,000 cycles

360,000 cycles



Station 11

359,000 cycles

360,000 cycles

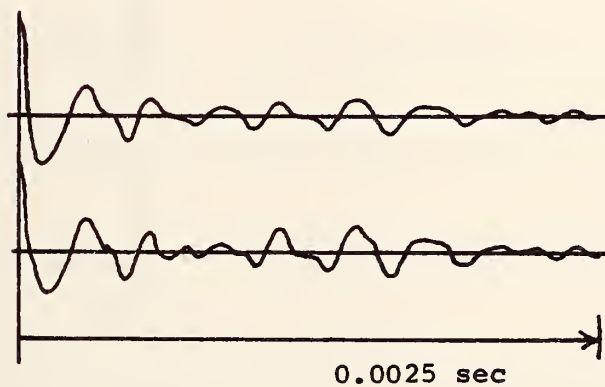


FIGURE 56.- CHECK OF REPEATABILITY;
FILTER: 2,400 - 12,00 Hz;
EXCITATION: ACTUATOR.

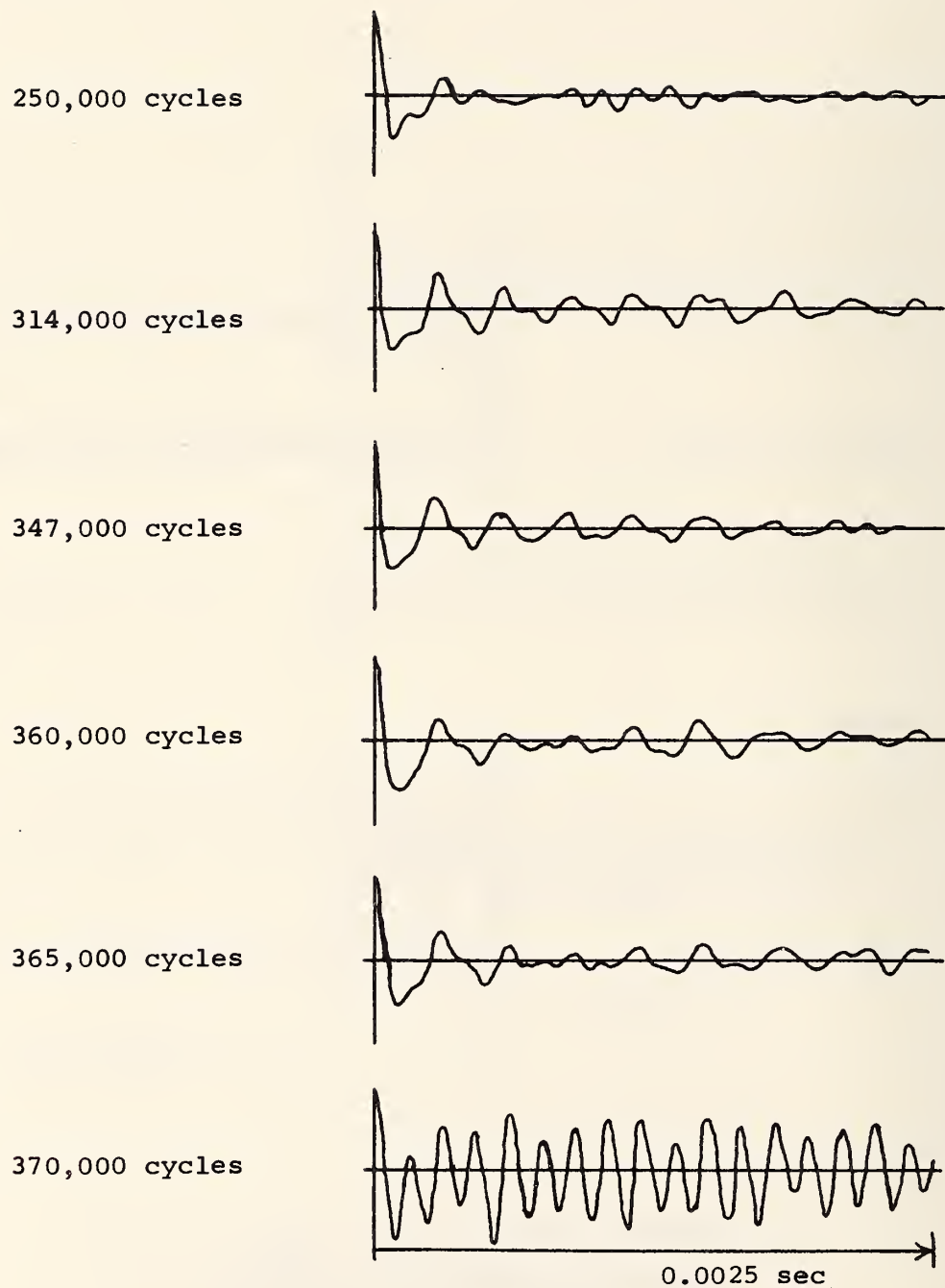


FIGURE 57.- STATION 10, BOTTOM FLANGE;
FILTER: 2,400 - 12,00 Hz;
EXCITATION: ACTUATOR.

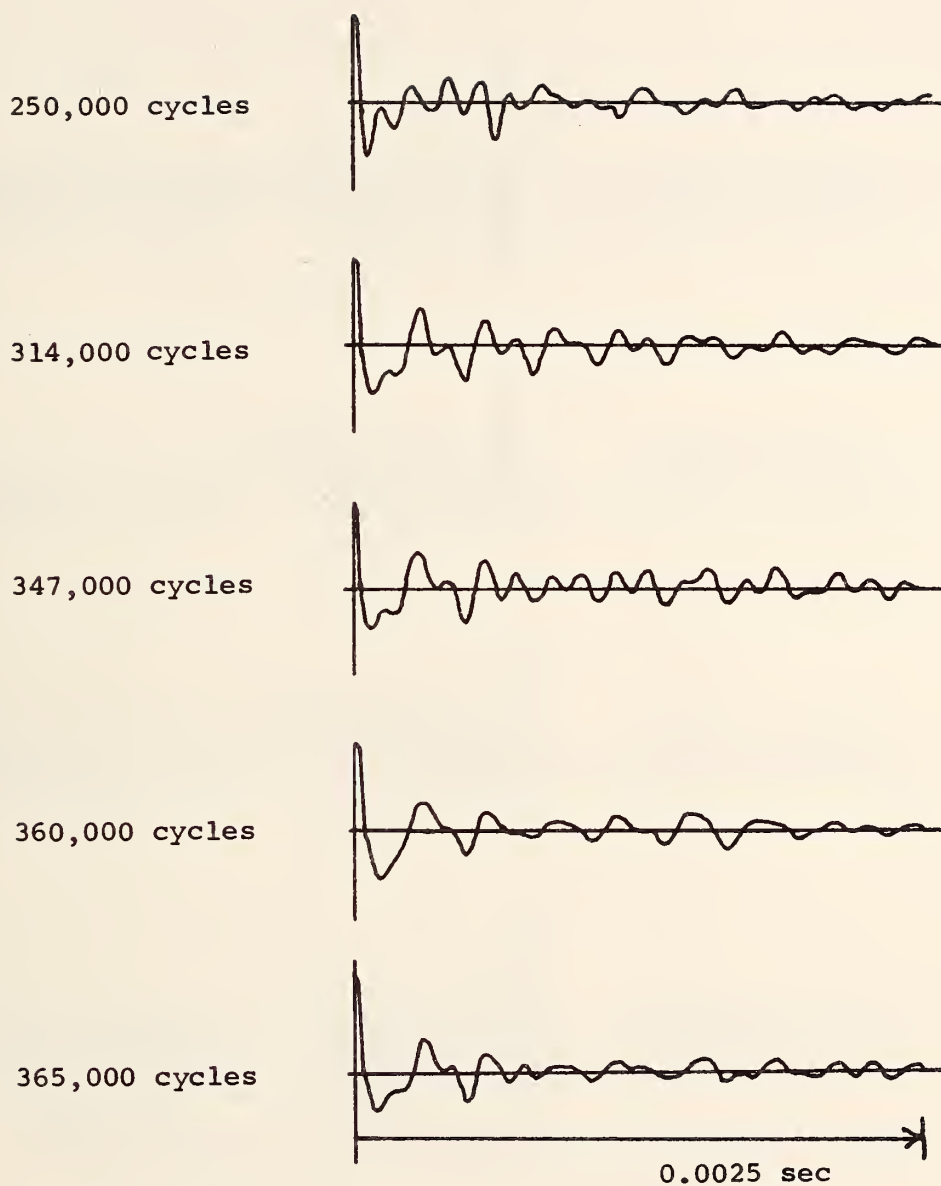


FIGURE 58.- STATION 11, BOTTOM FLANGE;
FILTER: 2,400 - 12,000 Hz;
EXCITATION: ACTUATOR.

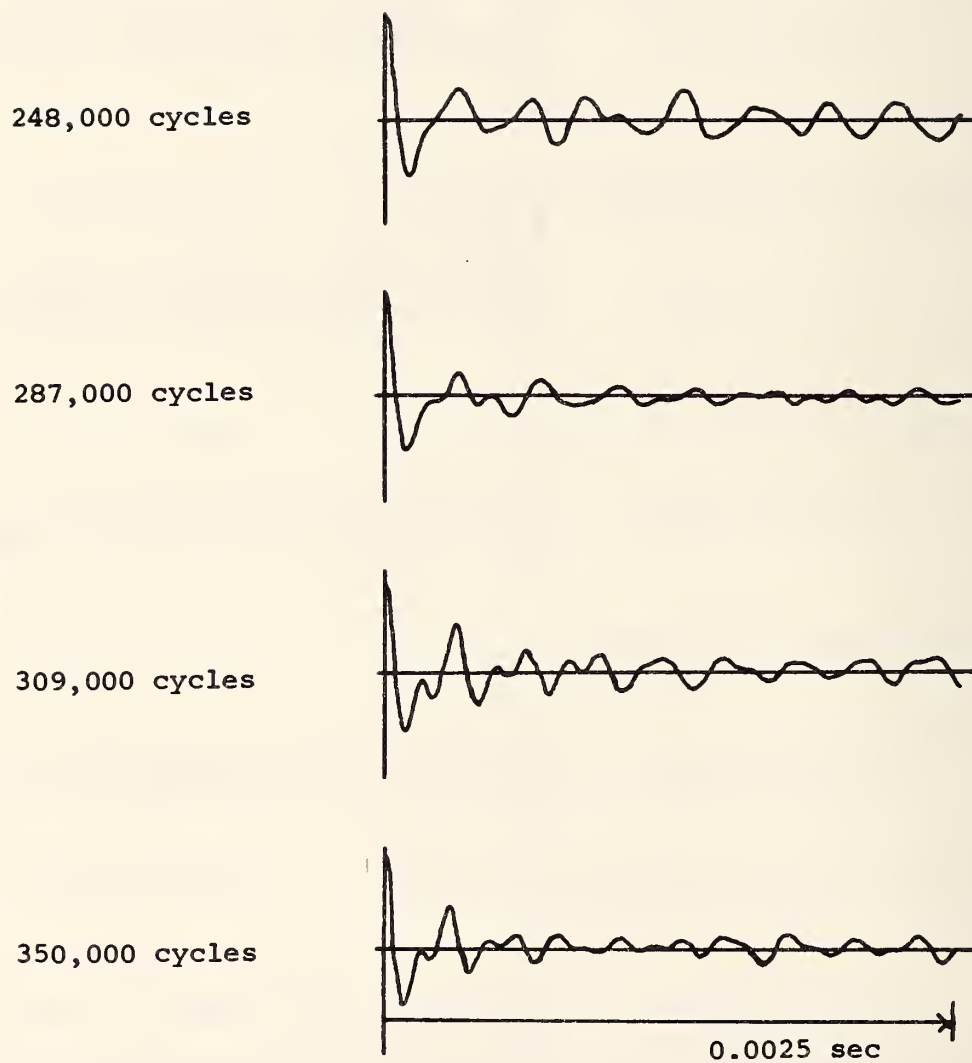


FIGURE 59.- STATION 1, BOTTOM FLANGE;
FILTER: 2,400 - 12,00 Hz;
EXCITATION: ACTUATOR.

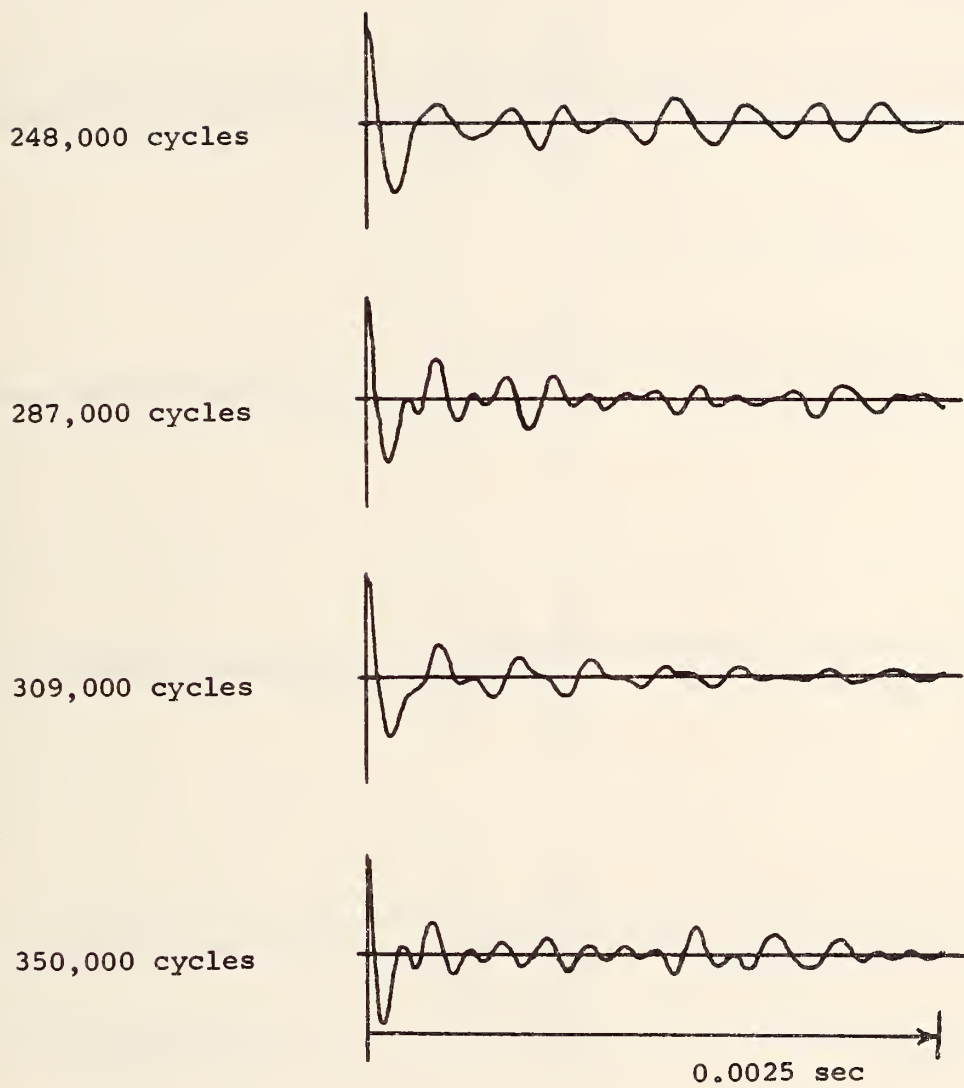


FIGURE 60.- STATION 2, BOTTOM FLANGE;
FILTER: 2,400 - 12,000 Hz;
EXCITATION: ACTUATOR.

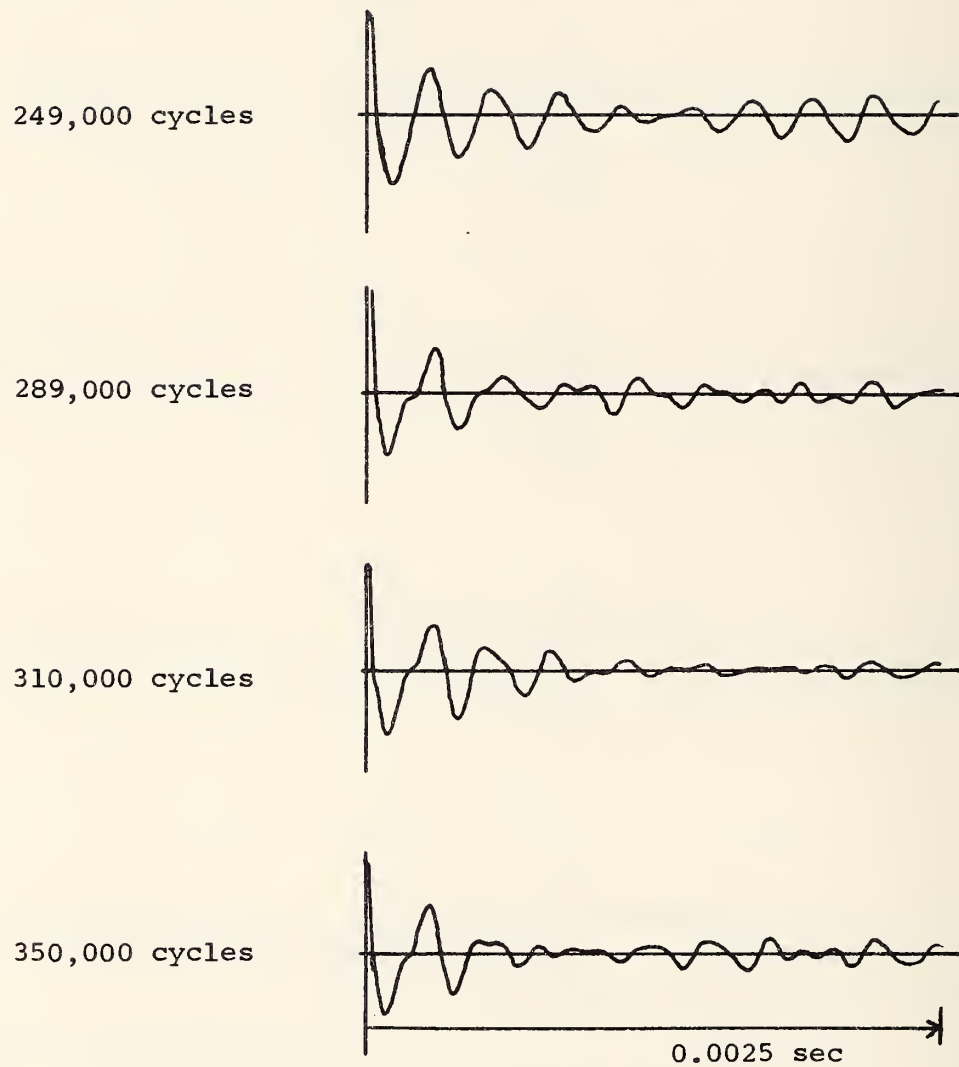


FIGURE 61.- STATION 3, TOP FLANGE;
FILTER: 2,400 - 12,000 Hz;
EXCITATION: ACTUATOR.

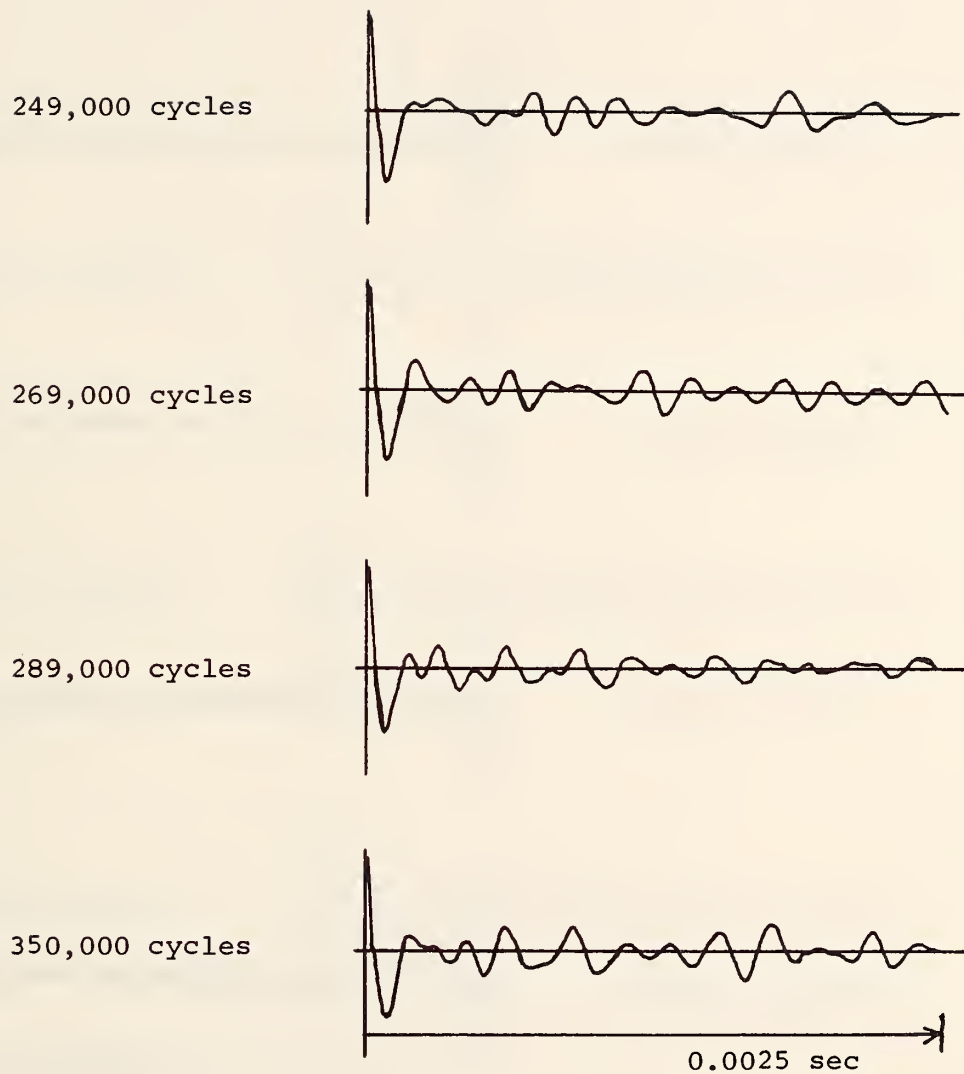


FIGURE 62.- STATION 6, TOP FLANGE;
FILTER: 2,400 - 12,00 Hz;
EXCITATION: ACTUATOR.

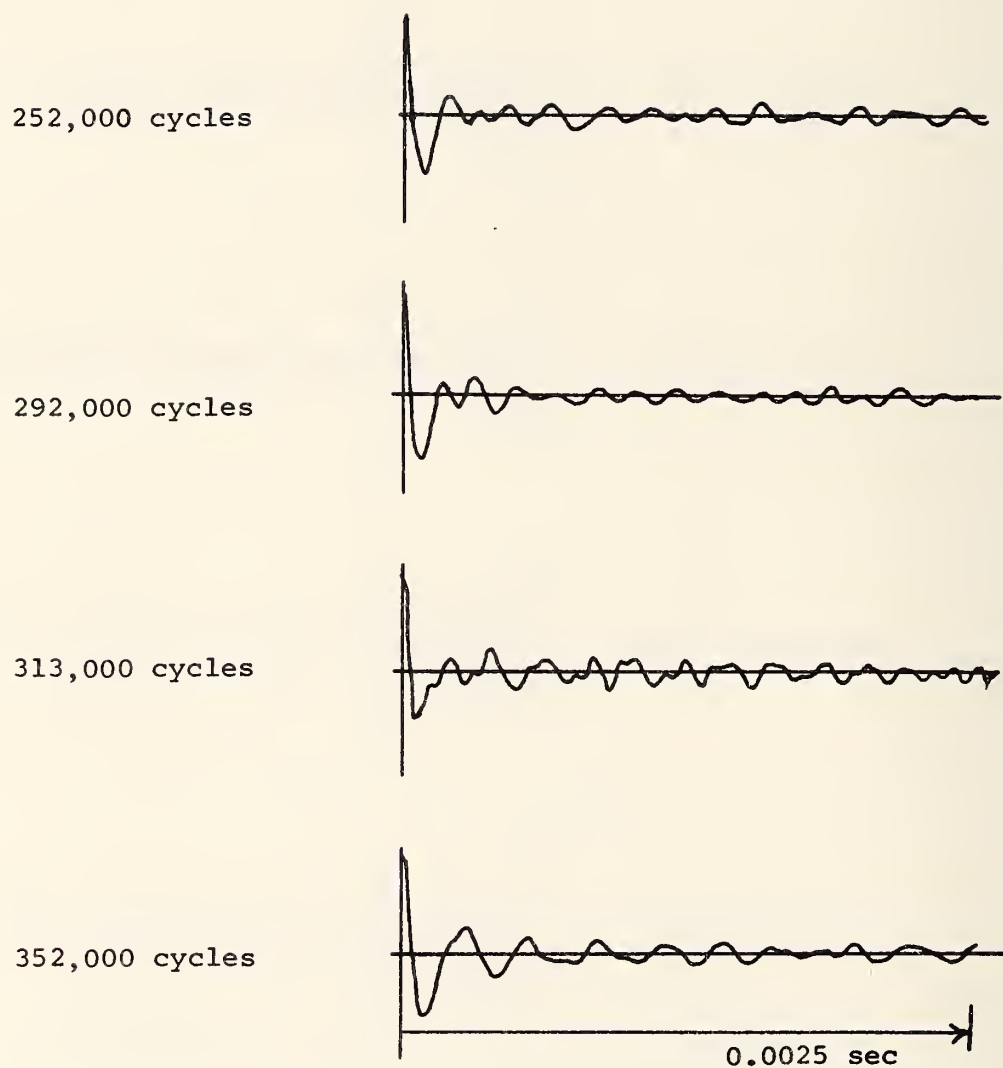


FIGURE 63.- STATION 9, TOP FLANGE;
FILTER: 2,400 - 12,000 Hz;
EXCITATION: ACTUATOR.

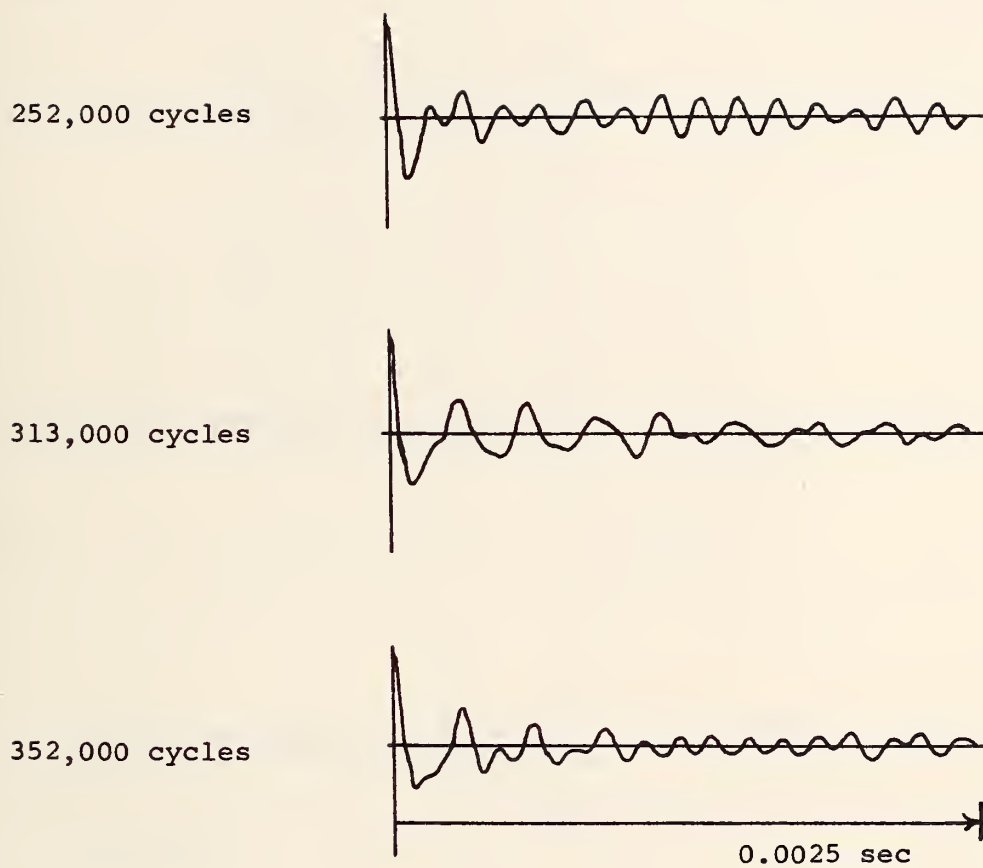
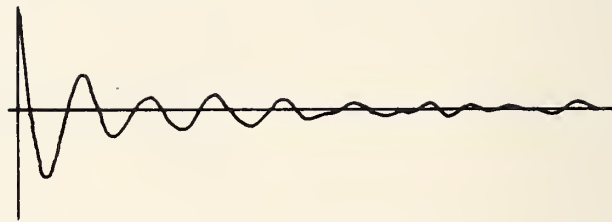
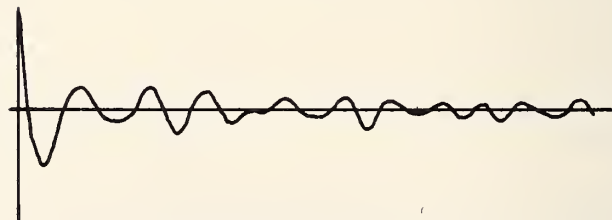


FIGURE 64.- STATION 12, TOP FLANGE;
FILTER: 2,400 - 12,000 Hz;
EXCITATION: ACTUATOR.

258,000 Fatigue
cycles



278,000 Fatigue
cycles



320,000 Fatigue
cycles

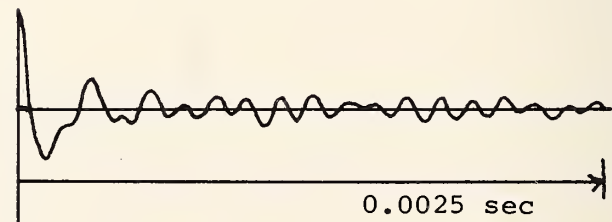


FIGURE 65.- STATION 19, BOTTOM FLANGE;
FILTER: 2,400 - 12,00 Hz;
EXCITATION: ACTUATOR.

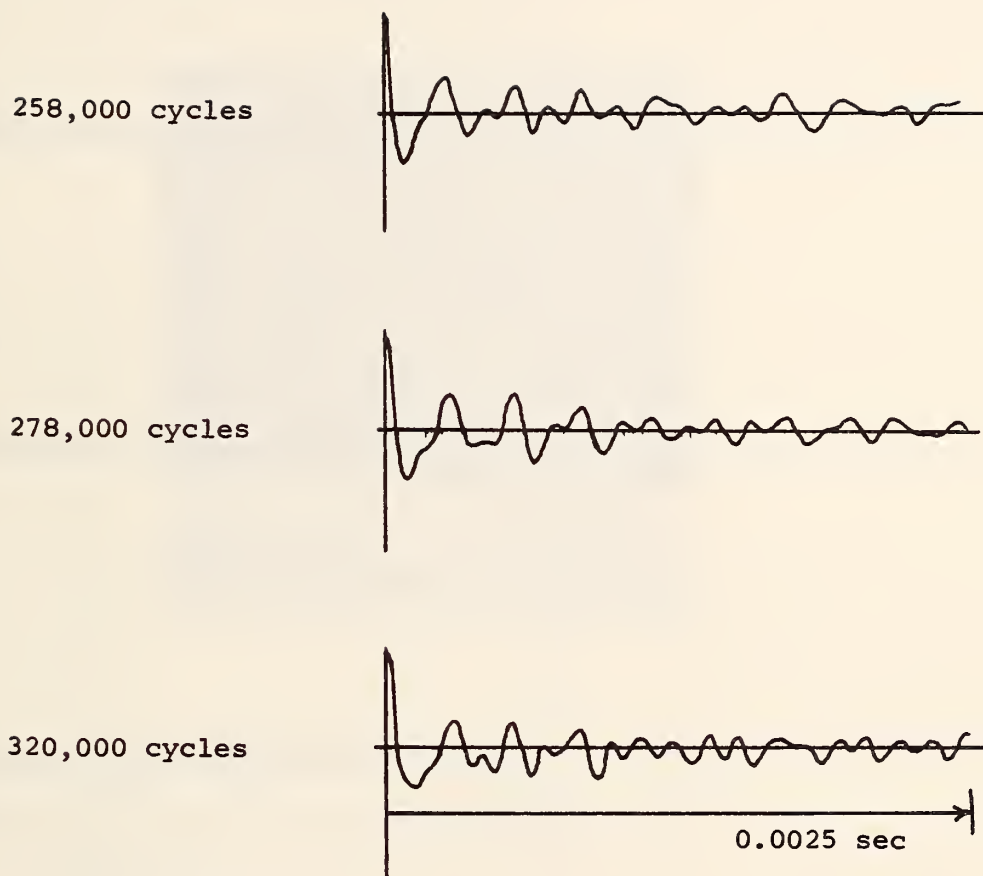


FIGURE 66.- STATION 20, BOTTOM FLANGE;
FILTER: 2,400 - 12,000 Hz;
EXCITATION: ACTUATOR.

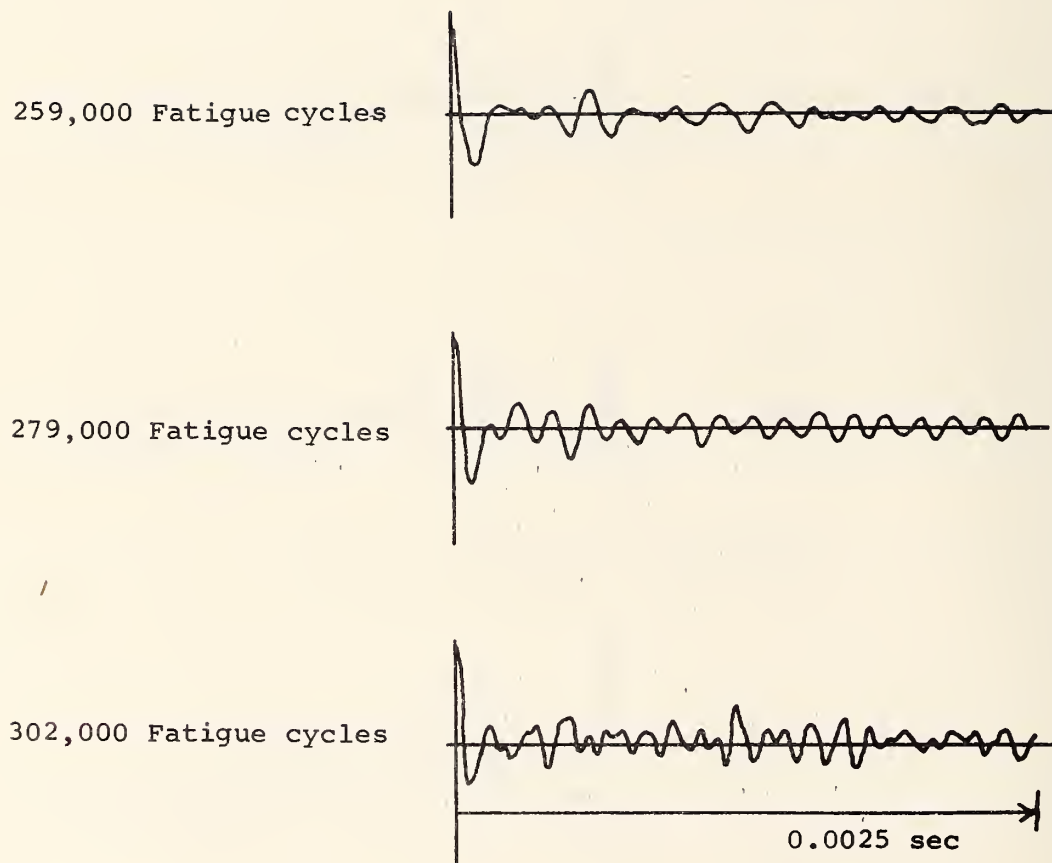


FIGURE 67.- STATION 21, TOP FLANGE;
FILTER: 2,400 - 12,000 Hz;
EXCITATION: ACTUATOR.

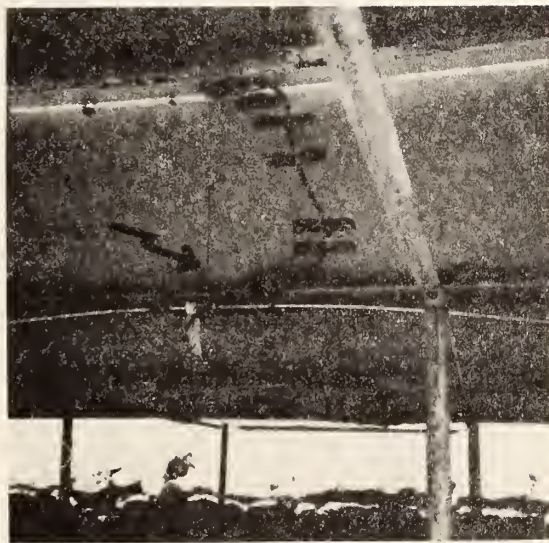


FIGURE 68.- FAILURE OF INTERIOR GIRDER AT
MIDSPAN ON MISSOURI BRIDGE.

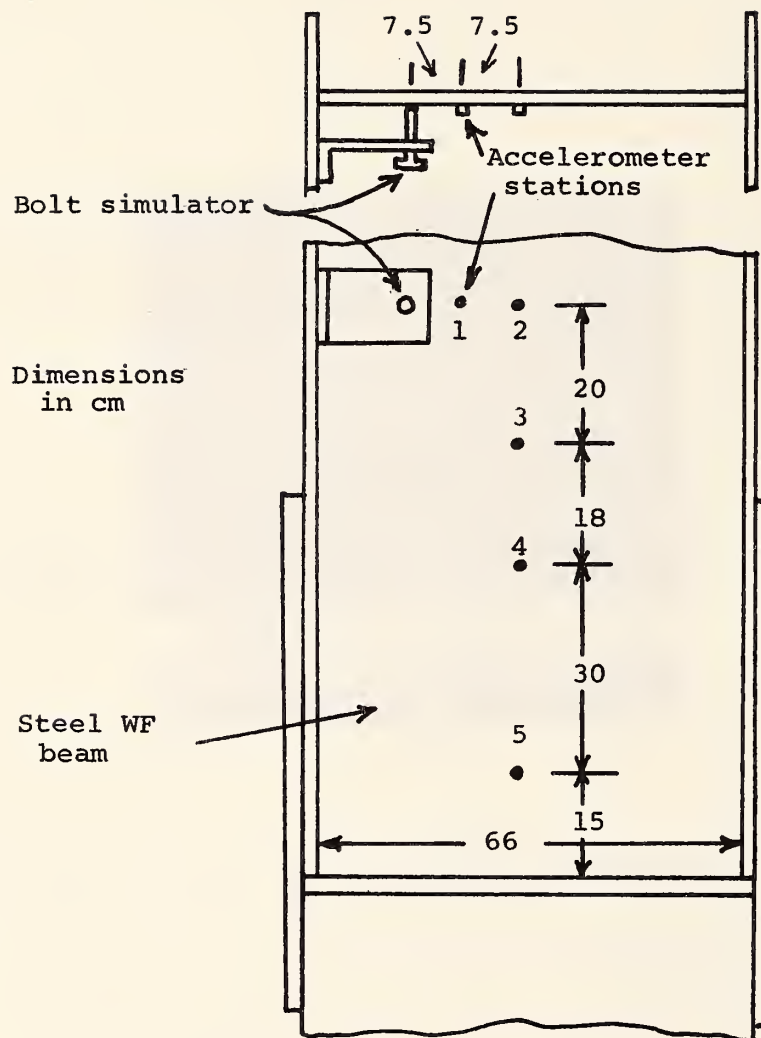


FIGURE 69.- BOLT SIMULATOR AND ACCELEROMETER STATIONS, EAST CARQUINEZ BRIDGE.

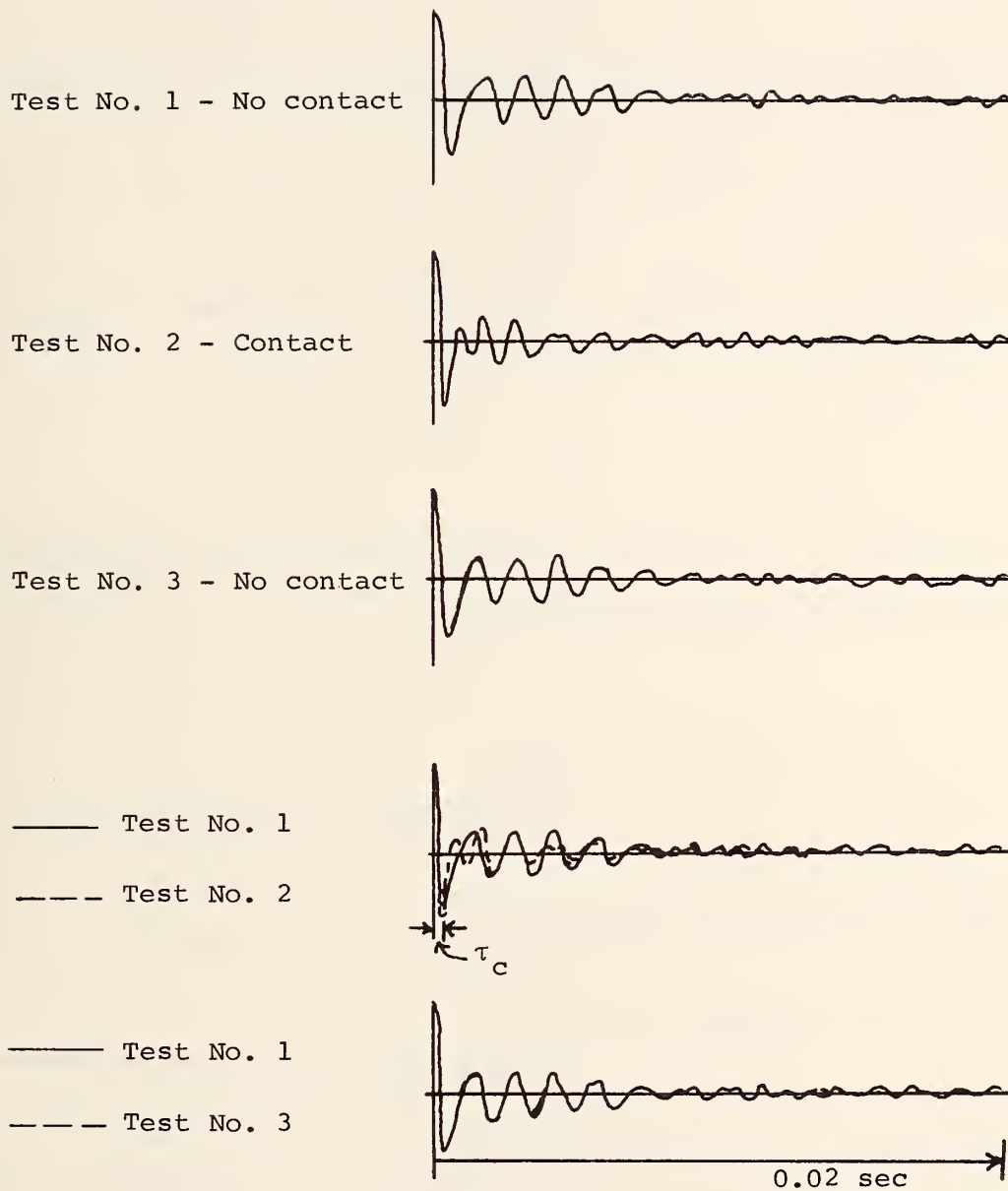


FIGURE 70.- STATION 1, FLAW SIMULATION;
FILTER: 700 - 1,500 Hz.

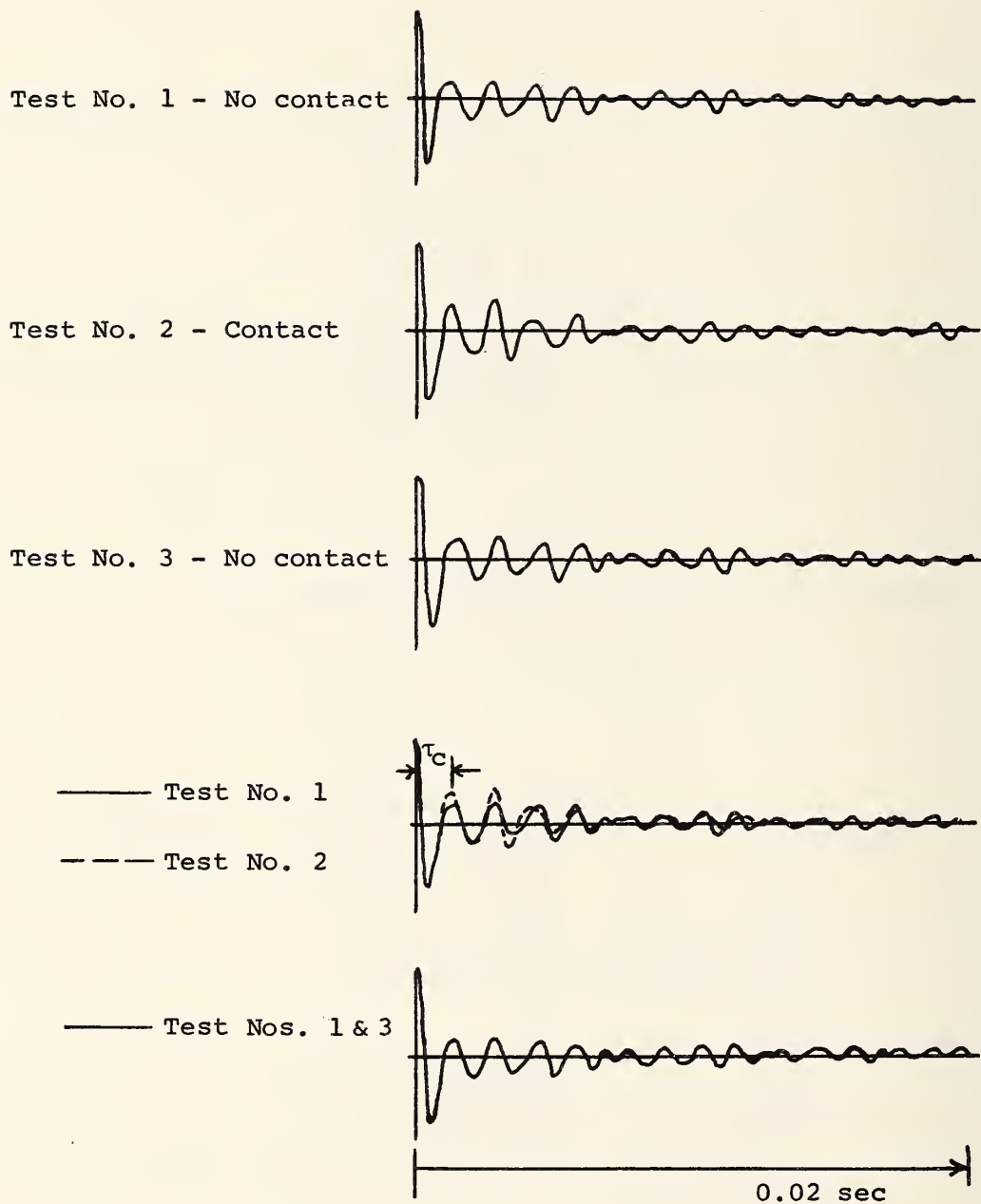


FIGURE 71.- STATION 2, FLAW SIMULATION;
FILTER: 700 - 1,500 Hz.

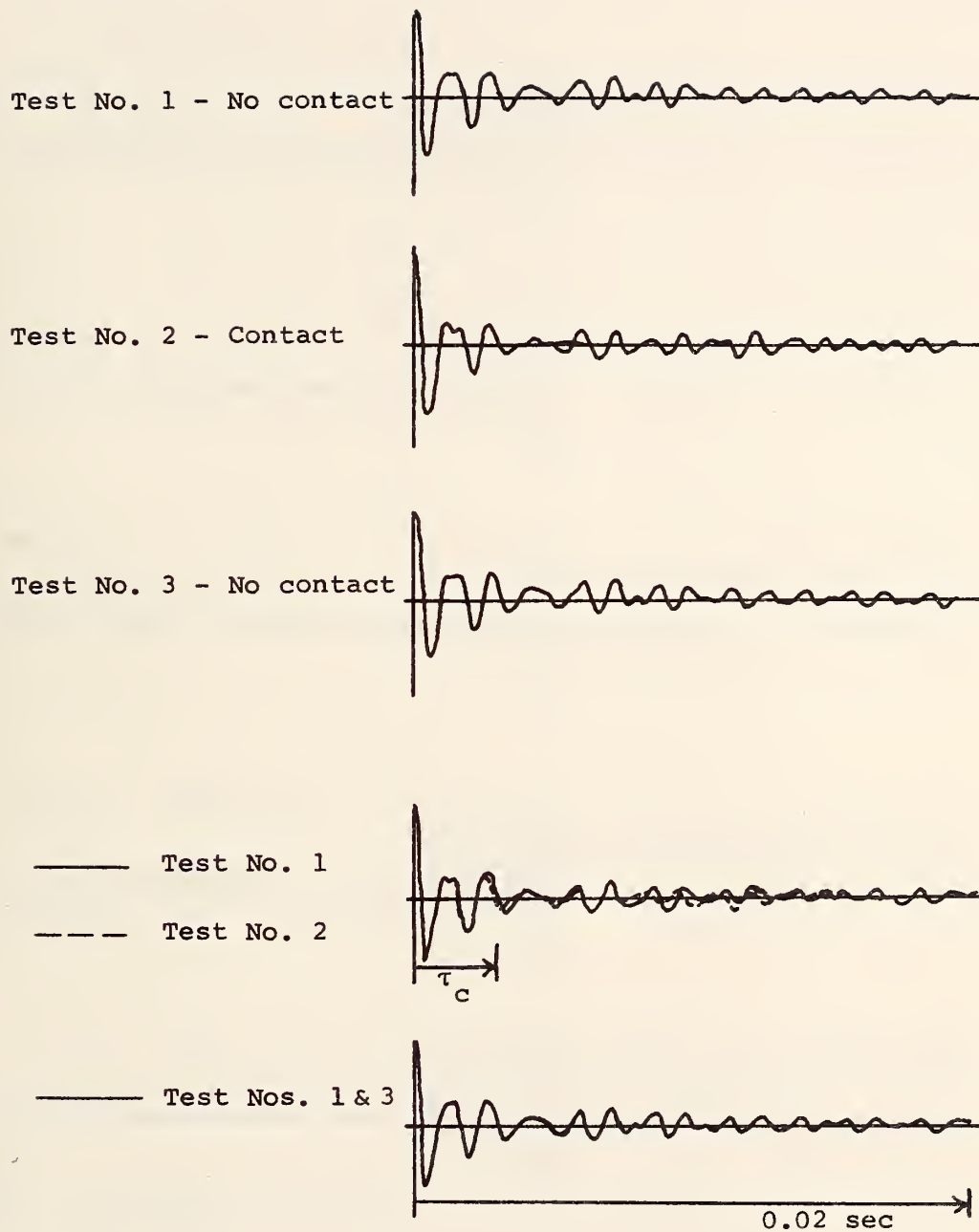


FIGURE 72.- STATION 3, FLAW SIMULATION;
FILTER: 700 - 1,500 Hz.

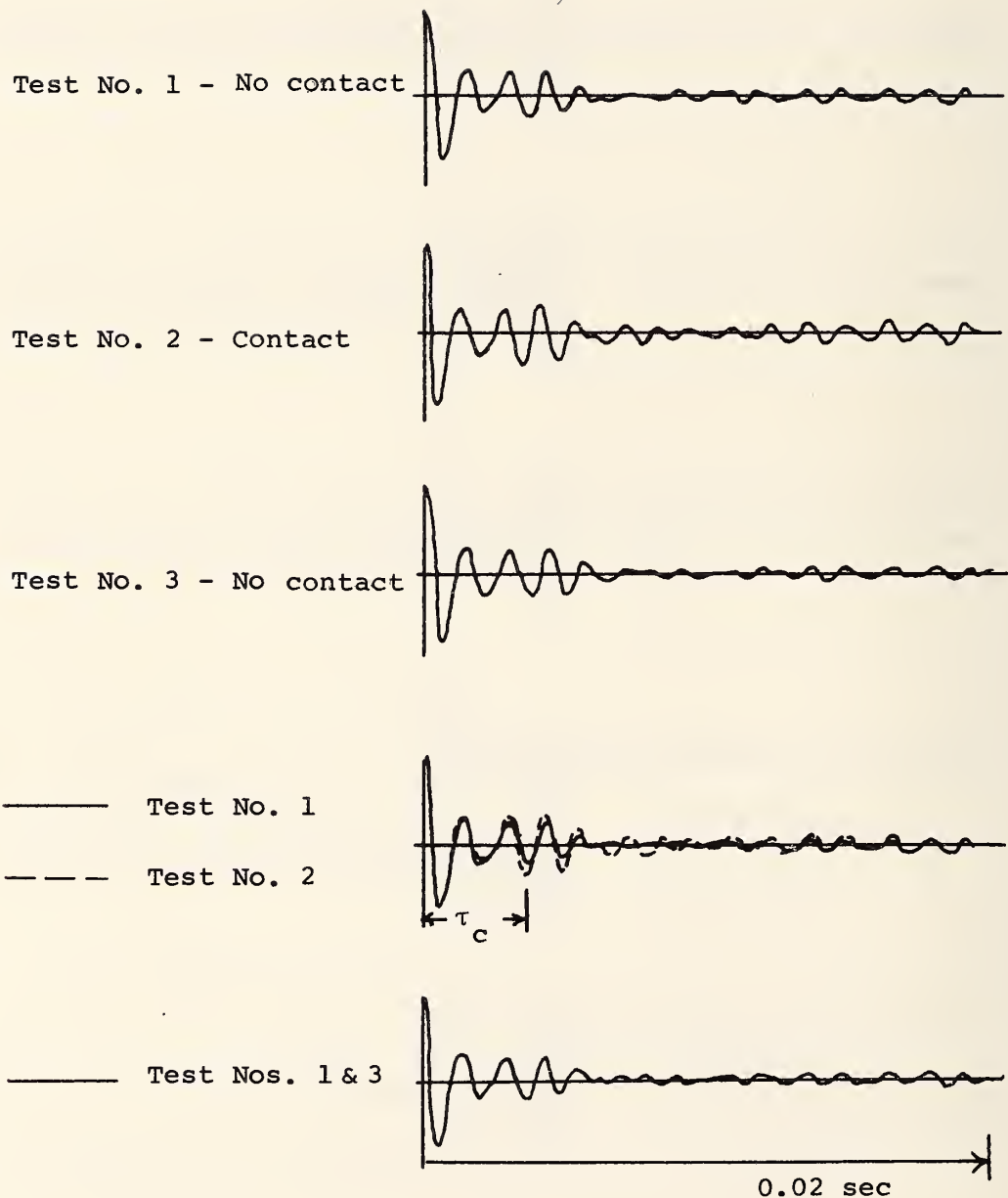


FIGURE 73.- STATION 4, FLAW SIMULATION;
FILTER: 700 - 1,500 Hz.

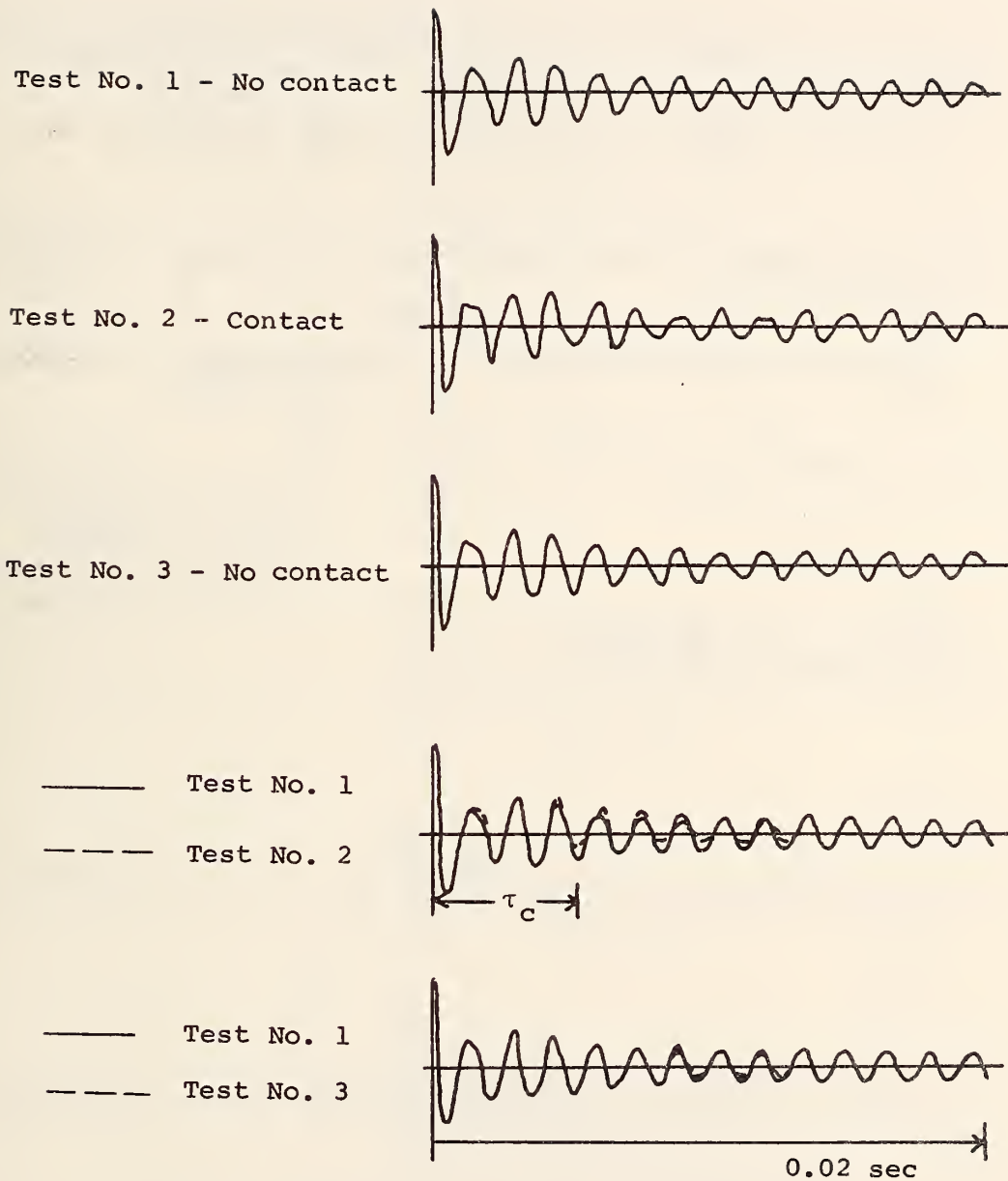
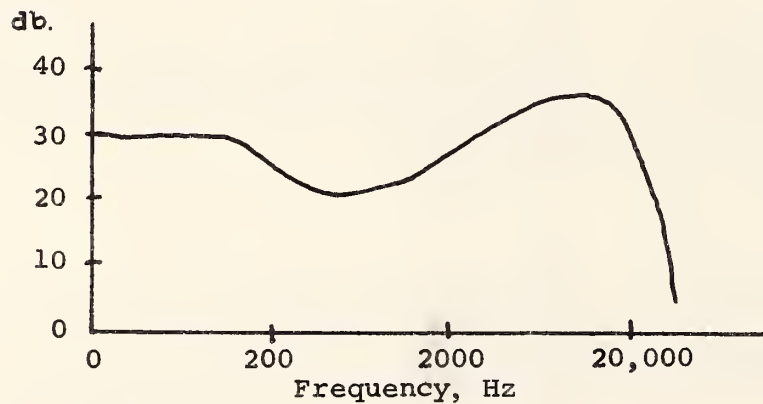
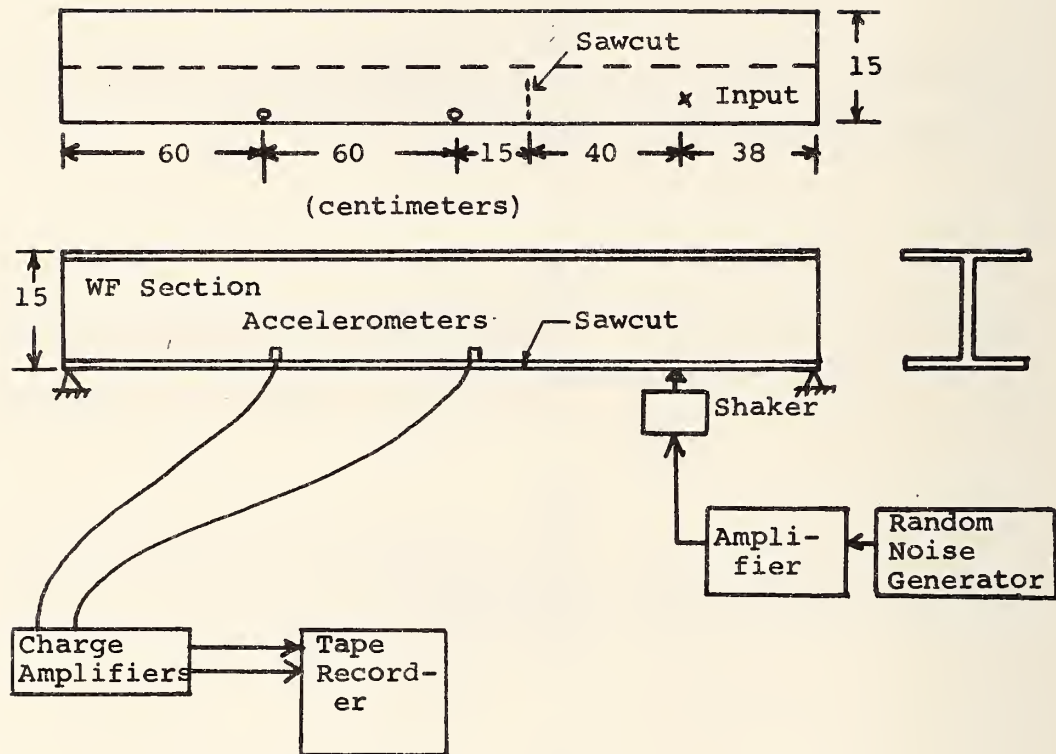


FIGURE 74.- STATION 5, FLAW SIMULATION;
 FILTER: 700 - 1,500 Hz.



Amplitude spectrum of shaker input

FIGURE 75.- SIMULATION OF CRACK WITH A SAWCUT IN BEAM.

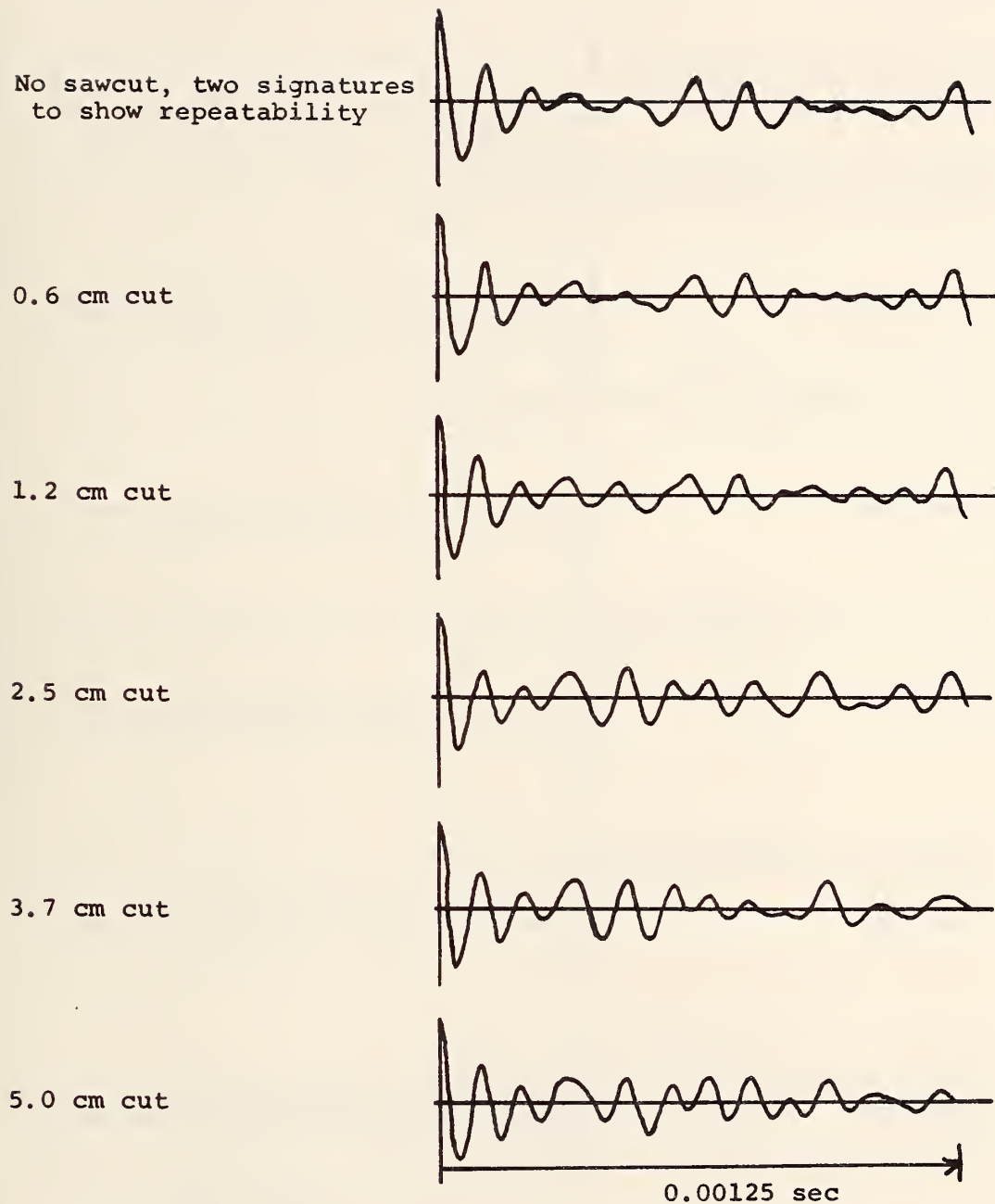


FIGURE 76.- SAWCUT IN BEAM, STATION 1;
FILTER: 4,000 - 20,800 Hz.

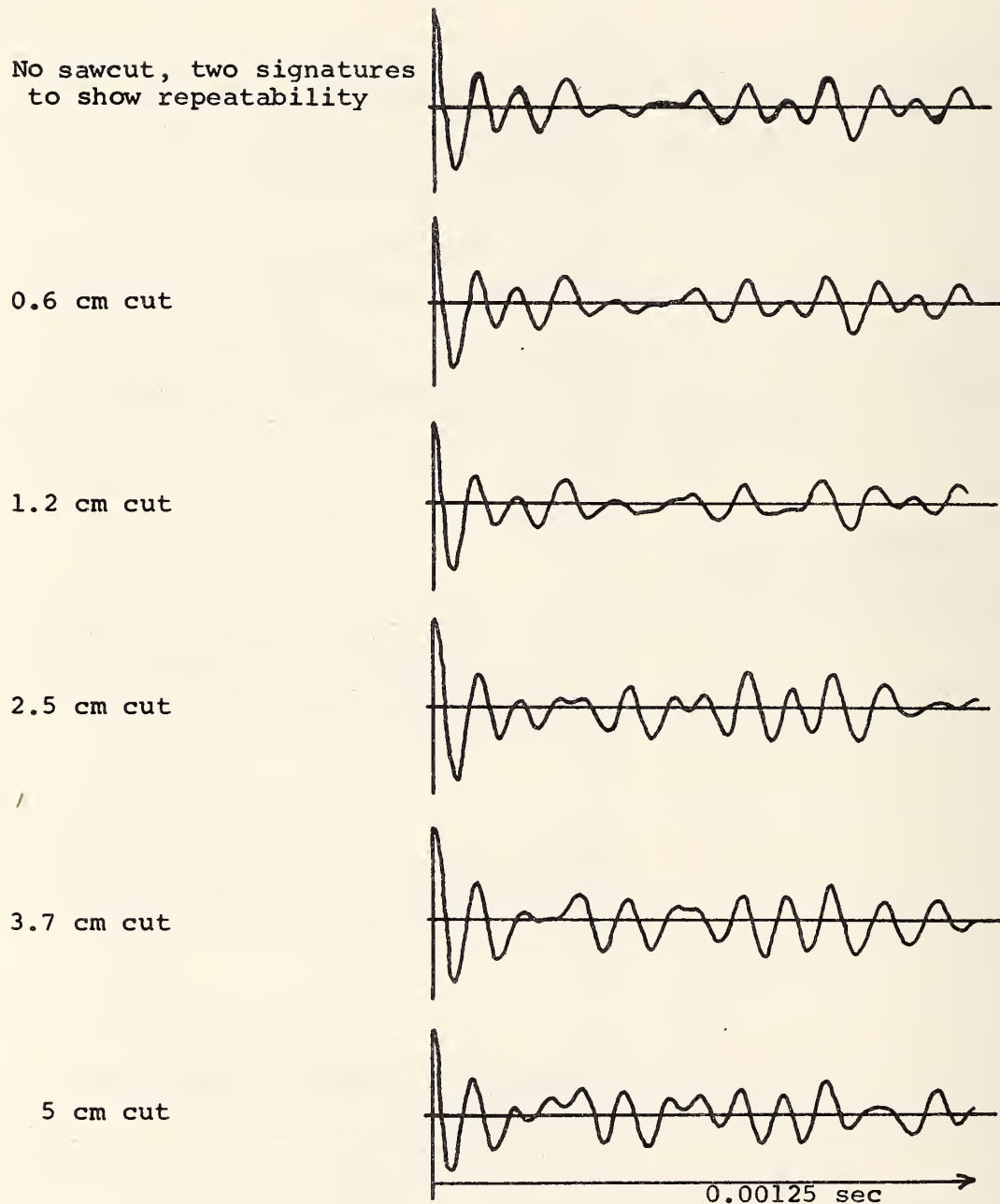


FIGURE 77.- SAWCUT IN BEAM, STATION 2;
FILTER: 4,000 - 20,800 Hz.

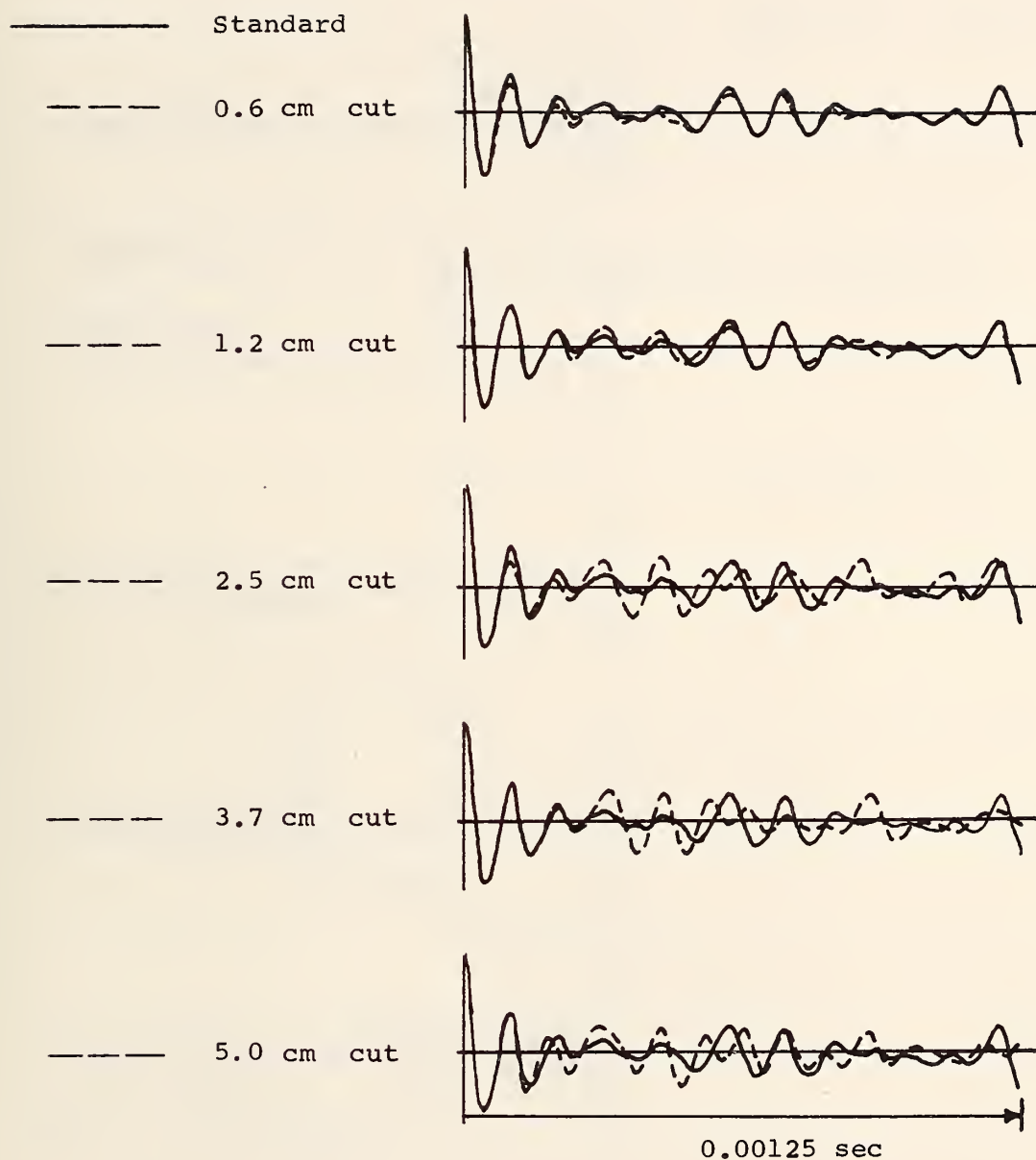


FIGURE 78.- SIGNATURES SUPERPOSED ON STANDARD,
STATION 1; FILTER: 4,000 - 20,800 Hz.

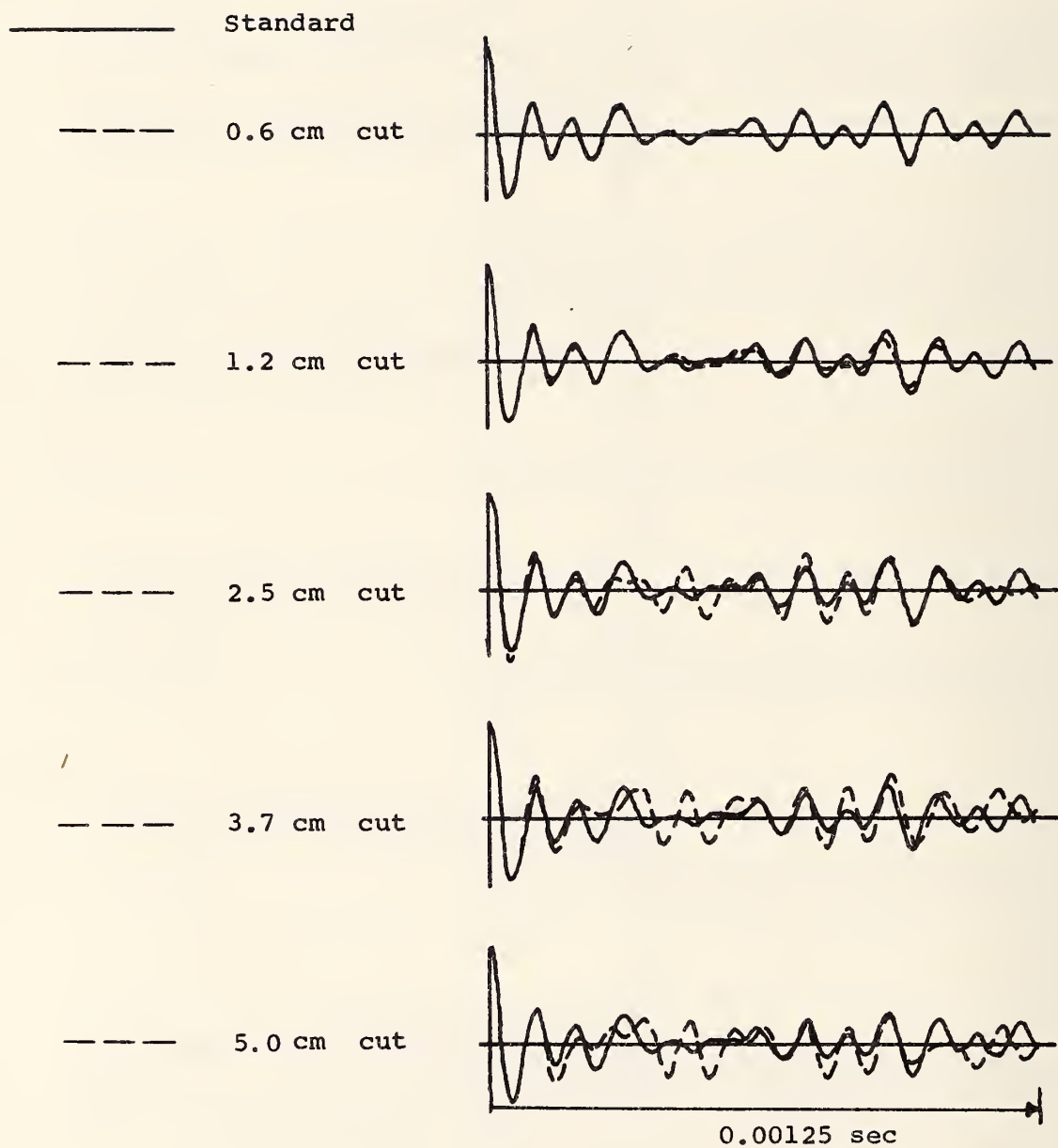
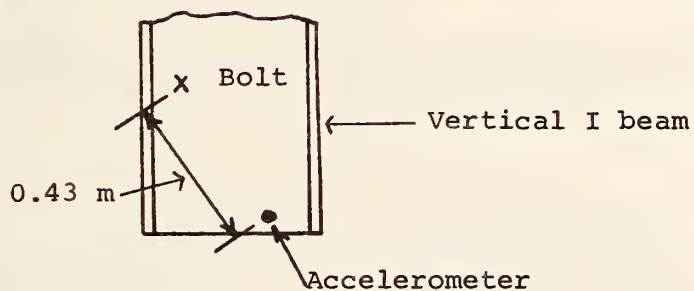
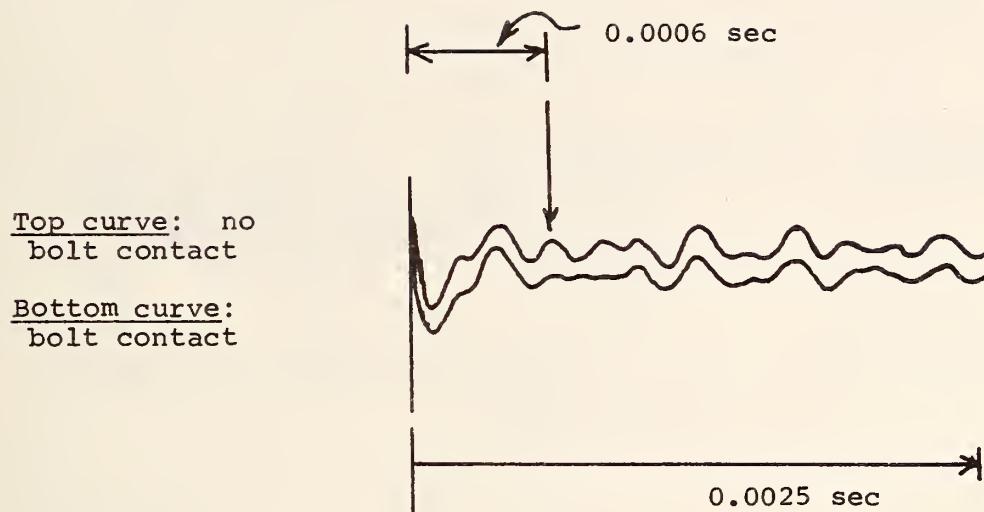


FIGURE 79.- SIGNATURES SUPERPOSED ON STANDARD,
STATION 2; FILTER: 4,000 - 20,800 Hz.



$$\text{Speed} = \frac{0.43}{0.0006} = 720 \frac{\text{m}}{\text{sec}}$$

FIGURE 80.- EFFECT OF FLAW SIMULATION AND POSSIBLE LOCATION OF FLAW; FILTER: 2,400 - 6,400 Hz.

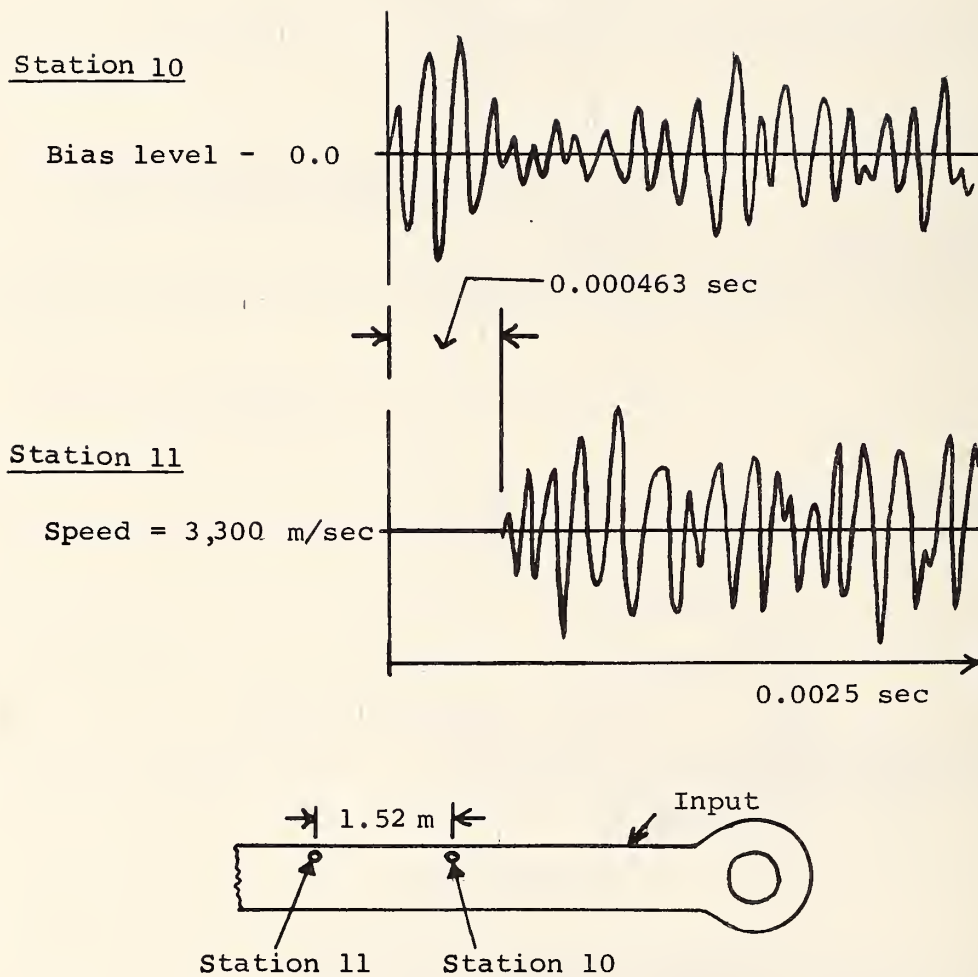


FIGURE 81.- TRAVELING WAVE IN WEST CARQUINEZ
EYEBAR; FILTER: 8,000 - 8,800 Hz.

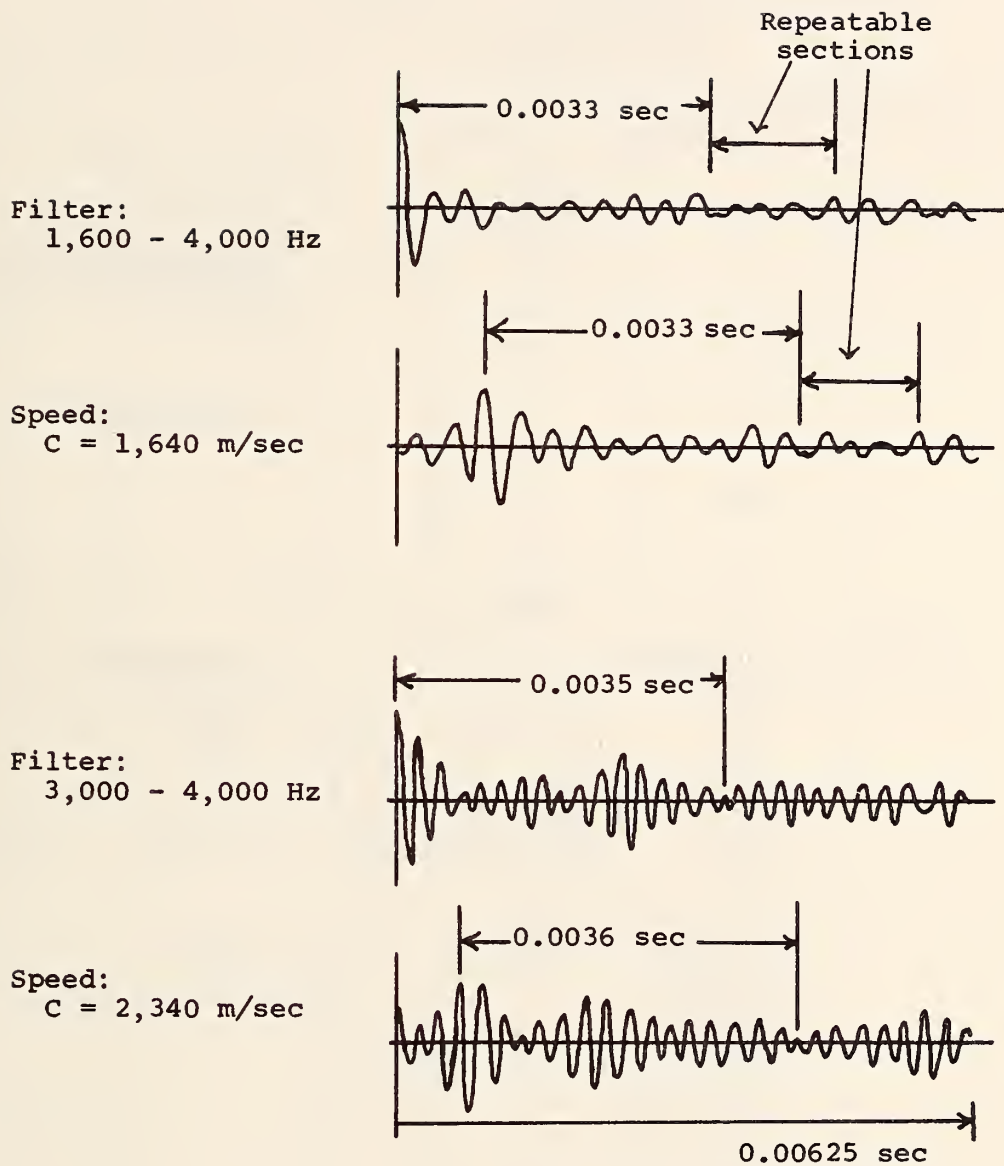


FIGURE 82.- TRAVELING WAVES IN WEST CARQUINEZ EYEBAR.

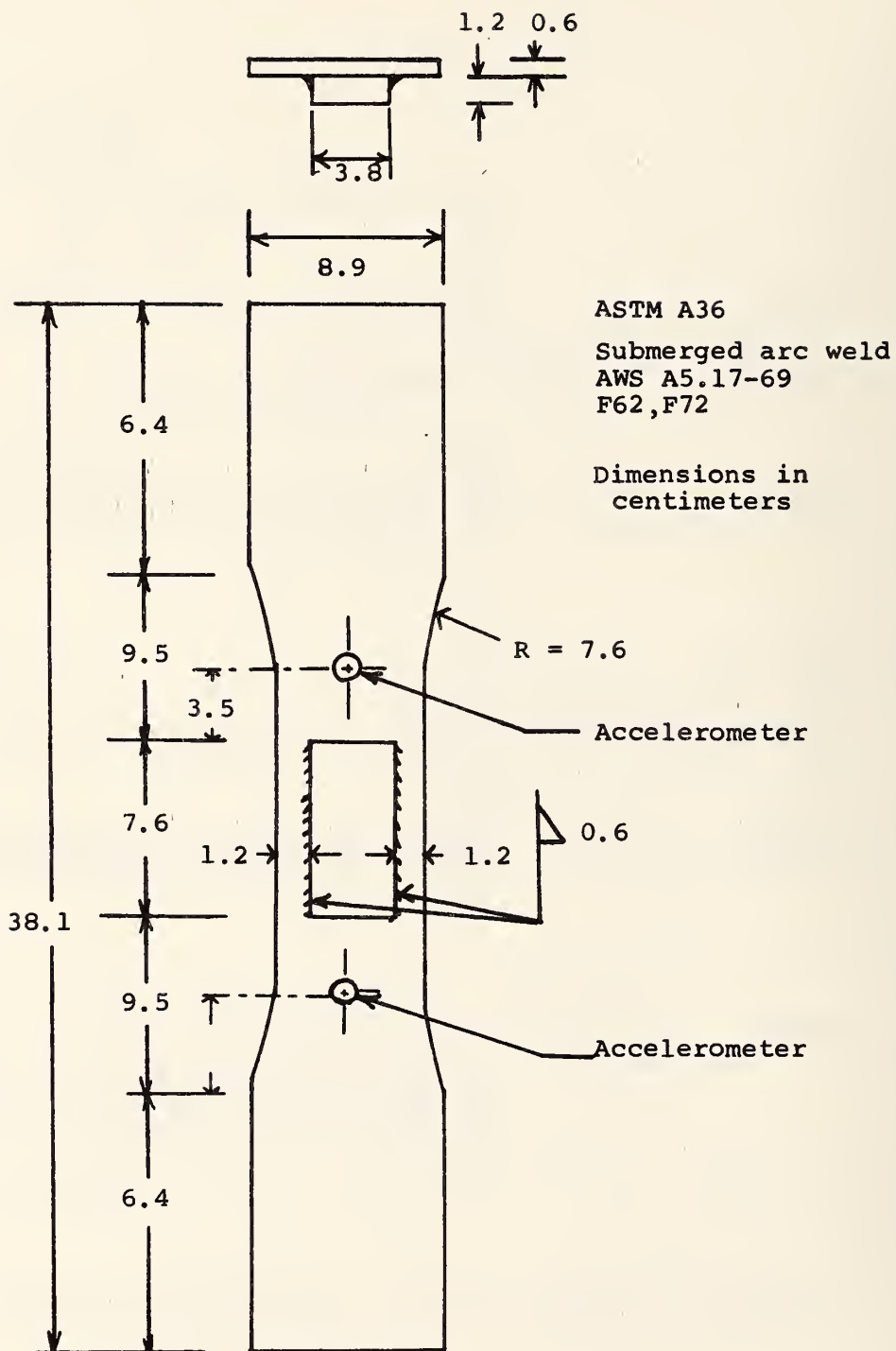


FIGURE 83.- LABORATORY SPECIMEN WITH
FILLET WELDED COVER PLATE.

ASTM A36

Submerged arc weld

AWS A5.17-69

F62, F72

Use end plate whz
starting and fin weld

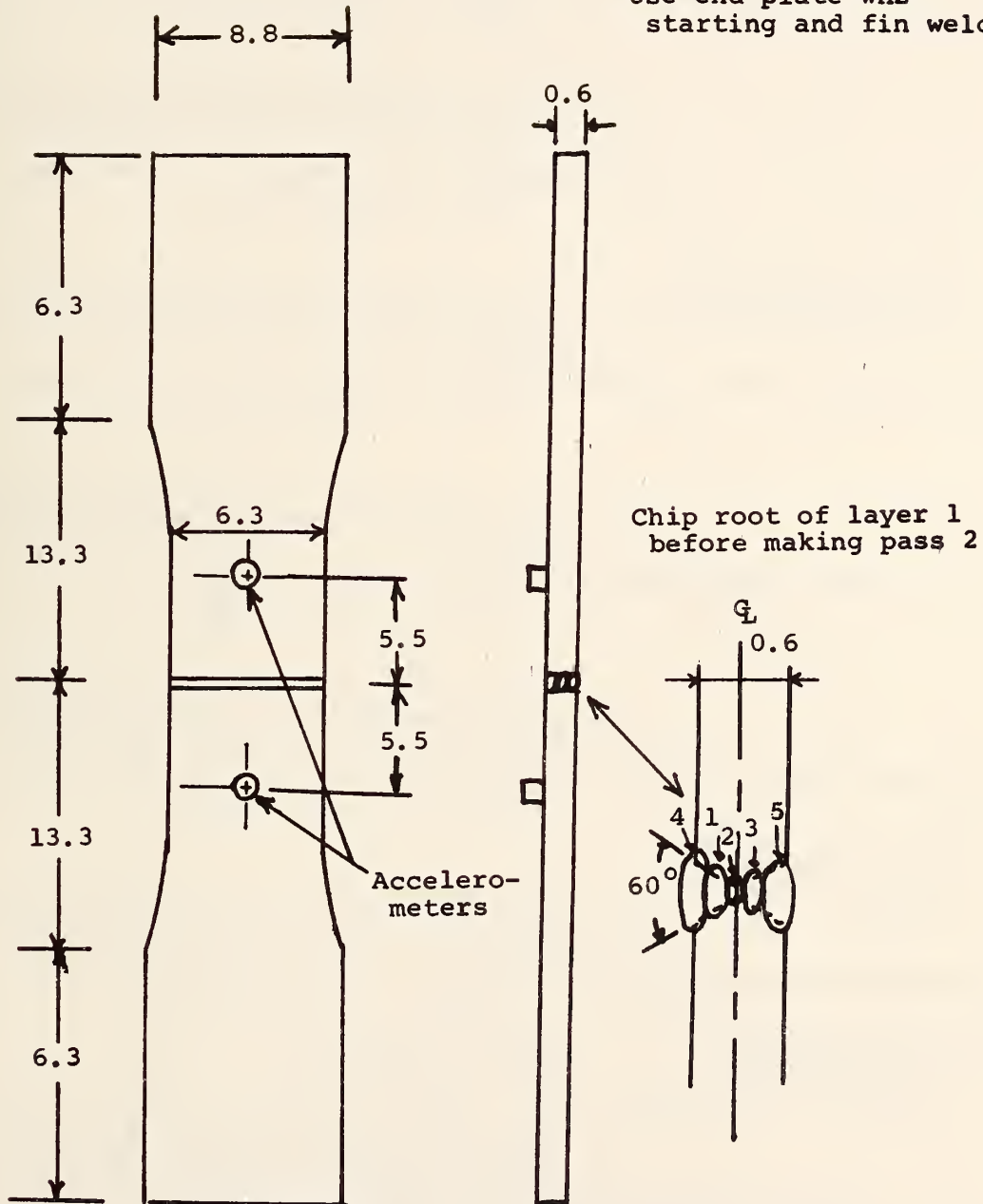


FIGURE 84.- LABORATORY SPECIMEN WITH BUTT WELD.

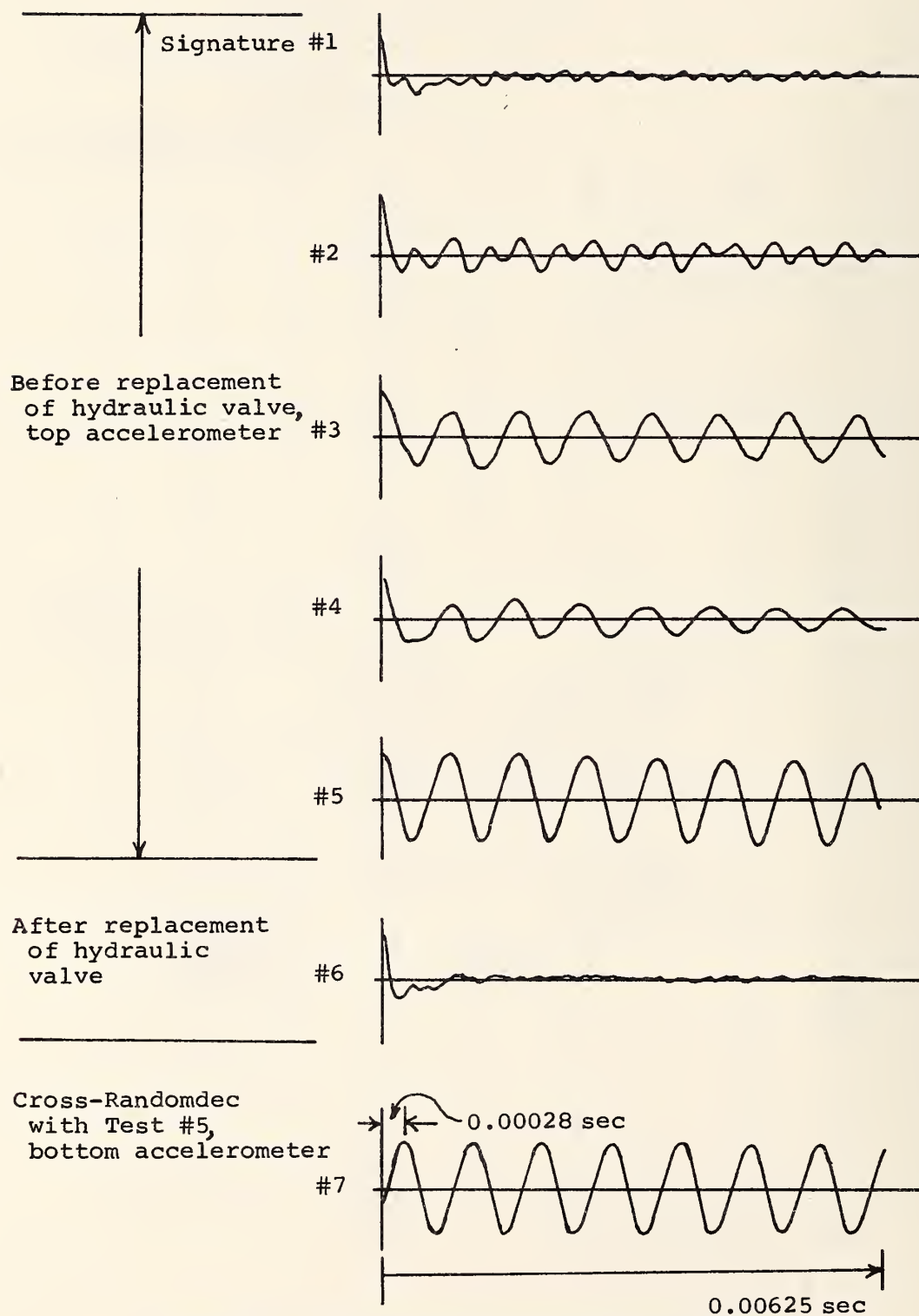


FIGURE 85 .- DEVELOPMENT OF MACHINE FAILURE;
FILTER: LOW-PASS AT 3,200 Hz.

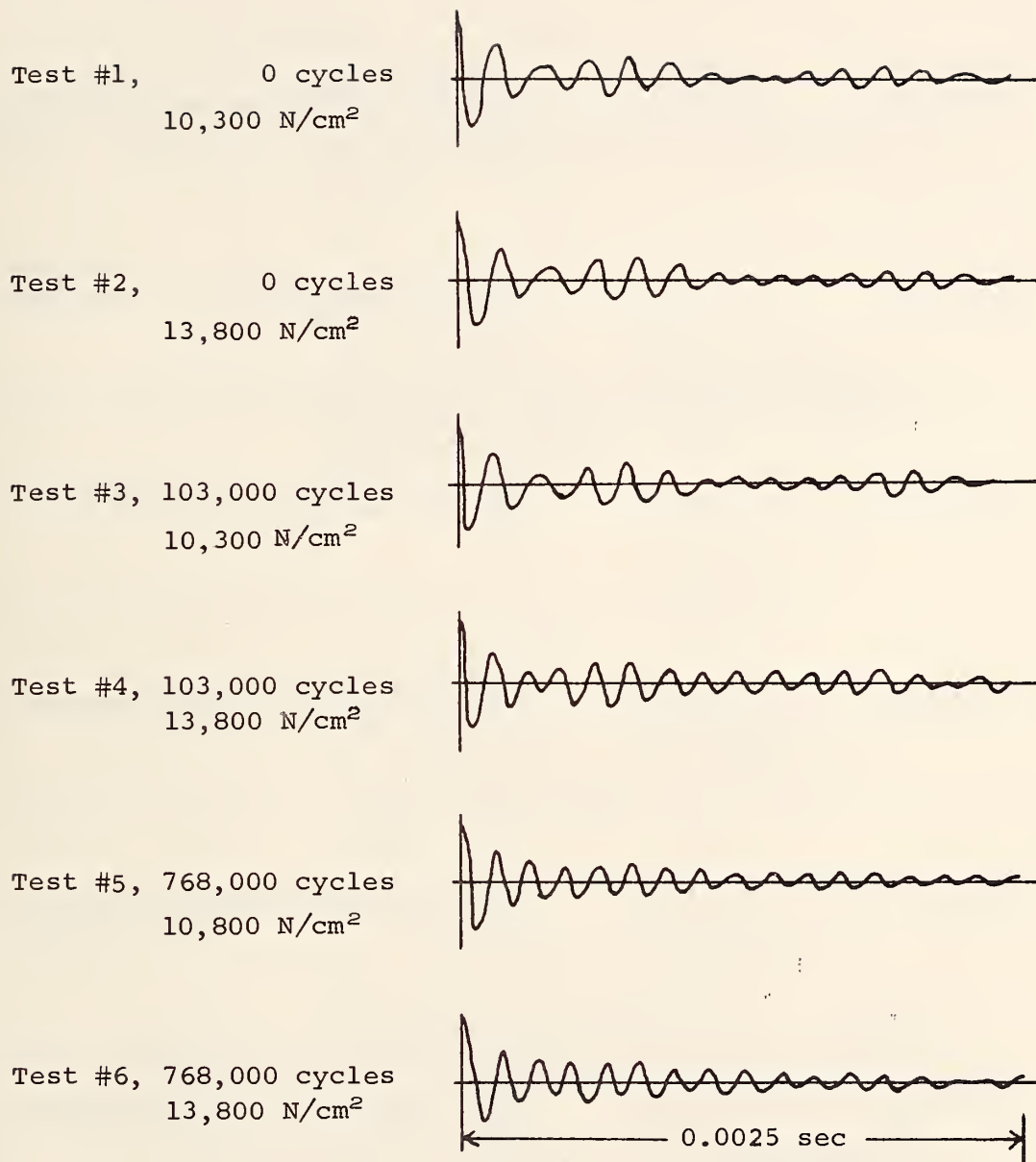


FIGURE 86.- SPECIMEN #1 - TOP ACCELEROMETER;
FILTER: 400 - 8,800 Hz.

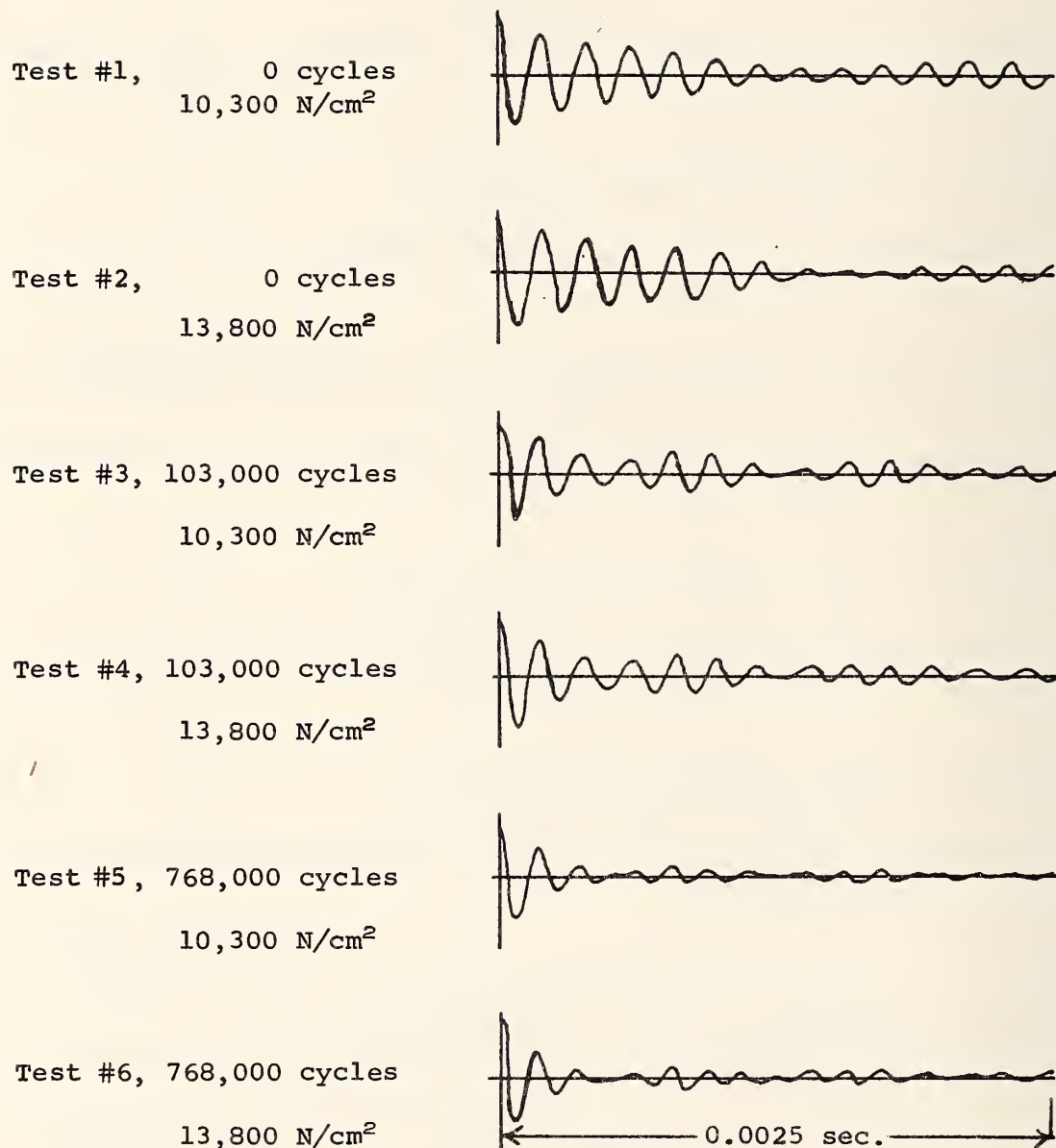
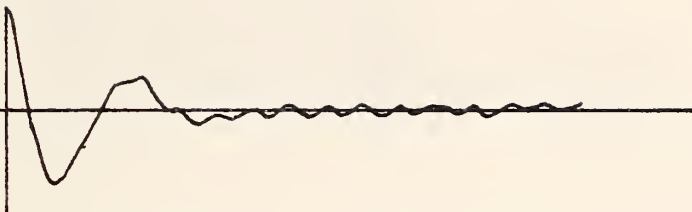


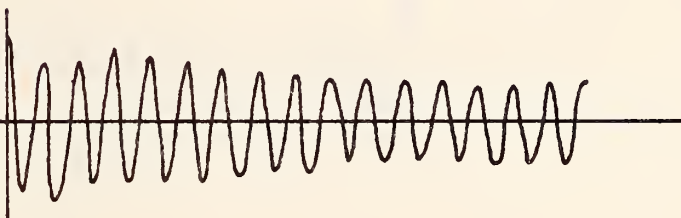
FIGURE 87.- SPECIMEN #1 - BOTTOM ACCELEROMETER;
 FILTER 4,400 - 8,800 Hz.

Filter: 560-1,600 Hz

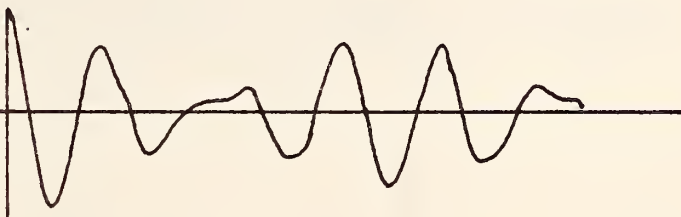


Test #1

Filter: 800-3,200 Hz



Filter: 560-1,600 Hz



Test #2

Filter: 800-3,200 Hz

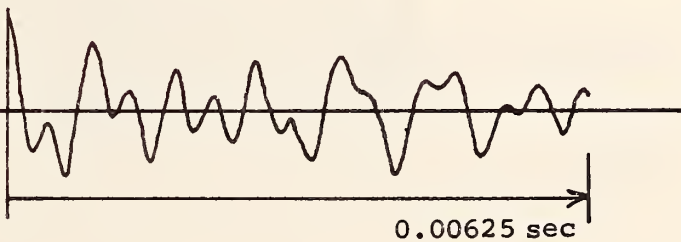


FIGURE 88.- SPECIMEN #2 - TOP ACCELEROMETER.

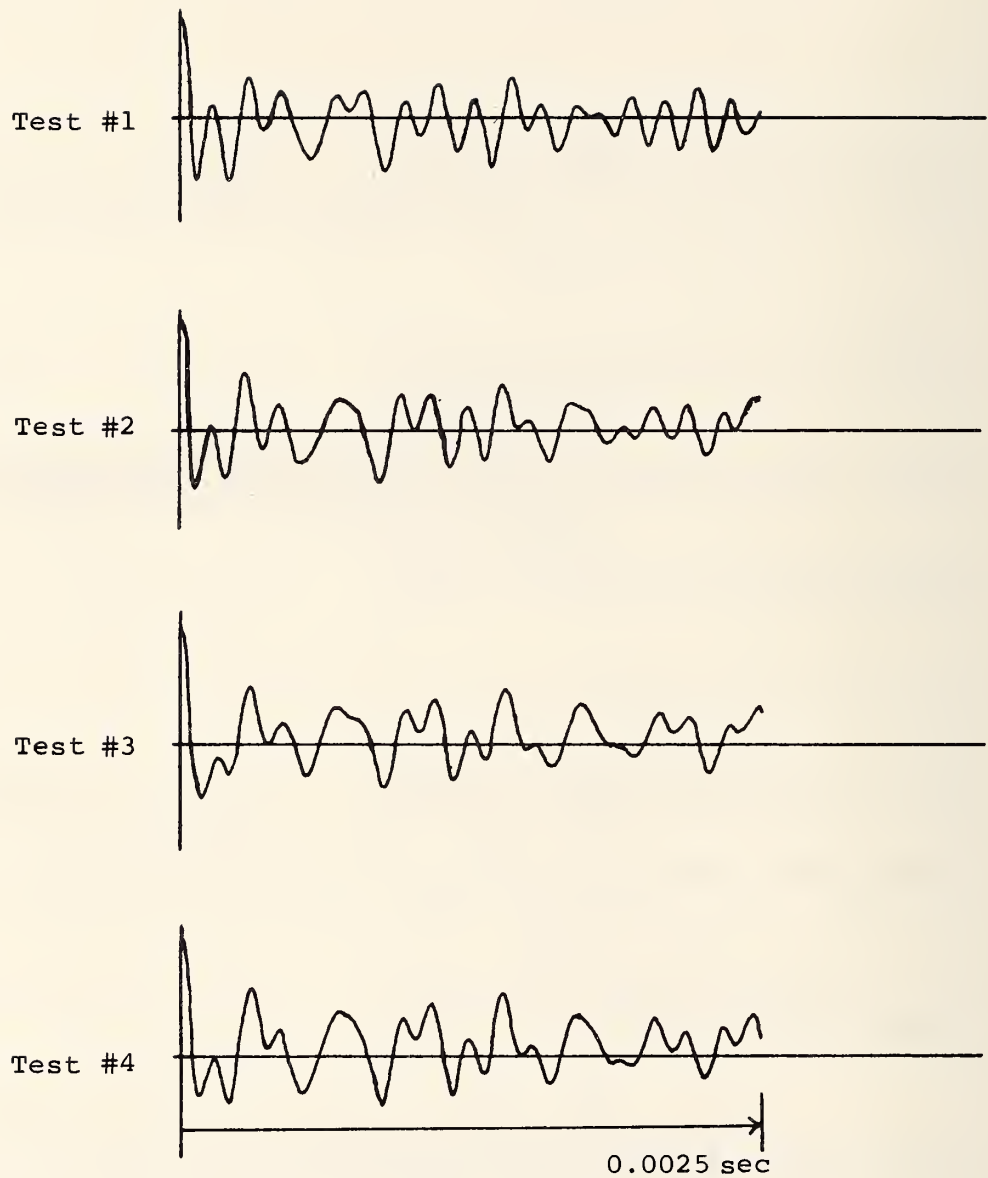
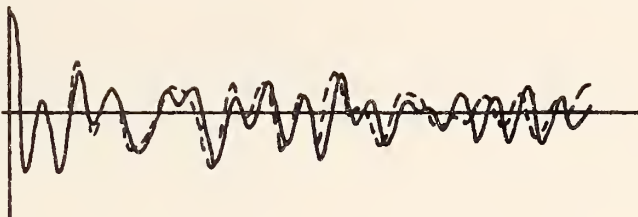


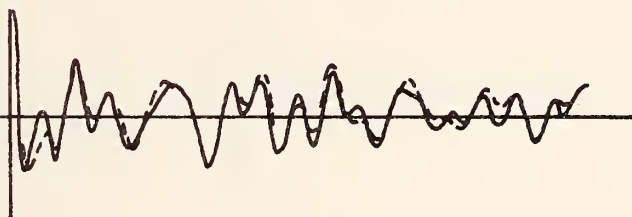
FIGURE 89.- SPECIMEN #3.- TOP ACCELEROMETER;
FILTER: 3,200 - 8,000 Hz.

Superposition of:

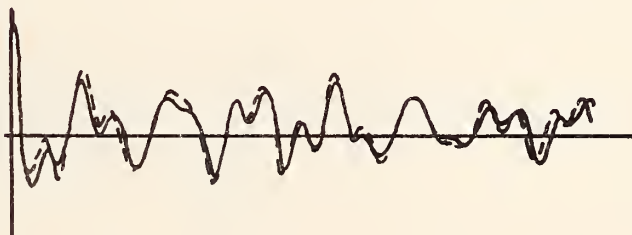
Tests 1 & 2



Tests 2 & 3



Tests 3 & 4



Tests 1 & 4

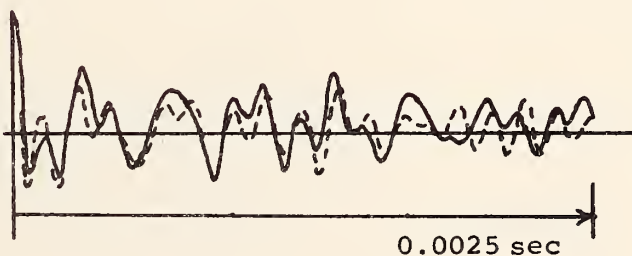


FIGURE 90.- SPECIMEN #3 - TOP ACCELEROMETER;
FILTER: 3,200 - 8,000 Hz.

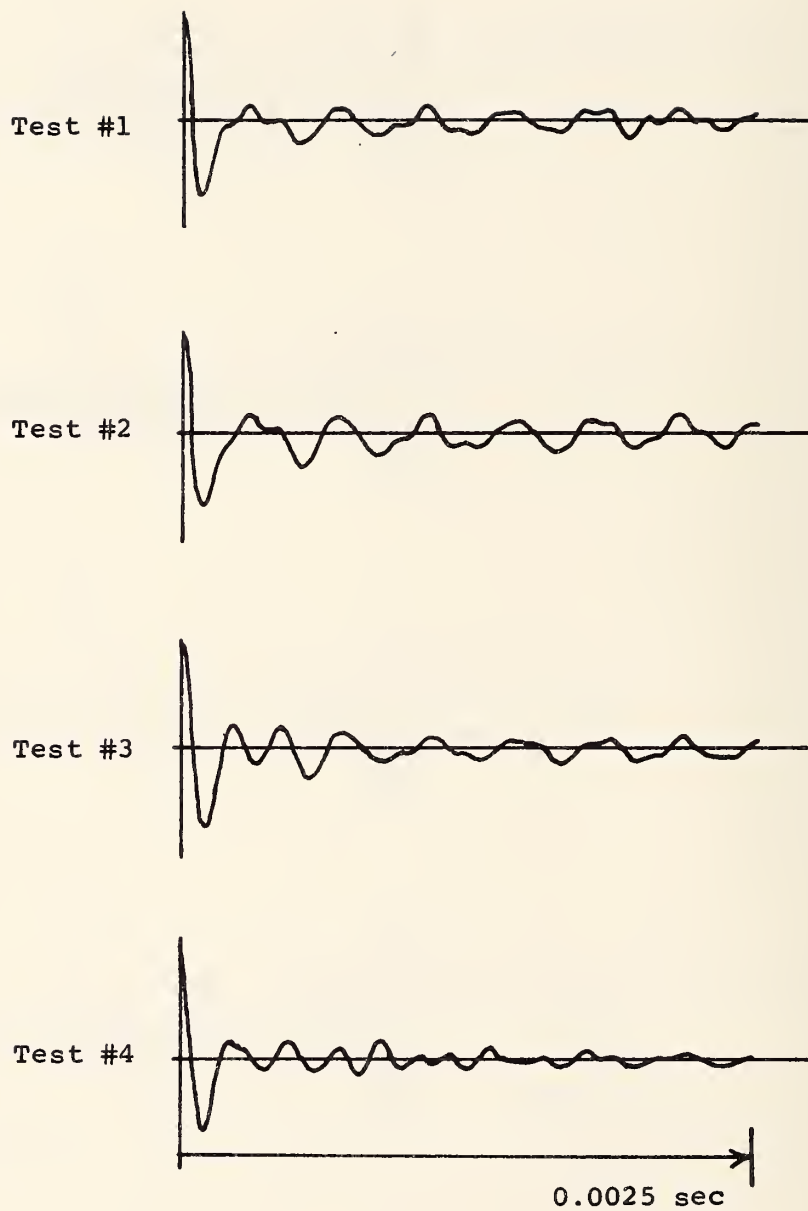


FIGURE 91.-- SPECIMEN #4 - TOP ACCELEROMETER;
FILTER: 3,200 - 8,000 Hz.

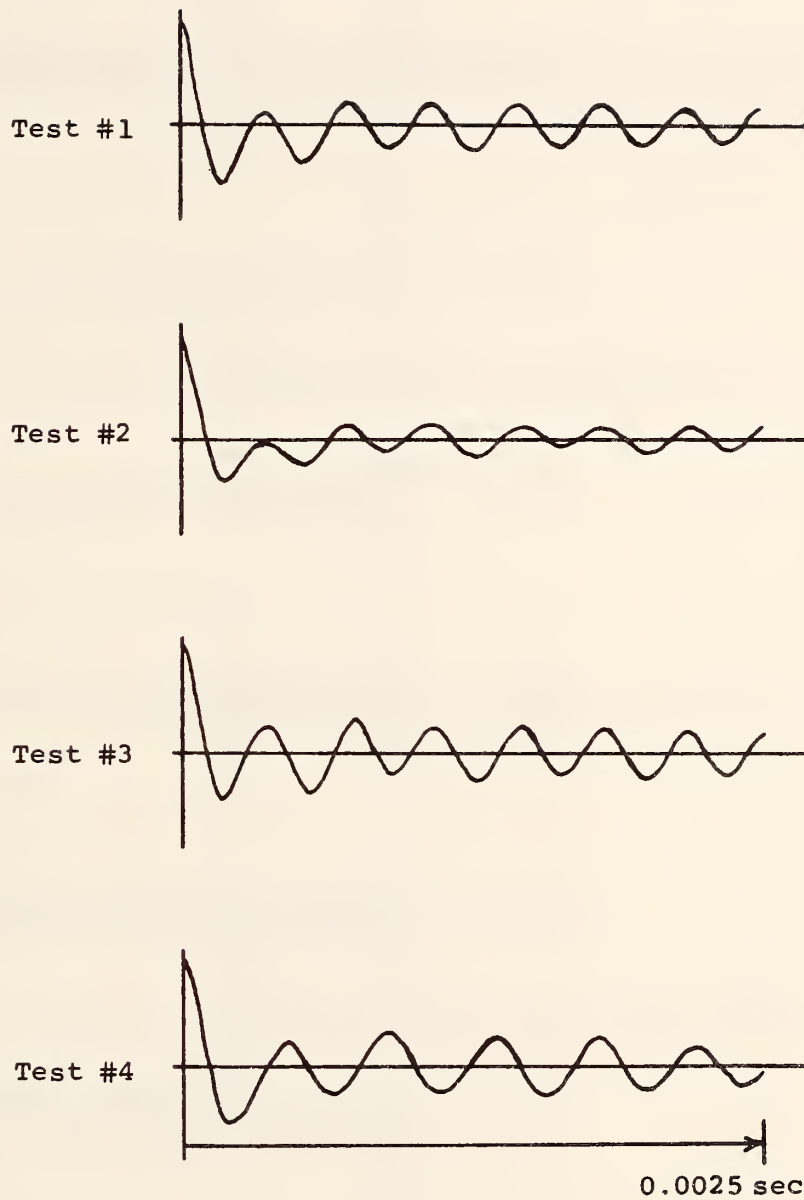


FIGURE 92.- SPECIMEN #4 - TOP ACCELEROMETER;
FILTER: 800 - 5,600 Hz.

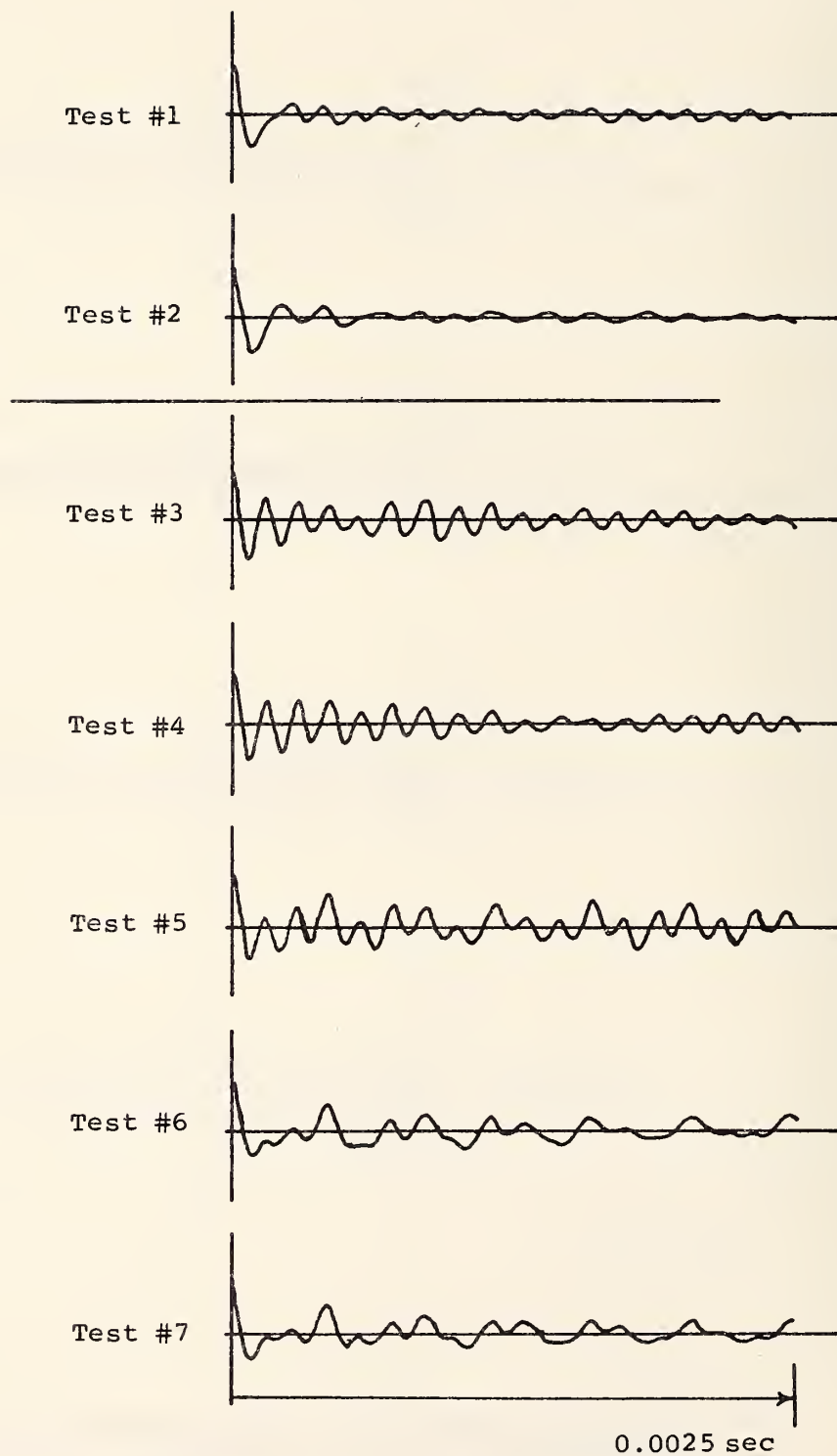


FIGURE 93.- SPECIMEN #5 - TOP ACCELEROMETER;
FILTER: 3,200 - 8,000 Hz.

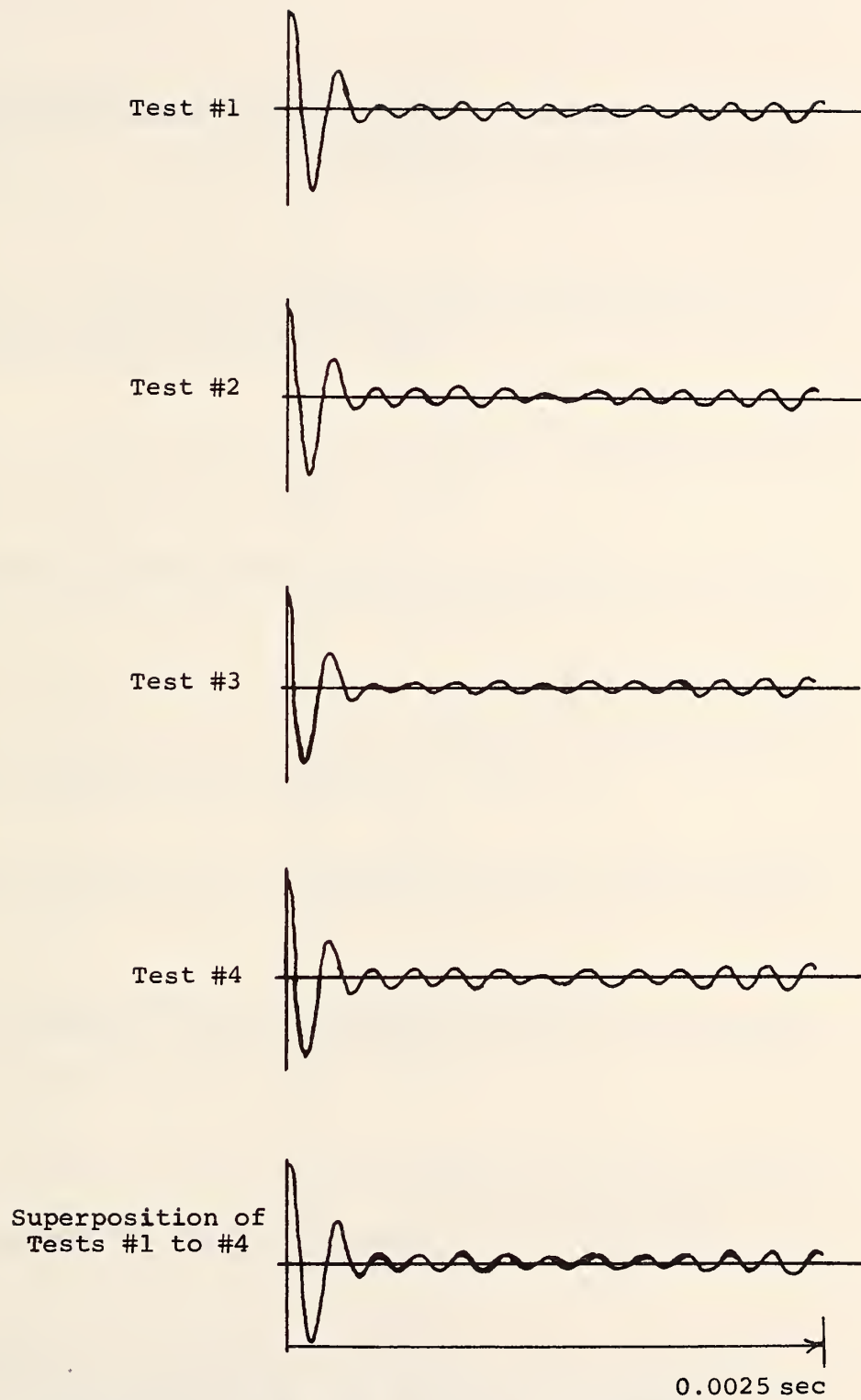


FIGURE 94.- SPECIMEN #6 - TOP ACCELEROMETER;
FILTER: 3,200 - 8,000 Hz.

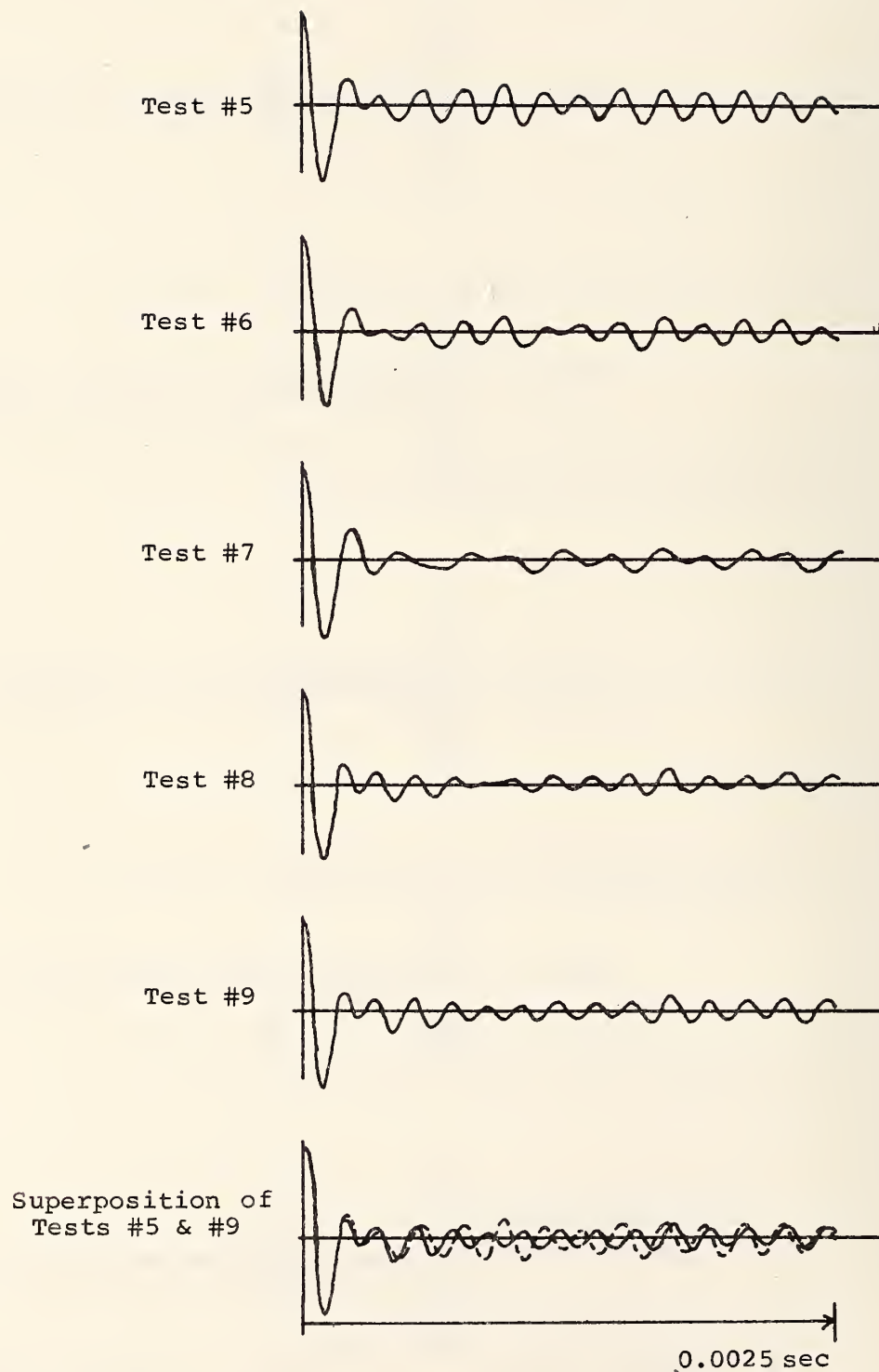


FIGURE 95.- SPECIMEN #6 - TOP ACCELEROMETER;
FILTER: 3,200 - 8,000 Hz.

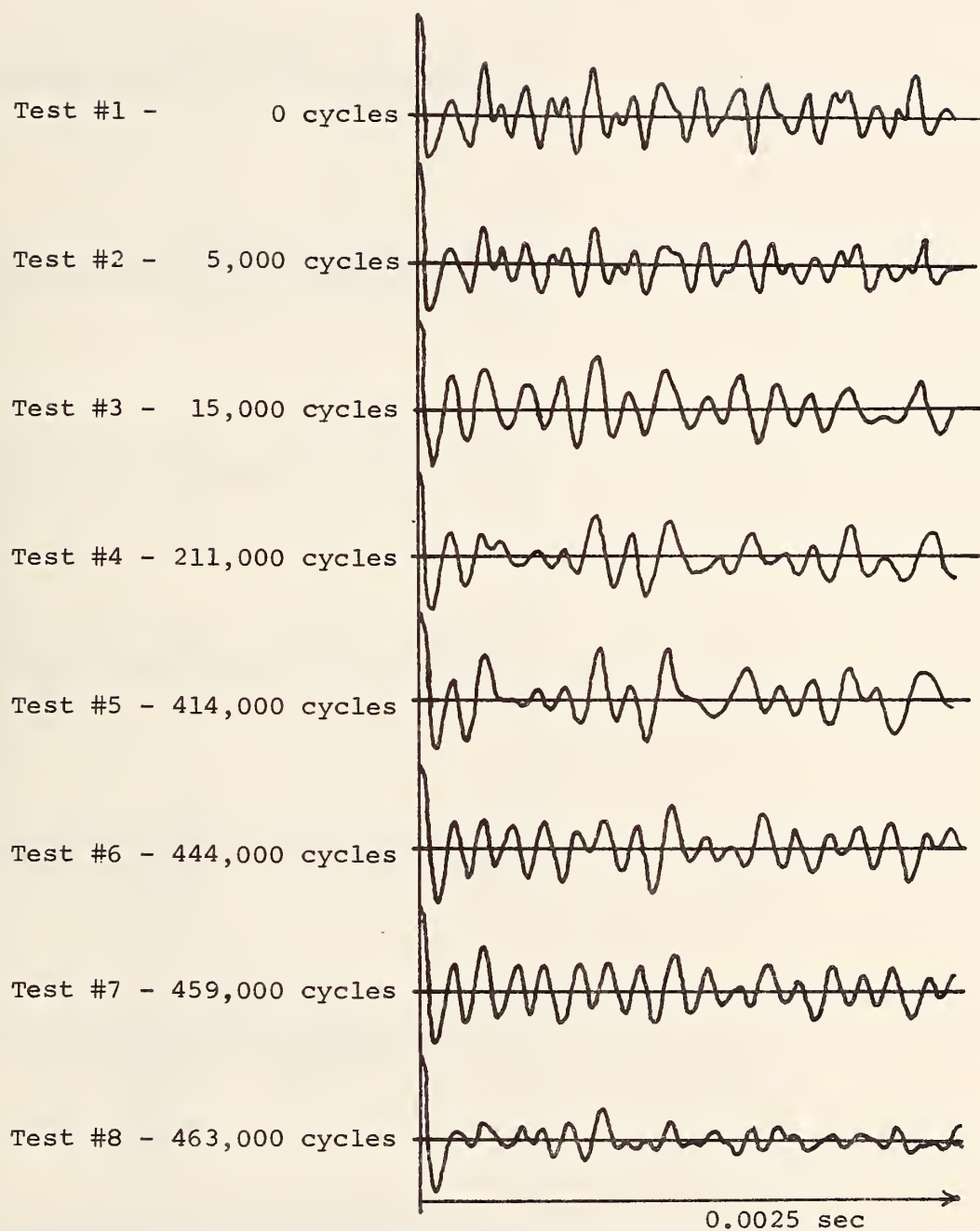


FIGURE 96.- SPECIMEN #7; FILTER: 4,000 - 8,000 Hz;
EXCITATION: SANDPAPER.

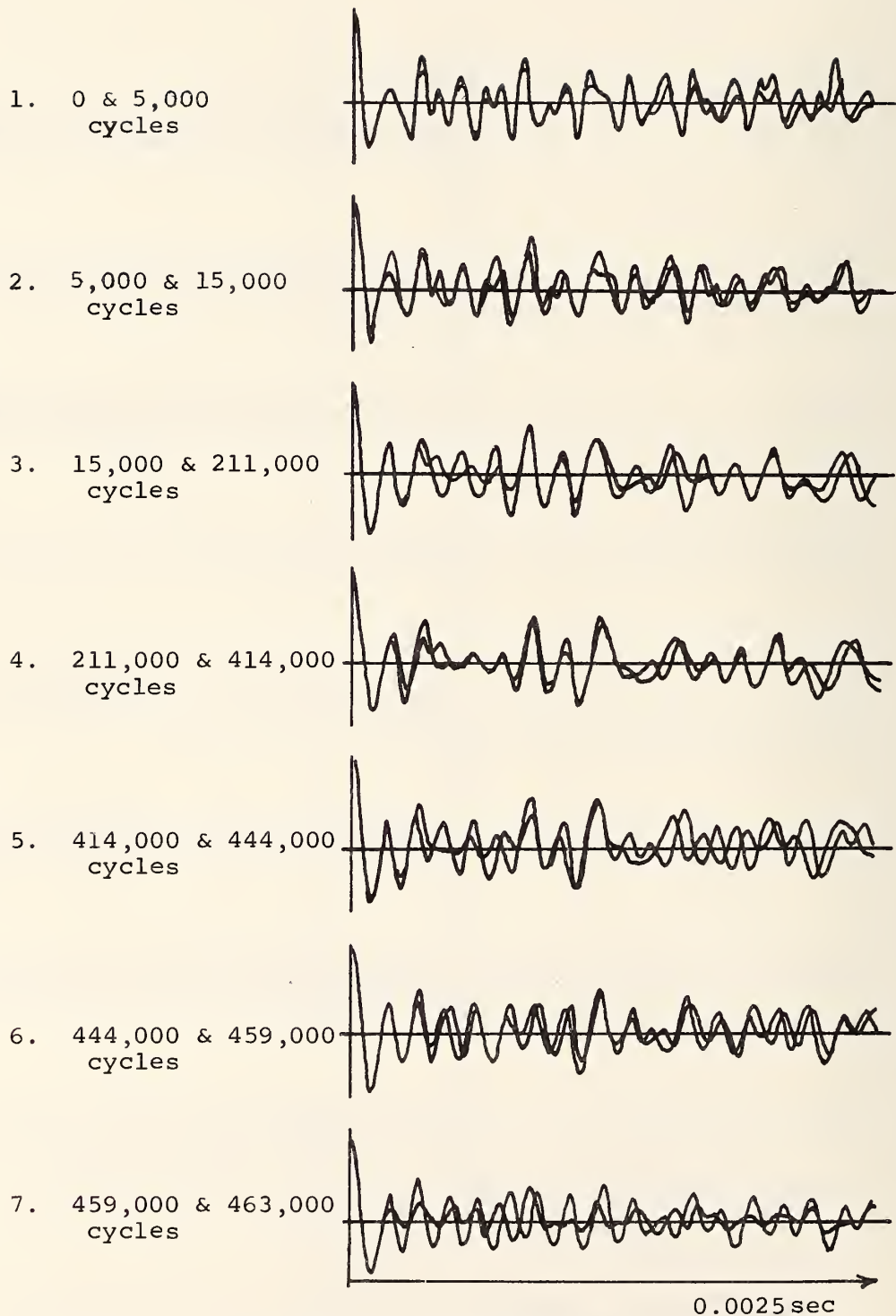


FIGURE 97.- SPECIMEN #7 - COMPARISON OF SIGNATURES;
FILTER: 4,000 - 8,000 Hz; EXCITATION: SANDPAPER.

TABLE 1.- TRANSDUCER LOCATIONS, 85-101 BRIDGE.

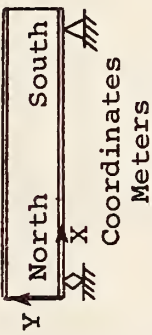
Station No.			Location and Description
	X	Y	
1A	3.53	0.69	Middle of web, west side of girder A, "Z
2A	3.53	0.02	Top of bottom flange, west side of girder A, "Y
3A	13.82	0.74	On web near cross base, west side "Z
4A	13.70	0.36	Cross bracing gusset, west side, "X
1B	3.53	0.69	Same as 1A, girder B
2B	3.53	0.02	Same as 2A, girder B
3B	13.82	0.74	Same as 3A, girder B
4B	13.70	0.36	Same as 4A, girder B

TABLE 2.- VISUAL CRACK SIZES ON LOWER
FLANGES OF MISSOURI BRIDGE.





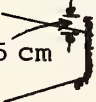
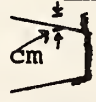
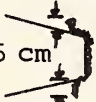
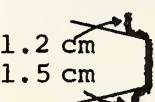
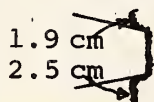
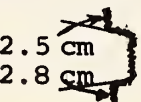
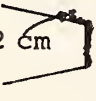



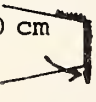

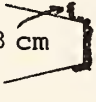

Station	Number of Fatigue Cycles			
	287,000	322,000	347,000	360,800
1				
4				
7	0.5 cm 		0.7 cm 	
10	0.6 cm 	1.2 cm  1.5 cm	1.9 cm  2.5 cm	2.5 cm  2.8 cm
13	0.2 cm 		0.2 cm 	
16				
19	1.0 cm 		1.8 cm 	
22	0.3 cm 		0.3 cm 	

TABLE 3.- NUMERICAL DIFFERENCES BETWEEN
SIGNATURES OF MISSOURI BRIDGE
BOTTOM FLANGE.

	Stations closest to cracks								Sum of rows
Tests	1	4	7	10	13	16	19	22	
0 & 95,000	0.31	1.0	0.31	0.52	0.77	1.23	0.94	0.10	5.18
95,000 & 377,000	0.52	0.10	0.63	0.11	0.35	0.35	0.48	0.16	2.70
	Stations furthest from cracks								
Tests	2	5	8	11	14	17	20	23	
0 & 95,000	0.52	0.69	0.18	0.10	0.70	0.22	0.10	0.13	2.64
95,000 & 377,000	0.27	0.48	0.26	0.22	0.12	0.08	0.26	0.30	1.99

TABLE 4.- LABORATORY TEST LOG.

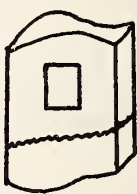
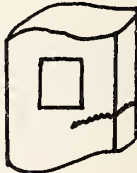
Specimen No. 1 - Fillet Weld, figures 76 and 77.				
Test No.	Static Stress $\frac{N}{\text{cm}^2} (10^{-3})$ $(\frac{1N}{\text{cm}^2} = 1.45\text{psi})$	Fatigue Cycles	Observed Crack Size, cm (2.54 cm = 1 in)	Locations
1	10.3	0	None	Complete failure occurred between 1.1 - 1.5x10 ⁶ cycles 
2	13.8	0	None	
3	10.3	130,000	None	
4	13.8	130,000	None	
5	10.3	768,000	None	
6	13.8	768,000	None	
Specimen No. 2 - Fillet Weld, figure 78.				
1	10.3	0	None	
2	10.3	0	None	
3	10.3	409,000	3.6	
4	10.3	409,000	3.6	

TABLE 4.- LABORATORY TEST LOG. (CONTINUED)

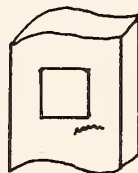
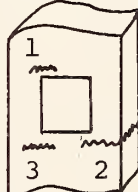
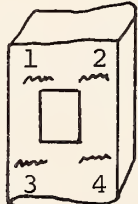

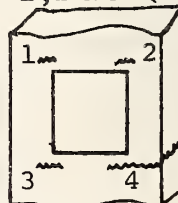
Specimen No. 3 - Fillet Weld, figures 79 and 80.				
Test No.	Static Stress $\frac{N}{\text{cm}^2}(10^{-3})$ $(\frac{1N}{\text{cm}^2} = 1.45\text{psi})$	Fatigue Cycles	Observed Crack Size, cm (2.54 cm) = 1 in)	Locations
1	10.3	0	None	
2	10.3	352,000	None	
3	10.3	369,000	0.25	
4	10.3	389,000	1.0	
Specimen No. 4 - Fillet Weld, figures 81 and 82.				
1	10.3	5,000	None	<div>Test No. 4</div>  <div>Crack #2 through specimen</div>
2	10.3	15,000	None	
3	10.3	264,000	1-0.5 2-1.0	
4	10.3	480,000	1-1.0 2-3.8 3-0.7	
Specimen No. 5 - Fillet Weld, figure 83.				
1	10.3	710,000	1-0.5	
2	13.8		2-0.6 3-1.0 4-1.4	
3	0.7		1-1.2	
4	3.5		2-0.6	
5	6.9	758,000	3-1.1	
6	10.3		4-2.9	
7	13.8			

TABLE 4.- LABORATORY TEST LOG. (CONCLUDED)

Specimen No. 6 - Butt Weld, figures 84 and 85.				
Test no.	Static Stress $\frac{N}{cm^2}(10^{-3})$ $(\frac{1N}{cm^2} = 1.45psi)$	Fatigue Cycles	Observed Crack Size, cm (2.54 cm = 1 in)	Locations
1	10.3	5,000	None	
2	13.8	15,000	None	
3	10.3		None	
4	13.8			
5	0.7			
6	3.5	567,000		
7	6.9		2.0	
8	10.3			
9	13.8			
Specimen No. 7 - Fillet Weld, figures 86 and 87.				
1		0	0	<p>1, 2 & 3 < 0.3 cm</p>  <p>Test No. 8 - Crack through specimen</p>
2		5,000	0	
3		10,000	0	
4		211,000	0	
5		414,000	1.5	
6		444,000	2.4	
7		459,000	3.0	
8		463,000	3.0	

TE662.A3 no.F

U.S. Federal

Report no.

Form DOT F 1720
FORMERLY FORM DO

FEDERALLY COORDINATED PROGRAM OF HIGHWAY RESEARCH AND DEVELOPMENT (FCP)

The Offices of Research and Development of the Federal Highway Administration are responsible for a broad program of research with resources including its own staff, contract programs, and a Federal-Aid program which is conducted by or through the State highway departments and which also finances the National Cooperative Highway Research Program managed by the Transportation Research Board. The Federally Coordinated Program of Highway Research and Development (FCP) is a carefully selected group of projects aimed at urgent, national problems, which concentrates these resources on these problems to obtain timely solutions. Virtually all of the available funds and staff resources are a part of the FCP, together with as much of the Federal-aid research funds of the States and the NCHRP resources as the States agree to devote to these projects.*

FCP Category Descriptions

1. Improved Highway Design and Operation for Safety

Safety R&D addresses problems connected with the responsibilities of the Federal Highway Administration under the Highway Safety Act and includes investigation of appropriate design standards, roadside hardware, signing, and physical and scientific data for the formulation of improved safety regulations.

2. Reduction of Traffic Congestion and Improved Operational Efficiency

Traffic R&D is concerned with increasing the operational efficiency of existing highways by advancing technology, by improving designs for existing as well as new facilities, and by keeping the demand-capacity relationship in better balance through traffic management techniques such as bus and carpool preferential treatment, motorist information, and rerouting of traffic.

3. Environmental Considerations in Highway Design, Location, Construction, and Operation

Environmental R&D is directed toward identifying and evaluating highway elements which affect the quality of the human environment. The ultimate goals are reduction of adverse highway and traffic impacts, and protection and enhancement of the environment.

4. Improved Materials Utilization and Durability

Materials R&D is concerned with expanding the knowledge of materials properties and technology to fully utilize available naturally occurring materials, to develop extender or substitute materials for materials in short supply, and to devise procedures for converting industrial and other wastes into useful highway products. These activities are all directed toward the common goals of lowering the cost of highway construction and extending the period of maintenance-free operation.

5. Improved Design to Reduce Costs, Extend Life Expectancy, and Insure Structural Safety

Structural R&D is concerned with furthering the latest technological advances in structural designs, fabrication processes, and construction techniques, to provide safe, efficient highways at reasonable cost.

6. Prototype Development and Implementation of Research

This category is concerned with developing and transferring research and technology into practice, or, as it has been commonly identified, "technology transfer."

7. Improved Technology for Highway Maintenance

Maintenance R&D objectives include the development and application of new technology to improve management, to augment the utilization of resources, and to increase operational efficiency and safety in the maintenance of highway facilities.

* The complete 7-volume official statement of the FCP is available from the National Technical Information Service (NTIS), Springfield, Virginia 22161 (Order No. PB 242057, price \$45 postpaid). Single copies of the introductory volume are obtainable without charge from Program Analysis (HRD-2), Offices of Research and Development, Federal Highway Administration, Washington, D.C. 20590.

DOT LIBRARY



00055341

